8-9-2022

Sustainable sidedress nitrogen applications for early corn and cotton crops using small unmanned aerial systems

James Nolan Parker
Mississippi State University, jp2403@msstate.edu

Sustainable sidedress nitrogen applications for early corn and cotton crops using small unmanned aerial systems

By

James Nolan Parker

Approved by:

Amelia A.A. Fox (Major Professor)
Jagmandeep S. Dhillon (Co-Major Professor)
Jac J. Varco
Rocky W. Lemus
Brian K. Pieralisi
Michael S. Cox (Graduate Coordinator)
Scott T. Willard (Dean, College of Agriculture and Life Sciences)

A Thesis
Submitted to the Faculty of
Mississippi State University
in Partial Fulfillment of the Requirements
for the Degree of Master of Science
in Agronomy
in the Department of Plant and Soil Sciences

Mississippi State, Mississippi

August 2022

Name: James Nolan Parker

Date of Degree: August 9, 2022

Institution: Mississippi State University

Major Field: Agronomy

Major Professor: Amelia A. A. Fox

Title of Study: Sustainable sidedress nitrogen applications for early corn and cotton crops using small unmanned aerial systems

Pages in Study: 132

Candidate for Degree of Master of Science

Nitrogen run-off from agriculture have been linked to human health problems on a global level. Large-scale conventional producers struggle to redefine themselves as sustainable because reducing nitrogen (N) inputs without justification or validation may lead to severe profit losses. Small unmanned aerial systems (sUAS) sensing may allow for decreased N runoff. Failure to address this problem will exacerbate already excessive N runoff into the Mississippi River and beyond. The purpose of this study was to reduce fertilizer N input using sUAS technology to assess crop canopy needs. In 2020 and 2021, variable rate nitrogen (VRN) side-dress N application maps were calculated on early corn and cotton crops sensed with MicaSense® technology. The SCCCI and FENDVI VIs most often were highly related by SEq to early corn and cotton canopy N status. VariRite™ technology was successfully implemented in producer's fields using VI calibrated imagery captured from sUAS.

DEDICATION

For Tap, Elaine, Brooks, Mark, Jennifer, Brockman, Elliott, and Adeline.

ACKNOWLEDGEMENTS

The author expresses thanks to Dr. Amelia Fox, and all committee members, for patience and persistence towards this common and crucial goal.

The flight team for this project also acknowledges the professional efforts of Mr. Dennis Lott (UAS Solutions, Clinton, MS) for the inspiration and design of the project's rotor craft. Moreover, we thank all at the Raspet Flight Laboratory (Starkville, MS) for providing the financial support and means to evaluate the fixed-wing aircraft piloted by Mr. Austin Wingo.

Finally, special thanks also go out to is given for the gracious support provided by Mississippi Corn Promotion Board and Southern SARE.

TABLE OF CONTENTS

LIST OF TABLES

LIST OF FIGURES

CHAPTER I

BACKGROUND

There are over 405 oceanic “Dead Zones” (hypoxic) according to Diaz (2018), and the Mississippi River Gulf dead zone covers approximately 15,540- 18,130 sq km (6,000-7,000 sq mi) (AP, 2021; Bruckner, 2019). Most dead zones are attributed to agricultural fertilizer nitrogen (N) runoff leading to aquatic deoxygenation. Fertilizer N overapplication can also contribute to health conditions such as “Blue Baby Syndrome” (Knobeloch et al., 2000). Methemoglobinemia is a form of Blue Baby Syndrome caused by nitrate (NO_{3-}) polluted drinking water. The nitrates in the water convert to nitrites and form methemoglobin in the bloodstream of infants (Christiano, 2017). Methemoglobin’s inability to bind oxygen in the infant’s blood stream creates oxygen deficiency and results in a blue tint in their skin color. Increasing N use efficiency in crop production systems may aid in reducing N in potable water.

Inefficient N use is a contributor to the pollution of major worldwide waterways (Kanter, 2019). In 2015, the U.S. applied 10.79 Tg (11.9 tn) of fertilizer N (Mosheim, 2019). The goal of reducing N fertilizer usage necessitates determining the optimal N rate for crops such as corn (*Zea mays* L.) and cotton (*Gossypium hirsutum* L.) against environmental challenges. In Mississippi, corn and cotton producers, being the primary consumer of commercial N fertilizer, planted 267,093 ha (660,000 ac) and 287,327 ha (710,000 ac), respectively (USDA Quick Stats, 2019). Corn and cotton have distinctive canopy architecture and related sunlight reflectance characteristics that aid in estimating N sidedress requirements through analysis by remote

sensing technologies (Baret et al., 2007; Cammarano et al., 2011). Corn and cotton canopy reflectance research, and related sustainable N applications, may also be translatable to other cropping systems.

Small Unmanned Aerial Systems (sUAS) missions equipped with MicaSense RedEdge® (Seattle, WA) technology may support estimating canopy N status in corn and cotton (Xu et al., 2019). From sUAS sensing missions, variable rate nitrogen (VRN) prescriptions may be estimated through quantitative calculation and delivered to the crop in need via fertilizer applicator at the most critical growth stages. Variable rate N prescription may aid producers in applying appropriate N fertilizer rates, thus lowering the whole-season fertilizer load. Reducing N fertilizer and maintaining optimal yields may also increase nitrogen use efficiency (NUE).

Failure to address farm N use may exacerbate already excessive N runoff into the waterways, may decrease yield and reduce producers' net profit. Excessive N fertilization is not sustainable as it leads to contaminated runoff and decreased profitability in southern states (Erisman et al., 2013). Persistent overapplication of N fertilizer will result in increased environmental perturbations. The current generation of farm producers are charged with the challenge of reducing inputs while producing sustainable outcomes (Green, 2019). The challenge calls for a revolution in new agricultural technology that will increase sustainability while also promote increasing yields. Increasing N and other nutrient efficiencies is the next step in finding solutions to long ignored problems in agriculture.

Purpose of Study

The overarching goal of this study is aimed at reducing fertilizer nitrogen (N) inputs through employment of technologies that may increase sustainability and, simultaneously, reduce environmental pollution related to fertilizer N use. The purpose of this study was to compare

techniques to aid in estimating early crop N status for supplementary, but reduced, fertilizer N sidedress applications at varying rates in corn and cotton. Commercial off-the-shelf aerial technology and sensors will be compared for their efficiency in estimating early N status.

Study Hypotheses

The first study hypothesis is that research conducted using a sUAS equipped with a multispectral sensor (visible-near infrared) will accurately estimate early corn and cotton crop leaf N percentage and aid in improving NUE through the production and employment of VRN sidedress maps.

The second study hypothesis is based on limited studies defining distinct differences between fixed-wing and quad-copter technologies. Based on induction, this study hypothesizes that fixed-wing may provide imaging data returns with higher efficacy due to factors such as speed and power consumption.

Study Objectives

For this study, the research objectives are:

1. Compare unmanned, fixed-wing flight technology to quad-copter to establish which system estimates early crop canopy N status most effectively
2. Evaluate five different VIs for estimating early corn and cotton canopy N status
3. Demonstrate a sensor-based VRN technology in a producer's field using VI calibrated imagery captured on unmanned flight systems

Expected Outcomes

The expected outcome of this study was improved fertilizer N distribution through prescription VRN mapping, which simultaneously supports both an increased NUE and crop

production sustainability. Moreover, it was expected that this study will demonstrate benefits of fixed-wing flight platforms as an alternative to conventional quad-copter platforms for overall sensing mission success.

Study Limitations

This study is limited to the 2020-2021 growing seasons for corn and cotton in Mississippi and (potentially) Louisiana Mississippi River Alluvium. Field operations (planting, fertilizing, harvesting) and sensing missions are highly dependent on weather. The sensing missions flown by sUAS will include two flight platforms that have flight distance limitations related to power supply systems. The study methods are limited to applications that are utile by farmers and farm service providers and cost less than a total of $10,000. This study also faced a flight platform limitation during year one due to a contractor failure.

CHAPTER II

LITERATURE REVIEW

Overview of Remote Sensing in Agriculture

Remote sensing and aerial imagery predate to the mid-19th century when hot air balloons equipped with large and cumbersome cameras were used to capture a bird's eye view from moderately low altitudes (Byrum, 2017). Military became dependent on aerial imagery during war time to help strategically plan attacks on the enemy. Remote sensing gained momentum in agriculture when the United States Department of Agriculture (USDA) began working with the National Oceanic and Atmospheric Administration (NOAA) and the National Aeronautics and Space Administration (NASA) on the large area crop inventory experiment in 1974 (Moore, 1981). The collaboration led to the launch of the AgRISTARS project in 1978 that assessed the future course of remote sensing in agriculture.

Along with the AgRISTARS program, the launching of earth observation satellites (EOS) into orbit also sparked interest for technological solutions within the agricultural community (Jarman and Dimmock, 2018). There are currently 4,550 satellites in operation with the majority being communication satellites (UCS, 2021; Chaturvedi, 2019). The ability to view data returns from satellites in the 1970's and 1980's gave farmers the opportunity to make management decisions from imagery for the first time. Once data for decision making filtered into agriculture, precision farming technologies were founded (Igor, 2017). Remote sensing technology allowed farmers to manage large land area on an acre-by-acre basis.

History of Agricultural Flight Systems for Sensing Missions

Low-orbiting satellites have collected data returns for agricultural purposes for the past six decades (Igor, 2017). Earth observing satellites (EOS) fly at approximately 708 km (438 mi) altitude and produce images with approximately 30 m (98ft) spatial resolution (Jarman and Dimmock, 2018). A common type of satellite used for agricultural data collection is the EOS, which typically circumnavigate the globe daily at 705 km altitude. Communication satellites in moderately high orbit and Global Positioning System (GPS) in high orbit also provide valuable services to precision agriculture.

While satellites still play a role in agricultural data collection, Small Unmanned Aerial systems (sUAS) provide a customizable technology to precision agriculture at much higher spatial and temporal resolutions (Tsouros et al., 2019). Colomina and Molina (2014) highlight the rapid growth of sUAS used for photogrammetry and remote sensing. The sUAS market was evaluated at $1.19 billion in 2018, and is predicted to reach $6.52 billion by 2026 (Watson, 2019). Originally, sUAS were primarily used for observational aerial imagery; but have recently shifted the focus to developing artificial intelligence (AI) autonomous applications. Although AI is a rapidly emerging technology, there is a need to increase efficacy of image-based flight systems in terms of speed and endurance (Tsouros et al., 2019). Fixed-wing flight platforms are the most efficient in terms of speed, but further testing to discover the most efficient system encompassing all necessary parameters is needed.

Modern Agricultural Sensors

Agricultural flight systems have evolved to carry a wide range of optical sensors including multispectral sensors, time-of-flight sensors, and others (Khot, 2017). When utilizing optical sensors, researchers must consider the sensor capabilities necessitated by their specific

research. Radiometric resolution is defined by the amount of information contained within a pixel; known as a single binary computer data value, or bit (Ose, 2016). Sensor sensitivity is directly related to a sensor's radiometric resolution. For example, a sensor with a finer radiometric resolution will produce high intensity returns with a broader range of digital number values directly related to the computational bit range.

The MicaSense RedEdge® (Seattle, WA), can produce images in 12- or 16-bit format (MicaSense, 2019). A 12-bit sensor produces image grayscale pixel values ranging from 0-4,096 (black to white, respectively) while a 16-bit image range spans 0-65,535. Also directly related to the radiometric resolution, spatial resolution is a critical consideration when choosing a sensor for flight operations.

A sensor's spatial resolution is determined by the measure of the smallest object detected by the sensor measured in ground sample distance (GSD) or pixel size (Leslie, 2018). MicaSense sensors have a GSD of 8 cm per pixel at 121 m (394 ft) above ground level (AGL). Another consideration when choosing a sensor is the desired, spectral resolution. Spectral resolution is defined as the number and width of the spectral bands within a sensor system. The MicaSense sensor captures five bands including blue (λ475 nm center, 20 nm bandwidth), green (λ 560 nm center, 20 nm bandwidth), red (λ 668 nm center, 10 nm bandwidth), red edge (λ 717 nm center, 10 nm bandwidth), and near-infrared (NIR) (λ 840 nm center, 40 nm bandwidth). The remaining resolution parameter, temporal resolution, is defined as the time necessary for a sensor to revisit the same spot on the earth's surface, or the revisit interval. Temporal resolution is primarily only measured on orbiting satellites.

Sensor function is classified as either passive or active (Mai, 2015). Active sensors rely on an external electromagnetic energy source, while passive sensors sample reflected, emitted, or

thermal electromagnetic energy during sensing operations. Agricultural sensors flown on sUAS, such as MicaSense RedEdge, are typically passive and sample reflected, radiant light.

Flight Sensing Platforms in Agriculture

Quad-copter flight systems are the most deployed platform in precision agriculture (Dukowitz, 2019). Multirotor aircraft may also be configured with five, six, and eight rotor-blade options. Quad-copters are ideal for sensing due to their stability, maneuverability, ability to hover, and vertical takeoff and landing (Herrick, 2017). Fixed-wing flight platforms are impacting precision agriculture due to their long endurance and faster flight speeds (Yinka-Banjo and Ajayi, 2019). Although fixed-wing platforms fly faster than quad-copter, increased speed may lead to distortion in data.

Flight Parameters

Quad-copter technology limitations include slower flight speed and less flight endurance, thus covering less land during sensing missions (Khot, 2016). While quad-copter is most common, fixed-wing flight systems may prove to be more efficient. Fixed-wing flight systems provide advantages such as faster flight speeds, and longer flight duration. Disadvantages of fixed-wing systems may include image blurriness related to speed distortion, inability to hover in place, and require a large area to make aerial turns and, finally, land. Fixed-wing platforms can cover an area in half of the time of quad-copter flight systems and may result in higher efficiency and a more productive sensing mission.

Sensor Efficacy for Fixed-Wing vs. Quad-Copter

Whether data clarity will be compromised on the fixed-wing platform due to increased speed is not clearly understood. According to Boon et al. (2017), fixed-wing flight data did

possess a decrease in data quality, but was satisfactory for the intended purpose. While fixed-wing data was considered utile, quad-copter data was preferred. Image overlap was constant for both platforms with 80 percent forward overlap and 60 percent side overlap. Although Moran et al. (2003) did not analyze data clarity, the quad-copter flight platform was found to follow waypoints closer than fixed-wing which may lead to higher data accuracy for precise points.

Estimating Early Corn and Cotton Canopy N Status

Corn Cultivation

Corn has a rich history predating back 9,000 years to the Balsas River Valley in Mexico (Katz, 2018). The origin of corn begins with the domestication of the grass teosinte (genus *Zea*). While genetic characteristics of corn and teosinte are very similar, the tough outer casing of teosinte was not ideal for human consumption. Ancient settlers selectively bred teosinte for its favorable traits that form current day corn.

Corn is typically planted approximately 5 cm (2 in) deep (Roozeboom and Sindelar, 2017). The seed requires a minimum soil temperature of 10 ^{o}C (50 ^{o}F) for germination. Emergence timing depends upon soil temperatures. Cooler soil temperatures will result in a later emergence date than warmer temperatures. Soil moisture is also required for successful germination and emergence. Once the seedling has emerged and began to grow, proper nutrient management is essential for a successful corn crop (McConnell, 2018). Nitrogen (N), Phosphorous (P), Potassium (K), Sulfur (S), Magnesium (Mg) and Zinc (Zn) are the primary nutrients that must be monitored to maintain a healthy corn plant (Larson and Oldham, 2021).

Corn growth stages are characterized as either vegetative or reproductive. The vegetative stages begin with VE at emergence and end at VT which is the tasseling stage. The first stage (VE) is characterized by the radicle emerging from the seed coat. After the emergence of the

radicle, the mesocotyl will begin to grow inside a protective casing called the coleoptile (Roozeboom and Sindelar, 2017). The following vegetative stages are identified by a V followed with the number of leaves (Licht, 2021). The V1 stage is noted when the bottom leaf has a collar and a rounded tip. During the second stage, known as V2, the second leaf appears with a visible collar. The second leaf and all following leaves will have a sharp point at the tip. The plants growing point will become visible above ground at V6 and the first leaf will die. The V6 stages may be a critical remote sensing sampling stage at which leaf N is highly detectable from low altitude missions. Ideal N application time is during the V4-V6 due to plant height restrictions. In-ground knife N application requires the plant to be below the toolbar of the implement. Nutrient and water requirements will become crucial during the V10 stage. The plant will possess multiple shoots that may become successful growing points. The final vegetative growth stage is tassel formation known as VT. Vegetative growth will now end and the reproductive stage will take over. At VT, it may be possible to estimate final corn crop yield using remote sensing technologies.

The reproductive stages initiate after the vegetative stages have completed their cycle (Roozeboom and Sindelar, 2017). Silking is the first reproductive stage in the corn plant. Silking produces reproductive silk strands elongating beginning at the bottom of the cob. Corn silk elongation is dependent upon turgor pressure; therefore, dry conditions can postpone silk development. Silk strands are responsible for capturing pollen and germinating the ovule from which they originate. The second reproductive stage is the kernel blister stage, which occurs approximately 11 days after silking. If the plant endures a high amount of weather-related or nutritional stress, kernels may be aborted during the kernel blister stage. Kernel milk stage is the third reproductive stage that occurs around 18 days after silking. “Milk” is the term used for the

white substance that begins to appear within the kernels during the milk stage. Reproductive stage four is termed the kernel dough stage. The kernels begin to harden from the milk stage and form into a dough type consistency. Kernel moisture is around 70% during the dough stage. Kernel dent stage is the fifth stage of reproduction. During the dent stage, a milk line begins to appear on the kernels. A dent line is used to determine the amount of "milk" left in the kernels. The milk line moves lower and lower on the kernel as the cob grows closer to physiological maturity.

Physiological maturity is the final stage of the reproductive growth cycle. The kernel milk line is gone, and a black layer appears on the tip of the kernels. A milk line forms typically when the farmer will stop irrigation since the corn has completed its reproductive growth. The final stage is harvest maturity when the corn has reached below 25 percent moisture.

Nitrogen uptake in corn can depend on a number of variable such as environment, soil type, N rate, and plant population (Ciampitti and Vyn, 2014). Nutrient replacement recommendations should also be monitored and accounted for each year when considering N rates. Best nutrient management practices must be implanted using the above-mentioned information.

Corn Production

The United States (U.S.) ranks first worldwide in corn producing approximately 377.5 Tg annually (Nag, 2017). The U.S. is also the leading corn exporter worldwide with $12.9 billion, which account for 38% of total worldwide exports, in 2018 (Workman, 2019). The majority of corn production in the U.S. comes from the Midwest with Iowa producing 68.5 million Tg (2.7 bill bu) of corn in 2016 (Cook, 2020). Mississippi produced three million Tg (119 mil bu) in 2016 ranking twentieth among all fifty states.

Markets, Uses, and Distribution

United States corn production is primarily used for biofuels and animal feed (Foley, 2013). Biofuel production consumes up to 40% of U.S. corn production while 36% of U.S. corn production is used for animal feed. Ethanol is the main biofuel manufactured from corn. Approximately 98% of U.S. gasoline contains ethanol thus making ethanol essential in the fueling of cars (Lewandrowski and Hohenstein, 2017). Corn is also a main ingredient in animal feed due to high protein content (Lardy, 2018). Additional to ethanol and animal feed, corn is a large factor in the production of corn meal and other foods (Cellania, 2010).

Cornmeal is used for various foods including batter, cornbread, pancakes, and donuts. Cornmeal is made by grinding whole corn and separating the remnants into different sized categories (Lardy, 2018). Starch is also another common product of corn made using the endosperm within the corn. The endosperm undergoes grounding and separation to release carbohydrates. Corn starch is primarily used to condense liquid food and is also a main ingredient in the creation of biodegradable plastics (Cellania, 2010). High-fructose corn syrup, often found in soft-drinks, is also a popular by-product of corn processing. Corn is an essential crop constituent many products in the U.S. and abroad.

Cotton Cultivation

The New World allopolyploid *Gossypium hirsutum* L., commonly referred to as upland cotton, originated in regions of Central and South America (Wendel et al., 2010). The climate of Central and South America is ideal for cotton growth due to cotton's desire for warm conditions within the temperature range of 32 to 35 ^{o}C (90-95 ^{o}F) (Sharpe, 2019). Cotton requires a significant amount of sunlight and a soil temperature of at least 16 ^{o} C (60 ^{o} F) for seed germination. After the cotton has emerged, the primary nutrients for cotton are Nitrogen (N),

Phosphorus (P), Potassium (K), and Boron (B) (Stevens, 2019). Secondary nutrients that are needed for cotton growth are Calcium (Ca), Magnesium (Mg), and Sulfur (S).

Ideal depth for cotton seeds at planting is 1.3 to 1.8 cm (0.5 – 0.7 in) deep (Collins, 2017). All necessary elements for germination, besides water, are encased in the cotton seed capsule (Main, 2012). The radical is the first to emerge from the swelling cotton seed. The "crook" stage is the period when the hypocotyl is growing towards the soil surface. Crook Stage is a crucial stage in the growth period due to the risk of the cotyledons being unable to penetrate through the soil surface. After the cotyledons develop successfully, growth of new plant tissues is driven by photosynthesis (Dodds et al., 2010). The first true leaf is created by photosynthesis drive and the following leaves will repeat the process. Sunlight reception increases directly in relation to new growth and the general increase of the overall surface area of the plant (Stewart et al., 2010). Carbohydrates are used by the plant to ensure continual growth throughout the season.

Historically, cotton is known as an indeterminate perennial grown as an annual (Dodds et al., 2010). The term "indeterminate" signifies the cotton does not have a genetically predetermined stopping point for growth. Also, indeterminate suggests the plant is constantly adding vegetative growth along with fruit. Plant growth regulators (PGRs) become necessary to transfer the excess vegetative growth to fruit formation. Several hormones in a cotton plant naturally regulate plant growth (Stevens, 2020). The PGRs currently deployed act with the same mode of action as the ones naturally present regulators.

Auxins, gibberellins, gibberellic acid and cytokinins are examples of hormones in the plant that contribute to regulating plant growth. Gibberellins play a role in stem elongation along with leaf growth (Stevens, 2020). Increased boll retention was also found associated with

gibberellins, but yield responses were inconclusive. Gibberellic acid primarily induces seed growth and cell elongation. Cell division and overall plant growth are promoted by cytokinins. A decrease in fruit abscission has also been found associated with cytokinins. Photosynthesis is also prolonged due to cytokinin delay of leaf aging (Stewart et al., 2010). The primary role of auxin is to contribute to leaf expansion, cell and stem elongation, and increased rooting. Application of additional auxins may lead to increased boll retention.

Simultaneously occurring with applications of PGR, a leaf "square," the first visible leaf structure containing the leaf-like bracts, is continually developing throughout the growing season. The true square development begins at the pinhead square stage, or at about 30-45 dap (Main, 2012). The square continues through match-head square and candle stage. Prior to bloom stage is considered optimal for remote sampling of reflectance to develop leaf N status. After candle stage, flowering occurs which pollinates to form the boll. It is at the flowering stage that most remote sensing imaging missions can begin to estimate crop yield.

Fifty days is the typical time period required for the boll to open, exposing the cotton within it (Stewart et al., 2010). The boll goes through three primary growth phases during the fifty-day span including enlargement, filling, and maturation. The enlargement stage is characterized by fibers elongating within the boll. Seed volume is maximized and the boll is prepared for the filling phase (Stevens, 2019). Secondary wall growth begins during the filling face as fiber elongation is terminated. During boll development, external factors such as weather can impact fiber quality, strength, and micronaire gradings. Boll maturation is the final stage of boll development. Maximum weight and size are achieved during boll maturation stage.

Cotton Production

During 2017, 26.3 billion Tg (120.86 bill bales) of cotton were produced worldwide with the majority being grown in India, China, and the United States (Shahbandeh, 2018). The United States alone produced 4.5 million Tg (20.9 mil bales) of the 26.3 billion Tg (120.86 bill bales) worldwide. Most cotton growth in the United States is based in the southern portion of the states. Cotton is the fourth largest agricultural product produced in Mississippi. In the year 2018, the Mississippi cotton market was valued at $623 million (USDA Quick Stats, 2019).

Markets, Uses, and Distribution

Cotton is traded globally in raw and finished products (Meyer, 2019). The United States plays a large role in the worldwide cotton market as the world's leading cotton exporter supplying over one third of world cotton exports. Cotton has a variety of uses ranging from clothing to oil (Worcester, 2017). Cotton is desirable for clothing production due to its comfort ability to absorb and release moisture quickly. Lint from cotton is classified into three separate groups to determine usage.

Fine lint, the first group which consists of primarily Pima cotton, is used for making stockings, yarn, and other fine fabrics (Weigmann, 2020). American upland cotton, commonly found growing in the United States, is classified as medium staple and is used for ring spinning in combed and carded yarn production (Chen et al., 2005). The final group, short staple, is used to produce carpets, blankets, and other inexpensive fabrics. While fiber is one part of cotton mill produce, oil and meal are also important products that come from cotton (Wickison, 2019).

Cotton seed oil is produced by extracting the oil from the seed within a cotton seed plant. Once in oil form, the product can be used for cooking, biodiesel, or as a natural pesticide (Chen et al., 2005). Along with the oil from cotton seed, meal is also a product from the cotton seed

mill (Wickison, 2019). Cotton seed meal is used for cattle feed alone. Due to the toxicity of gossypol, a chemical compound found in cotton seed meal, the meal can only be consumed and digested by ruminants. Gossypol has been used as an experimental contraception in male and female humans. Cotton has a variety of uses and is an important crop in worldwide agriculture.

Slope-, Distance -, and Orthogonal- based Indices

Three common types of vegetation indices (VI) used are slope, distance, and orthogonal based indices. Slope-based indices use a combination of red and near infrared (NIR) bands to formulate indices. One of the first slope-based VIs was the Ratio Vegetation Index (RATIO) (Birth and McVey, 1968). While RATIO was one of the earliest indices, normalized difference vegetation index (NDVI) (Rouse, 1974) is the most commonly used VI due to little topographic effects and ability to produce a linear measurement scale (Glenn et al., 2011). The Normalized Ratio Vegetation Index (NRVI) (Baret and Guyot, 1991) is a normalized version of the Ratio Vegetation Index (RVI) (Richardson and Wiegand, 1977), the inverse of RATIO, similar to the normalization of NDVI. Slope-based VIs are the basis for the majority of agricultural sensing indices.

Distance-based vegetation indices originated from the Perpendicular Vegetation Index (PVI) (Richardson and Wiegand, 1977). The goal of distance-based VIs is to remove the soil brightness factor where vegetation is scarce. The Ashburn Vegetation Index (AVI) (Ashburn, 1979) is a distance-based VI focused around measuring green growing vegetation. The most efficient distance-based VI is the Weighted Difference Vegetation Index (WDVI) (Clevers, 1988; Richardson and Wiegand, 1977), which is calculated by weighting the red band with soil slope line.

Orthogonal-based VIs are calculated by using the spectral bands to create a group of uncorrelated bands. Principal Components Analysis (PCA) is an orthogonal-based method that produces a group of uncorrelated images ordered by the variation within the original set of images. There is wide array of vegetation indices to choose from for each unique sensing mission in agriculture.

Overview of Remote Sensing N Status Sensing in Crops

Corn Sensing Methods

Several studies of N sensing in corn use a variety of sensing platforms to perform research. Paiao, (2018) conducted a N in corn study using SPAD (Spectrum Technologies, Aurora, IL), GreenSeeker 505 (Trimble, Sunnyvale, Ca), and RapidSCAN CS-45 (Holland Scientific, Lincoln, Ne) platforms. The goal of this study was to determine the best sensing and application time for N in corn. Among the VIs tested, Normalized Difference Red-Edge (NDRE) (Barnes et al., 2000) was found to have the most accurate prediction of grain yield and N requirements compared to NDVI. The SPAD readings were found to have a high level of accuracy but lacked full-scale N predictive capabilities.

Near-term, handheld, and tractor based sensors were tested during a study by Samborski et al., (2009). A well-fertilized reference plot, a no N reference plot, and relative yield were used to mitigate factors other than N than caused results to be biased. Sensor improvements such as footprint, and band availability are needed in near-term sensing. Needed is an algorithm that would be applicable in various soil and weather scenarios.

A study conducted by Corti et al., (2019) utilized small unmanned aerial systems (sUAS) to sense N status in corn. The UAS used for this study was an octocopter equipped with a Global Navigation Satellite System (GNSS) NEO-M8 N and a Canon® Powershot SX260 HS (Melville,

New York) camera converted to a color infrared (CIR) camera. The VIs used in this study were NDVI, Green normalized difference vegetation index (GNDVI) (Gitelson, 2004), Blue normalized difference vegetation index (BNDVI) (Yang et al., 2007), and calculated ground cover (GC). The results indicated GNDVI as most accurate index from this study with a R^2 value of 0.7 and a root mean square error (RMSE) of less than 25 percent.

Cotton Sensing Methods

Raper et al., (2013) led a study in cotton utilizing Yara N Sensor (Yara International ASA, Oslo, Norway), GreenSeeker (GS) Model 505 Optical Sensor Unit (NTech Industries, Inc., Ukiah, CA) and Crop Circle (CC) Model ACS-210 (Holland Scientific, Inc., Lincoln, NE). Cotton leaf N status was not successfully predicted through sensing methods, yet NDVI showed a strong relationship with plant height. Needed is a vegetation index that is not strongly related to plant height to increase accuracy of N sensing. The different sensors within the study produced inconsistent canopy reflectance-based NDVI values.

Utilizing remote sensing to determine N status in cotton has become popular in recent years. In 2017, Ballester et al., (2017) performed a study to test N status sensing and lint yield prediction using sUAS. The sUAS platform used was a Dà-Jiāng Innovations (DJI) Inspire® (Shenzhen, China) equipped with a MicaSense RedEdge multispectral sensor. The VIs employed were NDVI, NDRE, Simplified Canopy Chlorophyll Content Index (SCCCI), the Transformed Chlorophyll Absorption Reflectance Index normalized by the optimized soil adjusted vegetation index (TCARI/OSAVI), and the visible-band indices Triangular Greenness Index (TGI) and Visible Atmospherically Resistant Index (VARI). The results concluded that SCCCI had the highest coefficient of determination, making it the most accurate VI tested.

Chen, (2019) conducted a similar study utilizing sUAS to predict N status in cotton. The sensing platform used was a quadcopter, 3DR Solo, equipped with a MicaSense RedEdge multispectral sensor. This study tested nine different VIs including NDVI, GNDVI, Modified Soil-adjusted Vegetation Index (MSAVI) (Qi et al., 1994), Optimized Soil-adjusted Vegetation Index (OSAVI) (Rondeaux et al., 1996), Enhanced Vegetation Index (EVI) (Huete et al. 1994), Triangular Vegetation Index (TVI) (Broge and Leblanc, 2001), Modified Triangular Vegetation Index 2 (MTVI2) (Haboudane et al., 2004), RVI, and NDRE. Including all VIs evaluated, RVI proved to have the highest accuracy for predicting N status.

Selected Study Vegetation Indices

Normalized Difference Vegetation Index

Normalized Difference Vegetation Index (NDVI) was derived by Dr. John Rouse of Texas A&M University in 1973 (Tu, 2002). The establishment of NDVI revolutionized the way remote sensing analyst detect live green plant canopies and is calculated by (Equation 2.1).

$$\left(NDVI = \frac{(R_{840} - R_{650})}{(R_{840} + R_{650})} \right) \quad (2.1)$$

(Rouse et al., 1973)

The NDVI index has become the most well known in agriculture. Along with detecting live green plant canopies, NDVI is also used to quantify photosynthetic capacity of plants. Shaver et al. (2011) found NDVI to be the most efficient vegetation index for estimating N content.

Normalized Difference Red Edge

Barnes et al. (2000) founded Normalized Difference Red Edge Index (NDRE) during a study to assess crop water stress, N status, and canopy density. While NDVI uses a combination of visual red and near-infrared (NIR) light, NDRE combines NIR and a transitional region between red and NIR known as red edge Equation number (Equation 2.2).

$$\left(NDRE = \frac{(R_{780} - R_{720})}{(R_{780} + R_{720})}\right) \quad (2.2)$$

(Barnes et al., 2000; Varco et al., 2013; Taipale, 2019)

Due to the substitution of Red edge for red light band, NDRE has the ability to penetrate further into the canopy for permanent or later stage crops. Rodriguez et al. (2006) found that NDRE, along with NDVI, was efficient at detection N stress.

Simplified Canopy Chlorophyll Content Index

Barnes et al. (2000) originally formulated the equation for Simplified Canopy Chlorophyll Content Index (SCCCI) followed up by further analysis by Varco et al., (2013). The SCCCI index is calculated by dividing NDVI into NDRE (Equation 2.3).

$$\left(SCCCI = \frac{NDRE}{NDVI}\right) \quad (2.3)$$

(Barnes et al., 2000; Varco et al., 2013; Raper and Varco, 2014)

Among all indices tested by Ballester et al. (2017), SCCCI had the highest coefficient of determination for determining N status in plants.

Early Nitrogen Detection Vegetation Index

Early Nitrogen Detection Vegetation Index [(ENDVI) Fox, 2015] is a N specific index calculated by Dr. Amelia Fox of Mississippi State University. The SCCCI index, proposed by Varco et al., (2013), is divided into a transformed green bandwidth (R550) shown in (Equation 2.4) and taken in the inverse. During Fox's research, ENDVI was theoretically derived from spectroradiometer sampling at 10 nm intervals from 350-940 nm.

$$\left(ENDVI = -\left(\frac{R550^{.003}}{SCCCI}\right)\right) \quad (2.4)$$

(Fox, 2015)

The goal of ENDVI was to provide additional means of estimating N levels in crops. During Fox's study, ENDVI performed similar to SCCCI proving a high level of accuracy. For clarification, Fox's ENDVI will be referred to as FENDVI for this research.

Green Normalized Difference Vegetation Index

Gitelson et al. (1996) discovered Green Normalized Difference Vegetation Index (GNDVI) by incorporating the green band into the NDVI and removing the red band (Equation 2.5).

$$\left(GNDVI = \frac{(R_{840} - R_{550})}{(R_{840} + R_{550})}\right) \quad (2.5)$$

(Gitelson et al., 1996)

The GNDVI index was found to be more sensitive to chlorophyll content than the NDVI. Schmidt et al. (2009) found GNDVI may be advantageous for calculating N content for construction of prescription N applications.

Enhanced Normalized Difference Vegetation Index

Enhanced Normalized Difference Vegetation Index (ENDVI) was defined by Bulanon et al. (2016) during a study on irrigation in agriculture using aerial systems. The equation for ENDVI consists of the near infrared (NIR) band, green band, and blue band (Equation 2.6).

$$\left(ENDVI = \frac{NIR + G - 2(B)}{NIR + G + 2(B)}\right) \quad (2.6)$$

(Bulanon et al., 2016)

Bulanon et al. (2016) found that ENDVI performed best among five vegetation indices. There is interest in comparing sensitivity equivalence values of ENDVI to SCCCI. For the sake of this research, Bulanon's ENDVI will be referred to as BENDVI.

Sensitivity Equivalent (SEq) Modeling

Viña and Gitelson (2005) linked vegetation index (VI) sensitivity to biophysical parameters during a 2005 study. Solari et al. (2008) developed an equation to calculate sensitivity equivalents (*SEq*) using slope of the linear regression of the ANOVA and root mean square error created by relating the VI to each biophysical parameter tested (Equation 2.7).

$$\left(SEq = \frac{slope}{RMSE}\right) \quad (2.7)$$

(Solari et al., 2008; Fox, 2015)

The *SEq* calculation is a vital tool to compare results amongst indices. Studies suggest that *SEq* may allow for an alternate measure of accuracy between VIs.

CHAPTER III

METHODS AND MATERIALS

Site Description

The statistical design for the on-farm study was a randomized complete block. The variable rate nitrogen (VRN) treatments were established on 24-row plots with a full fixed-rate as a control and two different VRN applications (from two different aircraft imaging missions) as treatments. Four replications of the three treatments were established on 9 ha (20 ac) plots. All plots in this study included the same statistical design, VRN treatments and replications.

2020 Corn

The 2020 corn crop was located in a production plot (-90.989750, 33.873667) in Rosedale, MS, USA. The mapped soil series for the 2020 corn plot were identified as 30% Dowling clay (Very-fine, smectitic, nonacid, thermic, Vertic Endoaquepts), 46% Dundee silty clay loam (Fine-silty, mixed, active, thermic Typic Endoaqualfs), 14% Dundee very fine sandy loam, and 10% Dundee-clack silt loam. During the 2019 growing season, the field was leveled and hipped. A 116-day Dekalb 66-94 corn hybrid was planted at a population of 84,014 seeds ha^{-1} (34,000 seeds ac^{-1}). The plot was furrow irrigated according to grower recommendation.

Figure 3.1 identifies the research sites.

Figure 3.1 Research locations in Mississippi and Louisiana

Locations are denoted by stars.

2020 Cotton

The first 2020 cotton research site was located in a field (-91.200889, 32.847611) in Lake Providence, LA, USA. The mapped soil series for the 2020 cotton plot were identified as 50% Bruin silt (loam coarse-silty, mixed, superactive, thermic, Oxyaquic Eutrudepts), 35% Newellton

complex (Clayey over loamy, smectitic over mixed, superactive, nonacid, thermic, Fluvaquentic Epiaquepts), 10% Tunica clay (Clayey over loamy, smectitic over mixed, superactive, nonacid, thermic, Vertic Epiaquepts), and 5% Commerce silt (Fine-silty, mixed, superactive, nonacid, thermic Fluvaquentic Endoaquepts). An 8.1 ha (20 ac) plot area was situated in the northern end of a 16.2 ha (40 ac) field. Upon completion of the 2019 corn harvest, the stalks were shredded, and the field was hipper-rolled (hipped and rolled with a combination implement). After hipper-rolling, a cover crop of cereal rye (*Secale cereale*), black oats (*Avena strigose*), crimson clover (*Trifolium incarnatum*), and hairy vetch (*Vicia villosa*) was planted. During the spring of 2020, the cover crop was terminated before planting. A mid to full maturity Deltapine 1646 B2XF was planted at a rate of 103,530 seeds ha^{-1} (41,898 seeds ac^{-1}). An overhead pivot irrigated the plot in accordance with grower recommendation.

The second plot for the 2020 cotton crop was in a field (-91.200972, 32.833028) in Lake Providence, LA, USA. The mapped soil series for the 2020 cotton location were identified as 60% Bruin silt loam (Coarse-silty, mixed, superactive, thermic, Oxyaquic Eutrudepts) and 40% Newellton-Tunica complex (Clayey over loamy, smectitic over mixed, superactive, nonacid, thermic, Fluvaquentic Epiaquepts). The 8.1 ha (20 ac) study plot was located in the southern portion of a 48.6 ha (120 ac) field. After the 2019 cotton crop was harvested, the stalks were shredded, and a cover crop was planted consisting of cereal rye, black oats, crimson clover, and hairy vetch. During the spring of 2020, the cover crop was terminated, harrowed, and hipped to prepare for planting. A mid-maturity Phytogen 440W3FE was planted at 103,660 seeds ha^{-1} (41,950 seeds ac^{-1}). The plot was furrow irrigated with poly pipe according to grower recommendation.

2021 Corn

The 2021 Corn research plot was grown in a field (-91.200889, 32.847611) in Lake Providence, LA, USA. The mapped soil series for the 2021 corn plot were identified as 50% Bruin silt loam (Coarse-silty, mixed, superactive, thermic, Oxyaquic Eutrudepts), 35% Newellton complex (Clayey over loamy, smectitic over mixed, superactive, nonacid, thermic, Fluvaquentic Epiaquepts), and 10% Tunica clay (Clayey over loamy, smectitic over mixed, superactive, nonacid, thermic, Vertic Epiaquepts). An 8.1 ha (20 ac) plot area was situated in the northern end of a 16.2 ha (40 ac) field. Upon harvest of the 2020 cotton crop, the stalks were shredded, and a cover crop of black oat, cereal rye, and Austrian winter pea were planted. During the spring of 2020, the cover crop was terminated, harrowed, and hipped to prepare for planting. A 116-day Syngenta NK1677 corn hybrid was planted at 78,686 seeds ha^{-1} (31,843 seeds ac^{-1}). The plot was irrigated with an overhead pivot in accordance with grower recommendation.

2021 Cotton

The 2021 Cotton research plot was located in a field in Lake Providence (-91.200503, 32.845759), LA, USA. An 8.1 ha (20 ac) plot was located in the north end of a 31.5 ha (78 ac) field. The mapped soil series for the 2021 cotton plot consisted of 26% Bruin silt loam (Coarse-silty, mixed, superactive, thermic, Oxyaquic Eutrudepts), 71% Commerce silt loam (Fine-silty, mixed, superactive, nonacid, thermic Fluvaquentic Endoaquepts), and 3% Newellton-Tunica complex (Clayey over loamy, smectitic over mixed, superactive, nonacid, thermic, Fluvaquentic Epiaquepts). A mid-maturity DeltaPine 20r734 cotton variety was planted at 103,455 seeds ha^{-1} (41,868 seeds ac^{-1}). The plot was furrow irrigated with poly pipe according to grower recommendation.

Sampling and Nitrogen Treatments

Soil Sampling

Prior to planting, soil sample cores were taken in each plot at 0-15 cm (1-6 in) on a 1 ha (2.5 ac) grid. Soil samples were sent to Waypoint Analytical (Ridgeland, MS) for S3M package testing which includes pH, buffer pH, P, K, Mg, Ca, OM, CEC, percent cation saturation, B, S, Fe, Mn, Cu, Zn, and Na. Separate soil sample cores were taken at 0-30 cm (1-12 in) on a 1 ha (2.5 ac) grid, and sent to Waypoint Analytical for extractable N testing which includes NO_3^- and NH_4^+. The resulting available soil N map was derived through IDW (Inverse Distance Weighting) interpolation, thus aiding in establishing the difference between optimal crop performance occurring from the variable rate N application and residual soil N resources.

Starter Nitrogen Applications

At corn planting during the 2020 growing season, an initial application of 45 kg ha^{-1} (40 lb ac^{-1}) of N was applied using urea (46-0-0). When the corn was at the V1 stage, a second application of 53.8 kg ha^{-1} (48 lb ac^{-1}) of N was knifed in using a blend of diammonium phosphate (DAP) (18-46-0) and urea. A third fertilizer N application was a prescribed variable rate of liquid UAN 32% (32-0-0) calculated by sUAS sensing data with a low of 114 kg ha^{-1} (102 lb ac^{-1}) of fertilizer N to a high of 170 kg ha^{-1} (152 lb ac^{-1}) of N. The final application was a tassel shot of DAP applied by airplane at 45 kg ha^{-1} (40 lb ac^{-1}) of N. The method used for unit conversion was lb ac^{-1} multiplied by 1.121 resulted in kg ha^{-1}.

Multiple sources of N were used in this study based on grower recommendations. Varying cost of fertilizer sources were noted as the primary reason for multiple sources across applications. Soil fertility needs were also a consideration when choosing fertilizer N sources. Sources other than UAN 32% can fulfill multiple nutrient needs.

The 2021 corn crop received an initial application of DAP at 34 kg ha^{-1} (30 lb ac^{-1}) of N after planting. A second application of liquid UAN 32% was applied at 135 kg ha^{-1} (120 lb ac^{-1}) of N. When the corn was at V8 stage, a prescribed variable rate of liquid UAN 32% was applied with a low of 79 kg ha^{-1} (70 lb ac^{-1}) of fertilizer N and a high of 135 kg ha^{-1} (120 lb ac^{-1}) of fertilizer N. A tassel shot was not applied for the 2021 corn crop.

Following cotton planting in 2020, an initial application of 90 kg ha^{-1} (80 lb ac^{-1}) of N was spread using a blend of DAP and Urea. The final application of N was a prescribed rate of liquid UAN 32% (32-0-0) based on sUAS sensing data. The 2021 cotton crop received the same N rates and applications (Table 3.2).

Table 3.2 Timeline detailing research methods

Year 1-2020	Year 2 - 2021	Activity
March 26	March 5	• Extract soil samples pre plant for available soil N and calculate a residual soil N map. MSST extraction for total soil N. • Waypoint Analytical for analysis.
April 17 (corn) May 28 (cotton plot 1) May 11 (cotton plot 2)	March 13 (corn) May 16 (cotton)	• Plant and apply half rate N; 38in row 12 row planter; UAN®-32 (32-0-0); Max rate = 110-120 lb N/ac cotton and 240 - 280 lb N/ac corn depending on soil type.
June 6 (V6)	May 1 (V8)	• Collect Corn leaf N tissue samples and ship to Waypoint Analytical. Fly sUAS missions with MicaSense® (Seattle, WA) and calculate VRN sidedress; 400 ft above ground level Quad-copter at 20mph. (Additional Quad-copter flights at 10, 15 and 25mph for measuring *SEq* of VIs for 2020 season; no fixed-wing for 2020.)
June 8	May 8	• Corn VRN application.

Table 3.2 (continued)

Year 1-2020	Year 2 - 2021	Activity
July 11	July 28	• Collect Cotton leaf tissue N samples and deliver to Waypoint Analytical; Fly sUAS missions with MicaSense® (Seattle, WA) and calculate VRN sidedress; 400 ft above ground level Quad-copter at 20 mph. Additional Quad-copter flights at 10, 15 and 25mph for measuring *SEq* of VIs.
July 15	June 20	• Cotton VRN application
September 9	August 28	• Harvest Corn and relate yield to VRN prescription (corn harvester = 8-row).
October 17	October 23	• Harvest Cotton and relate yield to VRN prescription (cotton picker = 6-row).
Post-Harvest	Post-Harvest	• Calculate available N (residual soil N + VRN prescription) and relate to yield; SAS 9.4 analysis using LSD ($\alpha = 0.5$) PROC GLM.
---	December	• Disseminate Results

Sensing Missions, VRN Treatments, and Leaf N% Sampling

At early corn and cotton growth stages (V4-V8 and pinhead square, respectively) sUAS missions were flown at 121m (400 ft) above ground level with MicaSense RedEdge® (Seattle, WA) sensor technology. A quad-copter mission flown at 32 km h^{-1} (20 mi h^{-1}) was used for calculating the VRN application map.

Upon completion of flight missions, leaf tissue samples (corn most matured collard leaf, cotton first matured leaf) were shipped to Waypoint Analytical. Leaf samples allowed for relating of leaf N concentration to the VRN map and validation of imaging efficiency. Imaged datasets from all missions were processed and calibrated with a SCCCI (Fox, 2015) to estimate sensed canopy leaf N percentage. Optimal sensing method was described through a comparison

of calibrated imagery to actual, sampled corn canopy leaf N percentage. Within 24 hours after the sensing missions, MicaSense imagery datasets from the conventional quad-copter flights were used to calculate the variable rate N sidedress prescription. VariRite™ (Mississippi State University, MS) geospatial technology was used to generate the prescription N maps. VariRite is a proprietary copyrighted remote sensing algorithm used to estimate crop canopy N both off nadir and on nadir at distances of 4.6 – 121 m (15-400 ft), respectively. To estimate crop canopy N status and create a final, relational side-dress VRN prescription map, crop reflectance was sampled at some critical stage that best exemplifies future crop fertilizer N requirements. Resultant imagery outputs, created in Pix4D Mapper® (Prilly, Switzerland) and converted to VIs, are used to calibrate the remainder N fertilizer rate for the season, which equals the total maximum rate (or 'producer's preferred maximum rate'). The crop remainder fertilizer N balance was estimated by linearly stretching VI values from low to high over a normally distributed fertilizer N rate. The VRN rate map was calculated in gallons UAN 32% using ArcGIS Desktop software, after which maps were delivered to the equipment operator for application in WGS84 projection format.

Harvest and Aircraft Data Analysis

Harvest Data Analysis

Harvested yield data was collected in digital format for relating yield to VRN prescription. The yield data aided in determining the efficacy of the VRN mapping operations from unmanned systems. Yield data was compared to available N calculation (residual soil N + VRN prescription) to find the full N amount used throughout the growing season.
The unit bu ac^{-1} was multiplied by 0.0673 to achieve yield in Mt ha^{-1}.

Measuring Aircraft Efficiency

The quad-copter platform used during year one (2020) was a 650 commercial class copter with a 10,000 mAh 4S battery capable of 15 minutes sustained flight custom designed by Dennis Lott (UASSolutions, Clinton, MS). A MicaSense RedEdge sensor was employed for the missions. The quad-copter platform has the capability to fly approximately 40 ha h^{-1} (100 ac h^{-1}). Quad-copter missions [flown at 16 km h^{-1} (10 mi h^{-1}), 24 km h^{-1} (15 mi h^{-1}), 32 km h^{-1} (20 mi h^{-1}), 40 km h^{-1} (25 mi h^{-1})] were used to determine flight data accuracy at multiple speeds.

Year two (2021) of this study included flight missions with the quad-copter from the year one, and a fixed-wing platform. The fixed-wing platform was a custom-built Anaconda designed by Kevin Garland at KG Aviation (Oro Valley, AZ). A MicaSense RedEdge was employed aboard the Anaconda for data collection. The quad-copter was flown at 32 km h^{-1} (20 mi h^{-1}), and the Anaconda was flown at 64.37 km^{-1} (40 mi h^{-1}). Sensitivity Equivalents were calculated for each VI at both speeds.

Quad-copter flight in Rosedale, MS (Figure 3.2).

Figure 3.2 Parker flying quad-copter at Rosedale, MS research plot

Statistical Analysis of Data Sets

The statistical analysis of the data sets was performed in SAS® ver 9.4 (SAS Institute, Cary, NC). The analysis employed statistical classification methods to relate the factors to the outcomes for comparison of data returns. Statistical methods found if there are outliers that exist and determine data fitness. The commands "PROC REG" and "PROC GPLOT" in SAS coupled with r^2 modeling in Microsoft Excel (Microsoft Inc., Redmond, WA) were used to identify outliers within the leaf N point data.

Descriptive statistics were used to describe the different flight speeds. A linear regression coupled with Wald approximation was conducted in R® Statistical Software (R Foundation for Statistical Computing, Vienna, Austria) to determine the effect of speed on VI value. The command "PROC REG" in SAS was used to run a linear regression to determine the sensitivity

equivalents (*SEq*) for all VIs (Table 3.3). Calculations were performed by dividing the slope of the equation by the corresponding root-mean-square-error (Raper and Varco, 2014; Solari et al., 2008; Vina and Gitelson, 2005). When predominant or prevalent VIs were noted from the *SEq* analysis, means separation to determine statistically significant differences between the VIs was conducted using Tukey's studentized range test.

The PROC REG diagnostics tests (DFFITS and DFBetas) were employed to locate influential datasets when relating leaf N to the VIs. Yield was modeled in Microsoft Excel for comparison to both variable and fixed N rates. Yield means, as they relate to categorized VRN prescription rates, were separated using LSD Means protocol in SAS PROC GLM.

Table 3.3 details the vegetation indices used in this study.

Table 3.3 Vegetation indices employed in this study

Acronym	Name	Algorithm	Reference
NDVI	Normalized Difference Vegetation Index	$\left(NDVI = \frac{(R_{840} - R_{650})}{(R_{840} + R_{650})}\right)$	(Rouse et al., 1973)
NDRE	Normalized Difference Red Edge Index	$\left(NDRE = \frac{(R_{780} - R_{720})}{(R_{780} + R_{720})}\right)$	(Barnes et al., 2000; Varco et al., 2013; Taipale, 2019)
SCCCI	Simplified Canopy Chlorophyll Content Index	$\left(SCCCI = \frac{NDRE}{NDVI}\right)$	(Barnes et al., 2000; Varco et al., 2013; Raper and Varco, 2014)
FENDVI	Early Nitrogen Detection Vegetation Index	$\left(FENDVI = -\left(\frac{R550^{.003}}{SCCCI}\right)\right)$	(Fox, 2015)
GNDVI	Green Normalized Difference Vegetation Index	$\left(GNDVI = \frac{(R_{840} - R_{550})}{(R_{840} + R_{550})}\right)$	(Gitelson et al., 1996)
BENDVI	Enhanced Normalized Difference Vegetation Index	$\left(BENDVI = \frac{NIR + G - 2(B)}{NIR + G + 2(B)}\right)$	(Bulanon et al. 2016)

CHAPTER IV

RESULTS

Climate in Rosedale, MS

2020 Corn Crop

Average weekly temperature and rainfall for the 2020 corn plot was gathered from the USDA-NASS Cleveland, MS station (Table 4.1). The temperature during the growing season was slightly lower than normal during the beginning but increased toward the end of the season. Rainfall was recorded as sporadic with a high amount during the second half of the growing season. Ultimately, the crop was damaged by the high winds and heavy rainfall during the month of August.

Table 4.1 details the weekly average temperatures and precipitation in Cleveland, MS during 2020.

Table 4.1 Weekly average temperature and precipitation for the 2020 corn crop near Cleveland, MS

Temperature, °C			Precipitation, mm	
Period	Weekly Average	DFN	Weekly Average	DFN
April	12.5	-1.0	58.58	31.25
May	22.4	0.1	1.05	-34.62
June	25.5	-1.6	92.56	62.58
July	28.6	1.4	28.59	15.78
August	28.2	1.1	36.84	16.53
September	23.9	-1.2	88.12	64.32
October	20.4	3.5	58.17	32.52
Totals	23.1	0.3	51.98	26.91

Source: USDA-NASS-MS Crop Progress and Condition Report.
DFN=Departure from normal based on 1981-2010 average

Climate in Lake Providence, LA

2020 Cotton Crop

Weather conditions for the 2020 Cotton Plots in Lake Providence, LA were obtained from the USDA-NASS Eudora, AR reporting location (Table 4.2). The season began with dryer than normal conditions that resulted in a slow start for the plots. As the season progressed, the precipitation increased with a greater amount of rainfall in the month of September. The temperatures were slightly lower than normal for the duration of the growing season.

Table 4.2 details the weekly average temperatures and precipitation in Eudora, AR during 2020.

Table 4.2 Weekly average temperature and precipitation for the 2020 cotton crop near Eudora, AR

Temperature, °C			Precipitation, mm	
Period	Weekly Average	DFN	Weekly Average	DFN
April	17.5	-3.0	17.87	8.01
May	21.7	-2.9	33.44	-16.58
June	25.8	-2.1	98.96	75.89
July	29.4	1.5	3.58	-10.22
August	27.9	0.6	26.41	7.620
September	23.9	-0.4	90.58	65.62
October	19.1	4.9	5.78	-9.85
Totals	23.6	-0.2	39.52	17.21

Source: USDA-NASS-MS Crop Progress and Condition Report.
DFN=Departure from normal based on 1981-2010 average

2021 Cotton and Corn Crop

Weather conditions for the 2021 Cotton and Corn crops located in Lake Providence, LA were gathered from the USDA-NASS Eudora, AR reporting location (Table 4.3). The Pine Bluff and Crossett, AR sites were used when the Eudora, AR location was unavailable. The Eudora location data was unavailable from June through October.

Table 4.3 details the weekly average temperatures and precipitation in Eudora, AR during 2021.

Table 4.3 Weekly average temperature and precipitation for the 2021 corn and cotton crop near Eudora, AR

Temperature, °C			Precipitation, mm	
Period	Weekly Average	DFN	Weekly Average	DFN
April	10.3	-6.0	28.78	4.58
May	19.5	-4.5	28.75	1.87
June	24.3	-3.1	55.49	41.32
July	27.3	-1.3	14.78	-4.54
August	29.1	3.0	7.24	-7.58
September	22.5	-2.6	8.25	-12.68
October	20.0	3.0	1.02	-23.25
Totals	21.8	-1.6	20.61	-0.04

Source: USDA-NASS-MS Crop Progress and Condition Report.
DFN=Departure from normal based on 1981-2010 average

Residual Soil N

2020 Corn Crop

Residual Soil N levels for the 2020 corn crop were mapped prior to planting using ArcGIS Desktop 10.8.1® software (Esri, Redlands CA) Geostatistical Analyst Inverse Distance Weighted interpolation. Soil N levels ranged from 59 to 83 kg ha^{-1} with high concentration existing primarily in the northeast and southwest corners of the field (Figure 4.1). The northwest and southeast corners show very low residual N likely due to both corners being low elevation.

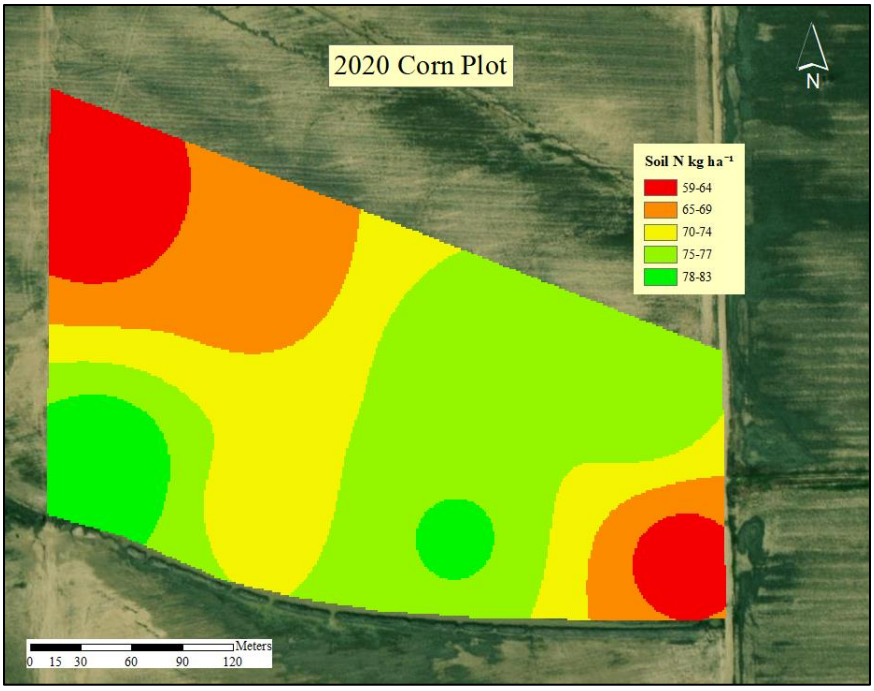

Figure 4.1 Soil N variability 2020 corn plot prior to planting

Total area: 8.1 ha (20 ac)

2020 Cotton Crop

Residual Soil N levels for the 2020 cotton crop were mapped prior to planting using ArcGIS Desktop 10.8.1® Geostatistical Analyst Inverse Distance Weighted interpolation (Figure 4.2). Soil N levels in the north plot ranged from 65 to 121 kg ha^{-1} with primarily high concentration along the southeast edge. The low N levels depicted in red at the far northwest corner was an area of low elevation in the plot.

Figure 4.2 Soil N variability in 2020 cotton plot north prior to planting

Total area: 8.1 ha (20 ac)

Residual Soil N levels for the 2020 south cotton plot ranged from 74 to 109 kg ha^{-1} (Figure 4.3). The majority of the plot consisted of low to mid-range N levels with two distinct low N areas. A drainage ditch runs through the red areas where low N levels were detected.

Figure 4.3 Soil N variability in 2020 cotton plot south prior to planting

Total area: 8.1 ha (20 ac)

2021 Corn Plot

ArcGIS Desktop 10.8.1® Geostatistical Analyst Inverse Distance Weighted interpolation was employed to map the Residual Soil N levels prior to planting for the 2021 corn crop (Figure 4.4). Soil N levels ranged from 69 to 116 kg ha^{-1} across the plot. The low N level areas of the field were consistent with last year's results prior to planting the plot. The red area in the northwest end continues to be a low elevation area that results in decreased residual N.

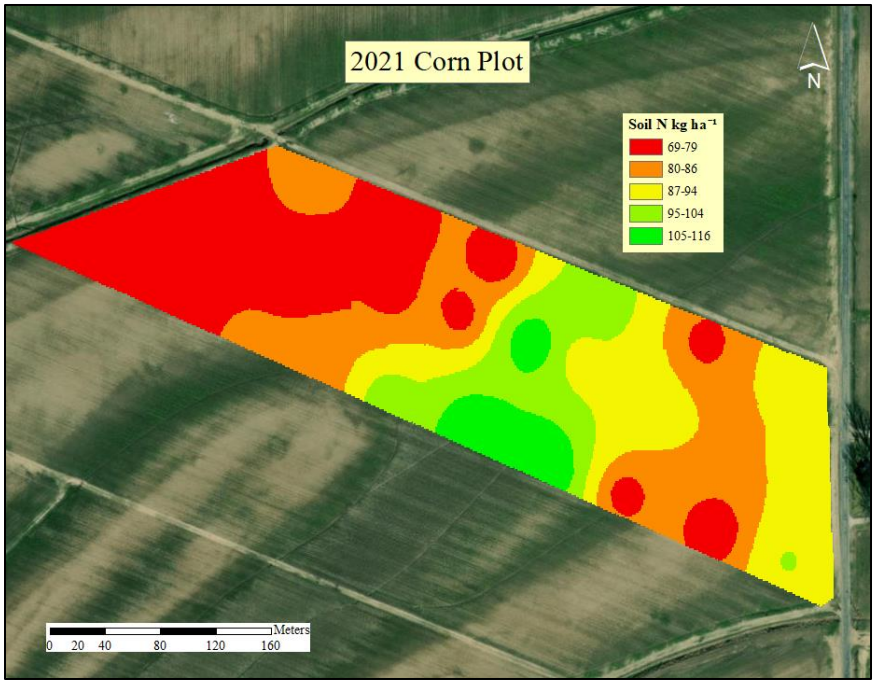

Figure 4.4 Soil N variability in 2021 corn plot prior to planting

Total area: 8.1 ha (20 ac)

2021 Cotton Plot

ArcGIS Desktop 10.8.1® Geostatistical Analyst Inverse Distance Weighted interpolation was employed to map the Residual Soil N levels prior to planting for the 2021 cotton crop (Figure 4.5). Soil N levels ranged from 69 to 107 kg ha^{-1} across the plot. Mid to low residual N levels persisted across the plot with few areas of extreme lows. The red area in the east section of the field falls along the irrigation pipeline, while the other red area lies in the low elevation area of the plot.

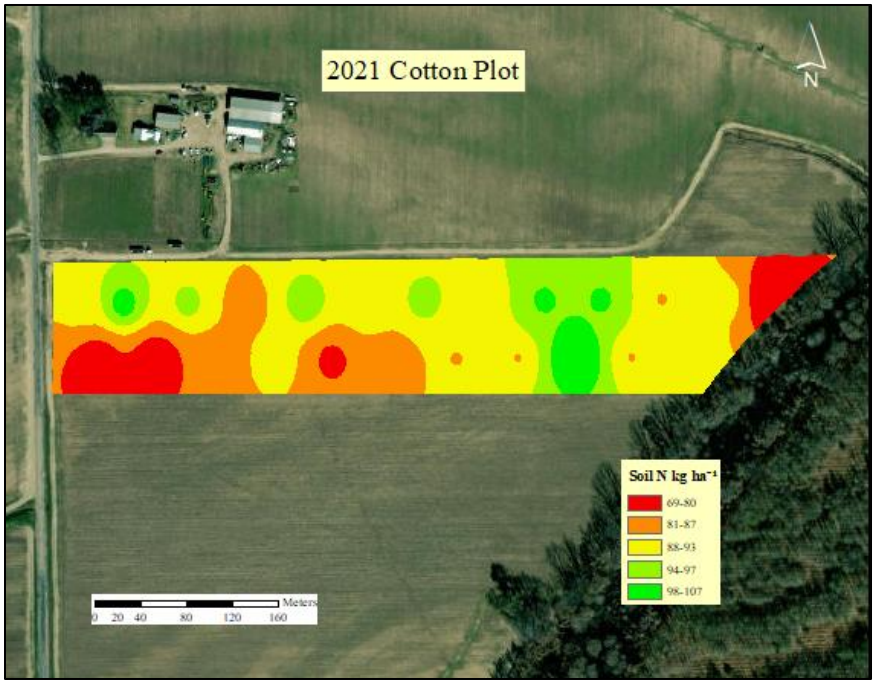

Figure 4.5 Soil N variability in 2021 cotton plot prior to planting

Total area: 8.1 ha (20 ac)

Crop Canopy Data Processing

2020 Growing Season

During the year 2020, eight sampling locations were used for soil sampling, leaf sampling, and VI comparison and analysis. Using these few locations limited the ability to cull out poor data points. For example, sample location five shown below was a known low area of the plot, yet the point could not be omitted due to the small number of available locations (Figure 4.6). The poorly performing data point was also verified with r^2 modeling in Microsoft Excel. Despite locating the single outlier, it was required to be included in the 2020 data. To reduce error, additional sampling points were added to the 2021 research studies.

Figure 4.6 2020 cotton plot north sampling locations

Total area: 8.1 ha (20 ac)

2021 Growing Season

Modeling selected sampling points was improved by adding additional sampling sites to the 2020 study. Sample population adjustments were made to include 24 total sampling points for the 2021 growing season. The increased sample size allowed for determination of outliers and removing them accordingly. Outliers were determined by analyzing the plot from an arial view and hypothesizing which points may be suspect. The primary areas that suspect points may arise are sample points in low elevation, drainage ditches, and along the edge of the plot. Figure 4.7 details the sampling point scheme and where they fall in the field in relation to field topographic features. Sample eleven, which was located in the low end of the plot, was noted among possible outliers, and is circled below (Figure 4.7).

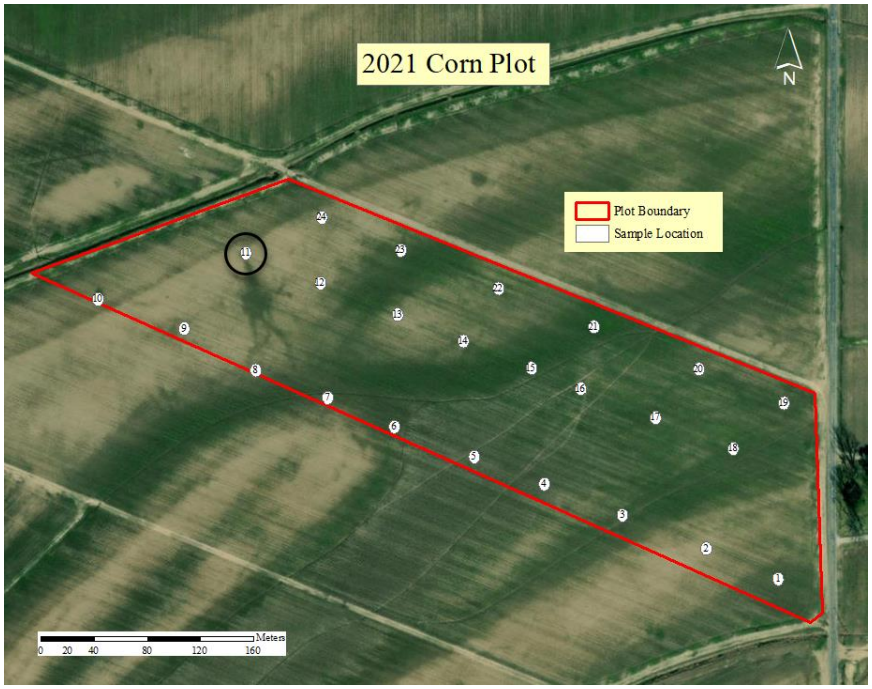

Figure 4.7 2021 corn plot sampling locations

Total area: 8.1 ha (20 ac)

After suspected outliers were identified, r^2 modeling was performed to further examine the points in question. Leaf N and SPAD were graphed against all VIs to determine if outliers were consistent among all VIs. The SCCCI was the standard measure against all other VIs. Clearly defined outliers in the chart below were consistent with anomalies in the field described previously. Sample point eleven proved to be an outlier in excel graphing as well. Once the outliers were consistent amongst both aerial view and Microsoft excel chart, SAS software was employed (Figure 4.8).

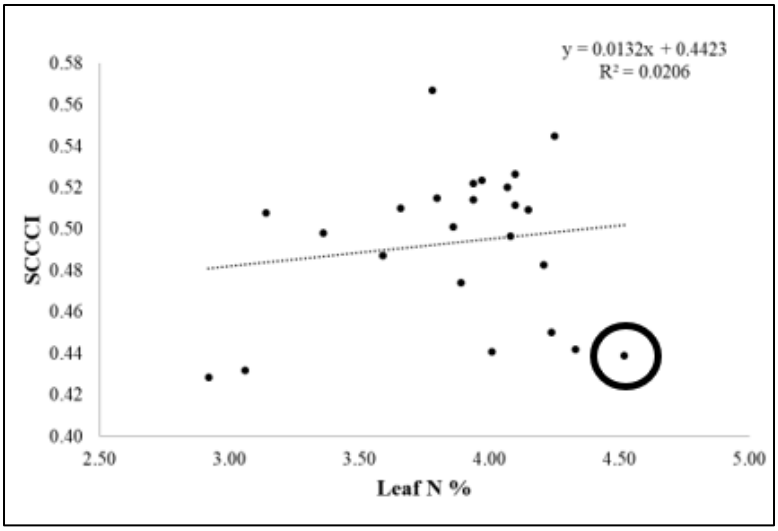

Figure 4.8 2021 corn plot SCCCI graphed against leaf N data in Microsoft Excel Sample point 11 is circled in black

Statistical DFBetas tests were run on all sample points to determine if outliers were consistent with the previous outlier selection methods. DFBetas measure the influence of each individual point on the entire dataset. If a DFBetas has a high value, then that value is a very influential point within the dataset (Mukherjee et al., 1998). High DFBetas values can skew data and create undue influence toward an outlier. Any value above two (2.0) is typically rejected in DFBetas testing, but the selective number should be adjusted based on sample size. The initial limit placed on the dataset was no greater than 0.6. Sample number 11 fell outside of the acceptable range, thus, sample 11 being identified as an outlier. Additional samples were removed based on a combination of aerial image analysis, r^2 modeling, and SAS DFBetas analysis (Table B.9).

Crop Canopy Sensing to Detect Early N Status

Results from crop canopy sensing missions, conducted between 2020-21 in corn and cotton, are discussed in relationship to flight speed trials, biophysical parameters relating crop

canopy N status to imagery outputs, and the fitting of vegetation indices (VIs) to sensitivity equivalents (*SEq*s). Data are presented in tabular format detailing the statistical outcomes that comprise the resulting quotient (linear regression slope divided by the root mean square error) from relating a biophysical parameter to extracted imagery VIs. It is worth noting the canopy sensing missions featured both corn (erectophile) and cotton (planophile) canopy types. Variations in canopy reflectance across many other crops may be strategically related to the data discussed herein.

Because of the unique nature of weather and technical events affecting mission quality during each year of this study, data will be presented by year instead of by crop. The crop canopy section concludes with a synopsis of the general findings and assumptions.

Speed Effects on VIs

Until this study, no research was found that tested speed effects on imagery outcomes while holding a constant altitude and shutter speed utilizing sUAS. The altitude was held constant at 121.9 m (400 ft) due to conventional and efficient sUAS standard operating procedures. Additionally, an altitude of 121.9 m produced a resolution of 8 cm pixel^{-1}. The shutter speed was held constant in order to reproduce the time constraints that would be present during the mission for farmers and farm service providers. Moreover, the shutter speed adjustment would increase processing time, thus, delaying data delivery to the N applicator. A possible explanation for a decrease in SCCCI value with increased speeds may be due to sampling error due to imperfect data in need of georeferencing. Sun angle may also provide explanation as to why SCCCI value decreased as speed increased. During each mission, the fixed-wing flight was performed before the quad-copter flight, thus, experiencing a different sun

angle. A different sun angle results in less brightness of soil albedo which may affect SCCCI value.

Linear regression models were performed in R software to determine the effect that speed has on VIs. The first test conducted was to determine the linear regression model of SCCCI as a function of leaf N (Figure 4.9).

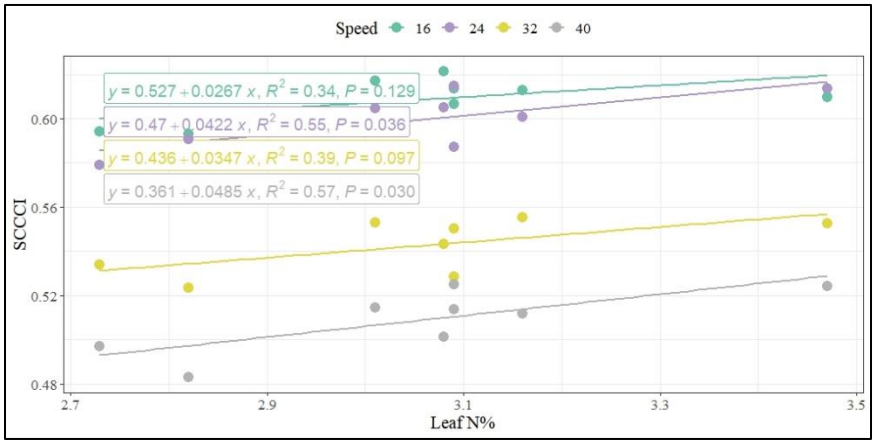

Figure 4.9 SCCCI as function of leaf N in 2020 corn plot.

Sensed at 16, 24, 32 and 40 km hr^{-1} at V6 growth stage. Different colors represent different speeds

Figure 4.9 depicts how SCCCI values reduced as speeds increased. There is a positive correlation between SCCCI and leaf N. Effects of leaf N on SCCCI were significant and positive only at 24 and 40 km h^{-1} speeds.

Table 4.4 details the regression analysis results for the 2020 corn crop. Analysis results were shown for all VIs regardless of significance. However, for the remainder of VI vs. speed and VI vs. platform analyses, only statistically significant results were included.

Table 4.4 Regression analysis output of leaf N and six different vegetation indices (VI) for 2020 corn plot.

	Leaf N, %			
VI/Speed	16	24	32	40
NDVI	y = 0.269 + 0.0341x; R^2 = 0.03; P = 0.664	y = 0.218 + 0.0498x; R^2 = 0.07; P = 0.513	y = 0.259 + 0.0458x; R^2 = 0.05; P = 0.613	y = 0.188 + 0.0476x; R^2 = 0.05; P = 0.588
GNDVI	y = 0.385 + 0.0323x; R^2 = 0.06; P = 0.546	y = 0.31 + 0.531x; R^2 = 0.16; P = 0.329	y = 0.355 + 0.044x; R^2 = 0.12; P = 0.406	y = 0.009 + 0.0204x; R^2 = 0.04; P = 0.637
NDRE	y = 0.133 + 0.0309x; R^2 = 0.08; P = 0.504	y = 0.080 + 0.0462x; R^2 = 0.17; P = 0.306	y = 0.0976 + 0.039x; R^2 = 0.10; P = 0.437	y = 0.0461 + 0.0405x; R^2 = 0.12; P = 0.401
SCCCI	y = 0.527 + 0.0267x; R^2 = 0.34; P = 0.129	y = 0.47 + 0.0422x; **R^2 = 0.55; P = 0.03**	y = 0.436 + 0.0347x; R^2 = 0.39; P = 0.097	y = 0.361 + 0.0485x; **R^2 = 0.57; P = 0.03**
FENDVI	y = 0.55 + 0.0256x; R^2 = 0.30; P = 0.158	y = 0.51 + 0.0368x; R^2 = 0.38; P = 0.103	y = 0.478 + 0.0249x; R^2 = 0.23; P = 0.232	y = 0.357 + 0.0543x; **R^2 = 0.52; P = 0.043**
BENDVI	y = 0.451 + 0.0232x; R^2 = 0.04; P = 0.652	y = 0.43 - 0.0414x; R^2 = 0.21; P = 0.257	y = 0.3 - 0.0111x; R^2 = 0.01; P = 0.788	y = 0.353 - 0.0199x; R^2 = 0.13; P = 0.388

Sensed at different speeds (16, 24, 32, and 40 km h^{-1}) at V6 growth stage

The regression analysis depicted in Table 4.4 suggests that SCCCI and FENDVI have the highest coefficient of determination when modeled with LN percentage at speeds of 24 km h^{-1} and 40 km h^{-1} speeds. Moreover, the p-value of both SCCCI and FENDVI at the aforementioned speeds were below 0.05, thus, indicating that they are statistically significant.

Figure 4.10 depicts SCCCI and FENDVI as a function of SPAD across all speeds for the 2020 corn crop.

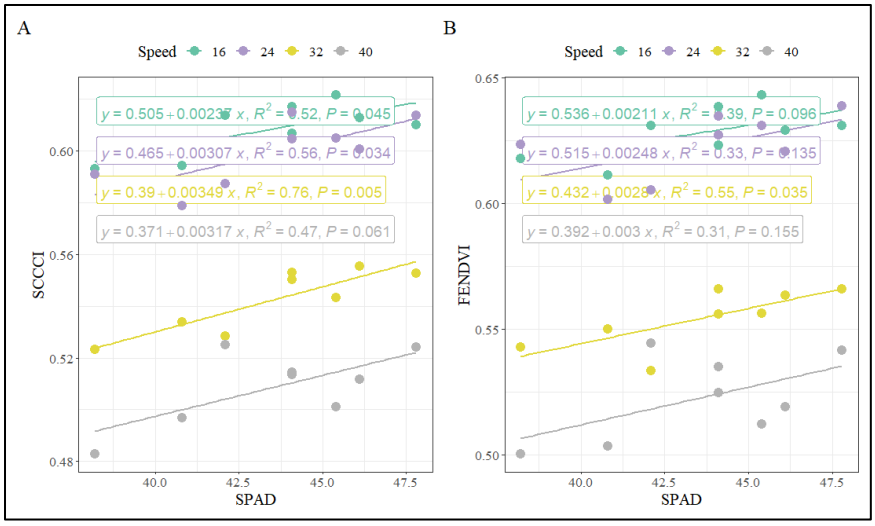

Figure 4.10 SCCCI (A) and FENDVI (B) as function of SPAD in the 2020 corn plot. Sensed at 16, 24, 32 and 40 km hr^{-1} at V6 growth stage. Different colors represent different speeds

According to Figure 4.10, SCCCI and FENDVI values reduced as speed increased. The relationship between SPAD and SCCCI was significant and positive at 16 km h^{-1}, 24 km h^{-1} and 32 km h^{-1}. The relationship between SPAD and FENDVI was significant and positive at the 32 km h^{-1} speed.

Results for the 2020 cotton plot north are not depicted due to neither LN nor SPAD significantly relating to VIs at all speeds. Table 4.5 depicts the regression analysis output of SPAD and six different VIs in the 2020 cotton crop south field.

Table 4.5 Regression analysis showing strength of relationship between SPAD readings and six different VIs in the 2020 cotton plot south

	SPAD			
VI/Speed	16	24	32	40
NDVI	y = 0.892 + 0.0001x; **R^2 = 0.51; P = 0.046**	y = 0.983 - 0.001x; R^2 = 0.11; P = 0.430	y = 0.716 + 0.004x; **R^2 = 0.63; P = 0.019**	y = 0.812 + 0.0024x; **R^2 = 0.54; P = 0.037**
GNDVI	y = 0.778 + 0.002x; **R^2 = 0.51; P = 0.048**	y = 0.934 - 0.000x; R^2 = 0.01; P = 0.954	y = 0.579 + 0.004x; **R^2 = 0.57; P = 0.030**	y = 0.656 + 0.0038x; **R^2 = 0.61; P = 0.022**
NDRE	y = 0.528 + 0.0035x; R^2 = 0.45; P = 0.069	y = 0.761 - 0.0026x; R^2 = 0.04; P = 0.652	y = 0.166 + 0.0078x; **R^2 = 0.62; P = 0.652**	y = 0.334 + 0.00052x; **R^2 = 0.62; P = 0.020**
SCCCI	y = 0.598 + 0.0026x; R^2 = 0.41; P = 0.088	y = 0.777 - 0.0020x; R^2 = 0.03 P = 0.702	y = 0.297 + 0.00603x; **R^2 = 0.58; P = 0.027**	y = 0.433 + 0.0041x; **R^2 = 0.63; P = 0.013**
FENDVI	y = 0.594 + 0.0267x; R^2 = 0.41; P = 0.086	y = 1.27 + 0.00397x; R^2 = 0.02; P = 0.710	y = 0.295 + 0.00597x; **R^2 = 0.59; P = 0.026**	y = 0.431 + 0.00407x; **R^2 = 0.63; P = 0.018**
BENDVI	y = 0.292 + 0.0279x; R^2 = 0.46; P = 0.063	y = 0.3 + 0.0552x; R^2 = 0.04; P = 0.641	y = 0.0726 - 0.0143x; R^2 = 0.10; P = 0.449	y = 0.183 - 0.0135x; **R^2 = 0.53; P = 0.042**

Sensed at four different speeds (16, 24, 32, and 40 km h^{-1}) for cotton crop – south field in 2020.

Interpretation of results shown in Table 4.5, SCCCI, FENDVI, and NDRE modeled with SPAD consistently achieved a high coefficient of determination at a speed of 32 km hr^{-1}. The p-value of SCCCI and FENDVI modeled with SPAD remained under 0.05 at a speed of 32 km hr^{-1}.

Figure 4.11 depicts SCCCI and FENDVI as a function of SPAD for the 2020 cotton plot south.

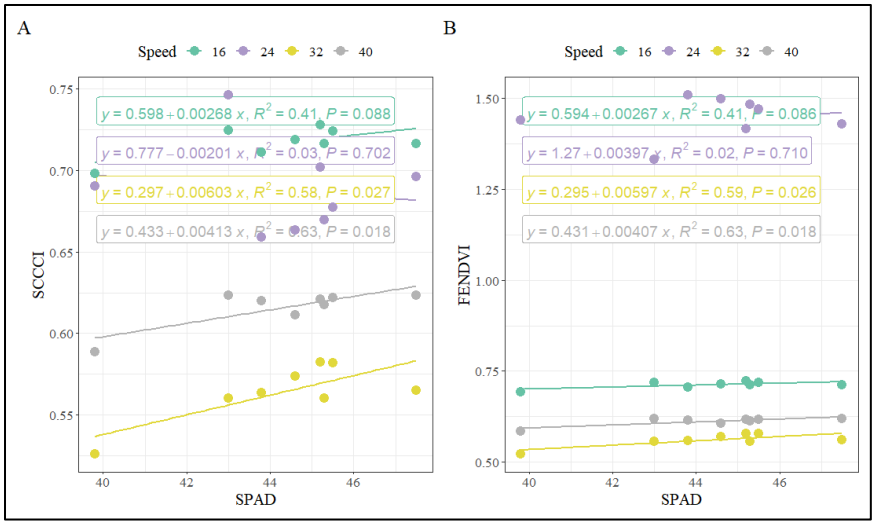

Figure 4.11 SCCCI (A) and FENDVI (B) as function of SPAD in the 2020 cotton south plot Sensed at 16, 24, 32 and 40 km hr^{-1} at mid-bloom stage in 2020. Different colors represent different speeds

According to figure 4.11, the relationship between SPAD and SCCCI and FENDVI was significant and positive at 32 and 40 km h^{-1}. As stated previously, the speed effects on VIs may be related to shutter speed settings on the camera.

For the 2021 corn crop, VIs were not affected by LN with change in flight platform. Figure 4.12 depicts NDRE, SCCCI, and FENDVI as a function of SPAD in the 2021 corn plot.

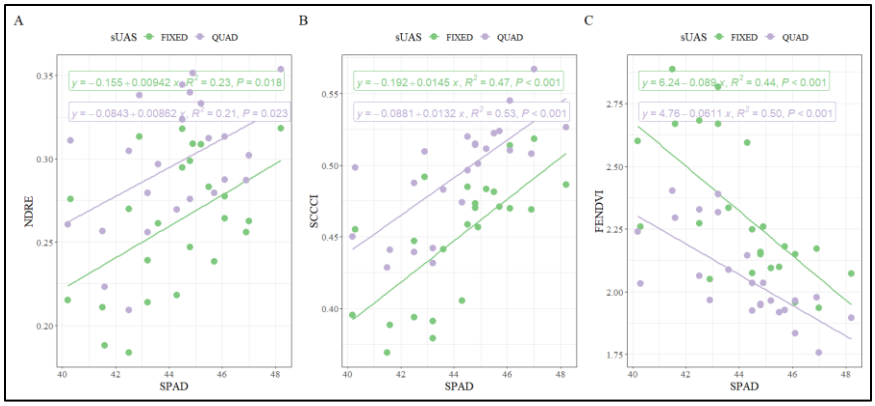

Figure 4.12 NDRE (A), SCCCI (B) and FENDVI (C) as function of SPAD in the 2021 corn plot.

Sensed with fixed wing (64 km h^{-1}) and quadcopter (32 km h^{-1}) at V8 growth stage. Different colors represent different platforms

In Figure 4.12, the relationship between SPAD on NDRE, and SCCCI was significant and positive. The relationship between SPAD on FENDVI was significant and negative with both platforms.

The 2021 cotton plot data showed that LN and SPAD did not affect the VI value with change in flight platform.

Corn 2020

In year one of this study, no fixed-wing aircraft was available to accomplish the prescribed goal of comparing fixed- to rotor-craft efficiency. Therefore, a quad-copter was deployed at four different speeds to develop a preliminary speed-related dataset.

The corn crop established for this study received a starter-rate fertilizer N treatment of 45 kg ha^{-1} (40 lb ac^{-1}) at planting. The 2020 corn canopy N sensing mission was flown on June 6, 2020. A quad-copter flew four separate flights at speeds of 16 km h^{-1} (10 mi h^{-1}), 24 km h^{-1} (15 mi h^{-1}), 32 km h^{-1} (20 mi h^{-1}) and 40 km h^{-1} (25 mi h^{-1}). From the June 6 sensing mission, both

fixed-rate N and VRN applications were calculated from the 16 km h^{-1} (10 mi h^{-1}) mission, and fertilizer N was applied on June 8, 2020. Corn yield data was lost in Hurricane Laura and was not included in the Yield data portion of this study (Table 4.6).

Table 4.6 Slope, root mean square error and sensitivity equivalents of indices of corn at V6 stage in 2020.

2020 Corn 16 km h^{-1}			2020 Corn 24 km h^{-1}		
SLOPE	SPAD	Leaf N%	*SLOPE*	SPAD	Leaf N%
NDVI	0.00285	0.0341	NDVI	0.00210	0.04985
GNDVI	0.00318	0.0323	GNDVI	0.00273	0.05313
NDRE	0.00259	0.0309	NDRE	0.00242	0.04620
SCCCI	0.00237	0.0267	SCCCI	0.00307	0.04220
FENDVI	0.00211	0.0256	FENDVI	0.00248	0.03678
BENDVI	0.00243	0.0232	BENDVI	-0.00260	-0.04140
RMSE			*RMSE*		
NDVI	0.04391	0.0442	NDVI	0.04353	0.04242
GNDVI	0.02899	0.0299	GNDVI	0.03093	0.02959
NDRE	0.02528	0.0257	NDRE	0.02556	0.02438
SCCCI	0.00768	0.0090	SCCCI	0.00919	0.00928
FENDVI	0.00876	0.0094	FENDVI	0.01174	0.01129
BENDVI	0.02830	0.0289	BENDVI	0.02017	0.01951
SEq			*SEq*		
NDVI	0.06491	0.7722	NDVI	0.04824	1.17515
GNDVI	0.10969	1.0813	GNDVI	0.08826	1.79554
NDRE	0.10245	1.2031	NDRE	0.09468	1.89500
SCCCI	**0.30859**	**2.9743**	SCCCI	**0.33406**	**4.54741**
FENDVI	0.24087	2.7274	FENDVI	0.21124	3.25775
BENDVI	0.08587	0.8028	BENDVI	-0.12740	-2.12050

Speeds are 16 km h^{-1} (10 mi h^{-1}) and 24 km h^{-1} (15 mi h^{-1})

Among all VIs in the 16 km h^{-1} (10 mi h^{-1}) and 24 km h^{-1} (15 mi h^{-1}) flights, SCCCI attained the greatest sensitivity equivalents when compared to both SPAD and leaf N variables. FENDVI performed second best behind SCCCI in all categories (Table 4.4). As speed increased from 16 km h^{-1} (10 mi h^{-1}) to 24 km h^{-1} (15 mi h^{-1}), SCCCI *SEq* increased by 0.02547 when modeled against SPAD. SCCCI modeled with leaf N increased by 1.57311 when comparing 16

km h^{-1} (10 mi h^{-1}) to 24 km h^{-1} (15 mi h^{-1}). The increase in value among both SCCCI with SPAD and SCCCI with leaf N indicates that the 24 km h^{-1} (15 mi h^{-1}) speed was superior to 16 km h^{-1} (10 mi h^{-1}) when related via *SEq* analysis. The 24 km h^{-1} (15 mi h^{-1}) was also a more efficient flight that was faster than the 16 km h^{-1} (10 mi h^{-1}) flight (Table 4.6).

The relative success of NDRE-based VIs (both NDRE and SCCCI) employed to estimate canopy leaf N in early corn complements earlier study findings (Fox, 2015; Raper and Varco, 2014). The precise biochemical nature of red-edge shift, as it relates to canopy leaf N%, remains unclear. Red-edge shift is a 'rubberbanding' effect caused by stretching of the red-to-NIR bands' respective decrease and increase of canopy reflectance and, therefore, may elicit a red-edge shift in conjunction with increased N treatment and canopy leaf N% expression. However, few, if any studies have been conducted to ascertain if a lateral, right red-edge shift relating to increased N status and/or availability is related to a biochemical phenomenon Therefore, the exact nature of the red-edge shift cannot be stated with certainty. Needed is research in a laboratory setting that might decouple red-edge shift from red-to-NIR reflectance decrease and increase, respectively.

Table 4.7 exhibits the double speed sampling from the previous (Table 4.6) flights.

Table 4.7 Slope, root mean square error and sensitivity equivalents of indices of corn at V6 stage in 2020.

2020 Corn 32 km h^{-1}			2020 Corn 40 km h^{-1}		
SLOPE	SPAD	Leaf N%	*SLOPE*	SPAD	Leaf N%
NDVI	0.00171	0.04582	NDVI	0.00096	0.04756
GNDVI	0.00283	0.04697	GNDVI	9.22222	0.02042
NDRE	0.00231	0.03896	NDRE	0.00153	0.04050
SCCCI	0.00349	0.03473	SCCCI	0.00317	0.04845
FENDVI	0.00280	-0.02492	FENDVI	0.00300	0.05426
BENDVI	-0.00040	-0.01110	BENDVI	-0.00205	-0.01990
RMSE			*RMSE*		
NDVI	0.05169	0.05082	NDVI	0.05029	0.04906
GNDVI	0.03170	0.03107	GNDVI	0.02481	0.02432
NDRE	0.02817	0.02765	NDRE	0.02777	0.02649
SCCCI	0.00660	0.01045	SCCCI	0.01128	0.01013
FENDVI	0.00843	0.01107	FENDVI	0.01509	0.01252
BENDVI	0.02338	0.02327	BENDVI	0.01165	0.01263
SEq			*SEq*		
NDVI	0.03308	0.90161	NDVI	0.01917	0.96943
GNDVI	0.08927	1.51175	GNDVI	0.00371	0.83964
NDRE	0.08200	1.40904	NDRE	0.05509	1.52888
SCCCI	**0.52879**	**3.32344**	SCCCI	**0.28102**	**4.78282**
FENDVI	0.33215	2.25113	FENDVI	0.19880	4.33387
BENDVI	-0.01740	-0.47490	BENDVI	-0.17596	-1.57480

Speeds are 32 km h^{-1} (20 mi h^{-1}) and 40 km h^{-1} (25 mi h^{-1})

Consistent with the 16 km h^{-1} (10 mi h^{-1}) and 24 km h^{-1} (15 mi h^{-1}) results, SCCCI achieved the highest sensitivity equivalents value among all VIs at both 32 km h^{-1} (20 mi h^{-1}) and 40 km h^{-1} (25 mi h^{-1}) speeds. When speed increased from 32 km h^{-1} (20 mi h^{-1}) to 40 km h^{-1} (25 mi h^{-1}), SCCCI with SPAD sensitivity equivalents exhibited an indirect relationship with a decrease of 0.25. The 0.25 decrease infers that a speed of 32 km h^{-1} (20 mi h^{-1}) was preferable to 40 km h^{-1} (25 mi h^{-1}) based on SCCCI and SPAD sensitivity equivalents. For SCCCI with leaf N sensitivity equivalents increased by 1.46 when speeds increased from 32 km h^{-1} (20 mi h^{-1}) to 40

km h^{-1} (25 mi h^{-1}), thus, revealing a direct relationship of speed to leaf N. The 1.46 increase from 32 km h^{-1} (20 mi h^{-1}) to 40 km h^{-1} (25 mi h^{-1}) implies that 40 km h^{-1} (25 mi h^{-1}) was desirable for the quad-copter flight platform when considering SCCCI with leaf N sensitivity equivalents.

Overall, the 2020 corn sensing missions revealed that SCCCI may be desirable compared to other VIs in this study. Noting that SCCCI is an NDRE-based VI, the SCCCI and SPAD sensitivity equivalents values were greatest at 32 km h^{-1} (20 mi h^{-1}), which infers that the 32 km h^{-1} (20 mi h^{-1}) speed was optimal to 16 km h^{-1} (10 mi h^{-1}), 24 km h^{-1} (15 mi h^{-1}), and 40 km h^{-1} (25 mi h^{-1}) when using SCCCI with SPAD to predict canopy N status. The 40 km h^{-1} (25 mi h^{-1}) produced the highest sensitivity equivalents for SCCCI and leaf N status. Again, what role aircraft attitude plays in increasing or decreasing VI sensitivity is yet unknown (Table 4.7).

One phenomenon that may explain the decrease in *SEq* value at different flight speeds was the tipping or pitching (an alteration of aircraft horizontal attitude towards the nose) of the quad-copter during increased acceleration. Witnessed by camera fly-by at 16 km h^{-1} (10 mi h^{-1}), 24 km h^{-1} (15 mi h^{-1}), 32 km h^{-1} (20 mi h^{-1}), and 40 km h^{-1} (25 mi h^{-1}), a noticeable upward shift in the aircraft aft that was succeeded by a downward shift in the aircraft forward nose created an angular tilt of the camera sensor backwards. The backwards shift will be referred to as NADIR-Aft and was most notable at 24 km h^{-1} (15 mi h^{-1}) and 40 km h^{-1} (25 mi h^{-1}). A remedy to control NADIR-Aft shift would be the installation of a sensor gimble but this study precludes deploying the device. Needed is research that will decouple aircraft attitude from speed by addition of a sensor gimbal that will horizontally align lenses to topography.

Cotton 2020

The 2020 cotton sensing mission was flown on July 11, 2020. A quad-copter was employed to fly four separate flights at speeds of 16 km h^{-1} (10 mi h^{-1}), 24 km h^{-1} (15 mi h^{-1}), 32 km h^{-1} (20 mi h^{-1}) and 40 km h^{-1} (25 mi h^{-1}). From the July 11 sensing mission, both fixed-rate N and VRN applications were made on July 15, 2020 (Table 4.8).

Table 4.8 Slope, root mean square error and sensitivity equivalents of indices of north cotton plot at mid bloom stage in 2020.

2020 Cotton North 16 km h^{-1}			2020 Cotton North 24 km h^{-1}		
SLOPE	SPAD	Leaf N%	*SLOPE*	SPAD	Leaf N%
NDVI	0.01154	-0.00039	NDVI	0.00190	-0.00007
GNDVI	0.00362	0.01864	GNDVI	-0.00137	0.00350
NDRE	0.01430	-0.00018	NDRE	-0.00156	0.01590
SCCCI	-0.02903	-0.00051	SCCCI	0.02302	-0.07329
FENDVI	0.00930	0.00074	FENDVI	-0.00465	0.01977
BENDVI	0.07537	0.20076	BENDVI	-0.00782	0.01484
RMSE			*RMSE*		
NDVI	0.10154	0.10327	NDVI	0.11607	0.11612
GNDVI	0.08538	0.08525	GNDVI	0.08353	0.08354
NDRE	0.06935	0.07316	NDRE	0.08591	0.08570
SCCCI	0.05515	0.07267	SCCCI	0.14393	0.14573
FENDVI	0.01656	0.02245	FENDVI	0.03541	0.03531
BENDVI	0.46194	0.47101	BENDVI	0.13078	0.13126
SEq			*SEq*		
NDVI	0.11365	-0.00375	NDVI	0.01637	-0.00058
GNDVI	0.04240	0.21865	GNDVI	-0.01640	0.04190
NDRE	0.20620	-0.00250	NDRE	-0.01816	0.18553
SCCCI	-0.52638	-0.00705	SCCCI	**0.15994**	-0.50292
FENDVI	**0.56159**	0.03317	FENDVI	-0.13132	**0.55990**
BENDVI	0.16316	**0.42623**	BENDVI	-0.05980	0.11306

Speeds are 16 km h^{-1} (10 mi h^{-1}) and 24 km h^{-1} (15 mi h^{-1})

There was no consistently high-performing VIs among speeds 16 km h^{-1} (10 mi h^{-1}) and 24 km h^{-1} (15 mi h^{-1}) in the 2020 North Cotton plot. FENDVI produced the highest sensitivity

equivalents for the 16 km h^{-1} (10 mi h^{-1}) when modeled with SPAD. The SPAD meter does not sample for green (550 nm) reflectance as is incorporated into the FENDVI but, instead, measures the absorbance in red and NIR wavelengths. Therefore, it is not possible to state whether FENDVI and SPAD are highly relatable other than through *SEq* modeling. The FENDVI algorithm incorporates NDRE, NDVI, and green bands of a sensor. Opposite of red-edge detection and shift relating to canopy N status, green band reflectance is indirectly related with canopy N status during photosynthesis and, therefore, inadvertently detectable by SPAD meters (Mutanga and Skidmore, 2004). However, research is needed to decouple green, red, red-edge, and NIR band reflectance behavior from other phenomenon especially considering SPAD does not account for red-colored soil albedo detected with the above-canopy sensing tools. Development of a SPAD tool that includes the green (550 nm) band may increase understanding of individual band reflectance's and improve canopy N detection through proximal and sUAS sensing methods.

The greatest sensitivity equivalents for 16 km h^{-1} (10 mi h^{-1}) when modeled with leaf N was achieved by BENDVI, a VI that incorporates NIR, blue, and green bands (Table 4.6). For the 24 km h^{-1} (15 mi h^{-1}) speed, SCCCI had the greatest sensitivity equivalents when modeled with SPAD. The 24 km h^{-1} (15 mi h^{-1}) speed for VIs modeled with leaf N resulted in FENDVI, a VI incorporating a modified green band with SCCCI, having the greatest sensitivity equivalents (Table 4.8).

Table 4.9 exhibits the double speed sampling from the previous (Table 4.6) flights.

Table 4.9 Slope, root mean square error and sensitivity equivalents of indices of north cotton plot at mid bloom stage in 2020.

2020 Cotton North 32 km h^{-1}			2020 Cotton North 40 km h^{-1}		
SLOPE	SPAD	Leaf N%	*SLOPE*	SPAD	Leaf N%
NDVI	-0.00013	-0.04011	NDVI	0.00429	0.08414
GNDVI	-0.00215	-0.02248	GNDVI	-0.00041	0.06394
NDRE	-0.00242	-0.01656	NDRE	-0.00300	0.06381
SCCCI	0.02171	-0.00478	SCCCI	0.03188	-0.08844
FENDVI	-0.00402	0.00228	FENDVI	-0.00764	0.02345
BENDVI	-0.00274	-0.02587	BENDVI	-0.01481	0.12881
RMSE			*RMSE*		
NDVI	0.11420	0.11303	NDVI	0.10626	0.10087
GNDVI	0.08349	0.08307	GNDVI	0.07977	0.07544
NDRE	0.08463	0.08446	NDRE	0.07904	0.07484
SCCCI	0.15956	0.16343	SCCCI	0.11946	0.12523
FENDVI	0.03755	0.03811	FENDVI	0.03004	0.03110
BENDVI	0.11652	0.11614	BENDVI	0.12046	0.11118
SEq			*SEq*		
NDVI	-0.00110	-0.35486	NDVI	0.04037	0.83414
GNDVI	-0.02575	-0.27062	GNDVI	-0.00515	0.84756
NDRE	-0.02860	-0.19607	NDRE	-0.03796	0.85262
SCCCI	**0.13606**	-0.02925	SCCCI	**0.26687**	-0.70622
FENDVI	-0.10706	**0.05983**	FENDVI	-0.25433	0.75402
BENDVI	-0.02352	-0.22275	BENDVI	-0.12295	**1.15857**

Speeds are 32 km h^{-1} (20 mi h^{-1}) and 40 km h^{-1} (25 mi h^{-1})

When canopy N status was assessed using SPAD, SCCCI attained the greatest sensitivity equivalents value for the 32 km h^{-1} (20 mi h^{-1}) speed. The greatest sensitivity equivalents result for the 32 km h^{-1} (20 mi h^{-1}) speed was FENDVI when modeled with leaf N. SCCCI modeled with SPAD achieved the greatest sensitivity equivalents for 40 km h^{-1} (25 mi h^{-1}). An increase of 0.13 was noted in SCCCI for the SPAD sensitivity equivalents with a speed increase from 32 km h^{-1} (20 mi h^{-1}) to 40 km h^{-1} (25 mi h^{-1}). Inconsistent with the 32 km h^{-1} (20 mi h^{-1}) speed, BENDVI modeled with Leaf N outperformed other VIs in terms of sensitivity equivalents.

Sensitivity Equivalents results across all speeds did not reveal a consistent ideal VI for modeling with SPAD or leaf N. A probable cause for the inconsistent results is related to the previously mentioned “tilt” of the quad-copter coupled with the inability to remove outliers due to small sample count (Table 4.9).

Table 4.10details the slope, root mean square error and sensitivity equivalents of indices of south cotton plot at mid bloom stage in 2020

Table 4.10 Slope, root mean square error and sensitivity equivalents of indices of south cotton plot at mid bloom stage in 2020.

2020 Cotton South 16 km h^{-1}			2020 Cotton South 24 km h^{-1}		
SLOPE	SPAD	Leaf N%	*SLOPE*	SPAD	Leaf N%
NDVI	0.00139	0.00504	NDVI	-0.00101	0.00024
GNDVI	0.00226	0.00648	GNDVI	-0.00056	-0.00635
NDRE	0.00354	0.00503	NDRE	-0.00261	-0.00951
SCCCI	0.00534	0.00332	SCCCI	-0.00201	-0.01005
FENDVI	0.00267	0.00164	FENDVI	-0.00397	-0.01995
BENDVI	0.02790	0.12982	BENDVI	0.05523	-0.03256
RMSE			*RMSE*		
NDVI	0.00332	0.00462	NDVI	0.00715	0.00756
GNDVI	0.00546	0.00762	GNDVI	0.00571	0.00553
NDRE	0.00958	0.01285	NDRE	0.0328	0.03334
SCCCI	0.01535	0.02012	SCCCI	0.03001	0.03033
FENDVI	0.00779	0.01015	FENDVI	0.06084	0.06145
BENDVI	0.07325	0.09574	BENDVI	0.67367	0.68700
SEq			*SEq*		
NDVI	**0.41867**	1.09090	NDVI	-0.14125	**0.03267**
GNDVI	0.41391	0.85039	GNDVI	-0.09964	-1.14828
NDRE	0.36951	0.39143	NDRE	-0.07957	-0.28524
SCCCI	0.34788	0.16500	SCCCI	-0.06697	-0.33135
FENDVI	0.34274	0.16157	FENDVI	-0.06525	-0.32465
BENDVI	0.38088	**1.35596**	BENDVI	**0.08198**	-0.04739

Speeds are 16 km h^{-1} (10 mi h^{-1}) and 24 km h^{-1} (15 mi h^{-1})

The 2020 south cotton plot results imply that NDVI modeled with SPAD produced the greatest sensitivity equivalents value at a speed of 16 km h^{-1} (10 mi h^{-1}). Both SPAD and NDVI employ red and NIR bands to estimate chlorophyll (and thus, related N status). BENDVI modeled with leaf N sensitivity equivalents results revealed that BENDVI may be preferred to other VIs at the 16 km h^{-1} (10 mi h^{-1}) speed. At 24 km h^{-1} (15 mi h^{-1}) results indicated that BENDVI modeled with SPAD may be favored compared to alternative VIs.

At a value of 0.03267, NDVI modeled with leaf N sensitivity equivalents results achieved a greatest value than comparable VIs. One single VI sensitivity equivalents value was not identified as consistently higher at speeds of 16 km h^{-1} (10 mi h^{-1}) and 24 km h^{-1} (15 mi h^{-1}). Subsequent studies using sUAS and sensing technologies necessitate an increase in sample size collection that will likely mitigate sampling errors related to on-farm topographic changes. Moreover, a highly consistent and uniform off-farm research methodology made up of similar small-plot research sites on limited soil substrate may also improve VI sensitivity Table 4.10.

Table 4.11 details the doubling of speed over the Table 4.10 sampling values.

Table 4.11 Slope, root mean square error and sensitivity equivalents of indices of north cotton plot at mid bloom stage in 2020.

2020 Cotton South 32 km h^{-1}			2020 Cotton South 40 km h^{-1}		
SLOPE	SPAD	Leaf N%	*SLOPE*	SPAD	Leaf N%
NDVI	0.00444	0.02621	NDVI	0.00246	0.0177
GNDVI	0.00494	0.02318	GNDVI	0.00380	0.01839
NDRE	0.00787	0.03397	NDRE	0.00526	0.03051
SCCCI	0.00603	0.07127	SCCCI	0.00413	0.02144
FENDVI	0.00597	0.02160	FENDVI	-0.00407	-0.02109
BENDVI	0.01429	0.22557	BENDVI	0.01348	0.06615
RMSE			*RMSE*		
NDVI	0.00835	0.01238	NDVI	0.00549	0.00711
GNDVI	0.01043	0.01508	GNDVI	0.00743	0.01116
NDRE	0.01496	0.02315	NDRE	0.01007	0.01483
SCCCI	0.01241	0.06084	SCCCI	0.00768	0.01175
FENDVI	0.01219	0.01838	FENDVI	0.00756	0.01155
BENDVI	0.10553	0.09913	BENDVI	0.03124	0.04291
SEq			*SEq*		
NDVI	**0.53173**	2.11712	NDVI	0.44808	**2.48945**
GNDVI	0.47363	1.53713	GNDVI	0.51144	1.64784
NDRE	0.52606	1.46738	NDRE	0.52234	2.05731
SCCCI	0.48589	1.15075	SCCCI	0.53776	1.82468
FENDVI	0.48974	1.17519	FENDVI	**0.53835**	1.82597
BENDVI	0.13541	**2.27549**	BENDVI	0.43149	1.54159

Speeds are 32 km h^{-1} (20 mi h^{-1}) and 40 km h^{-1} (25 mi h^{-1})

NDVI modeled with SPAD produced greater sensitivity equivalents value than other VIs at a speed of 32 km h^{-1} (20 mi h^{-1}) for cotton. A value of 2.28 resulted with BENDVI modeled with SPAD, thus, implying that BENDVI is optimal to other VIs at a speed of 32 km h^{-1} (20 mi h^{-1}). For the 40 km h^{-1} (25 mi h^{-1}) speed, FENDVI had the greatest sensitivity equivalents when modeled with SPAD. NDVI modeled with Leaf N sensitivity equivalents resulted in higher values than compared VIs for the 40 km h^{-1} (25 mi h^{-1}) speed.

Consistent with the 2020 cotton plot north results, the 2020 cotton plot south results did not have a persistent VI that ranked above other VI sensitivity equivalents. The quad-copter tilt and small sample count may factor into inconsistent results.

Corn 2021

The sensing mission for the 2021 corn crop was flown on May 1, 2021. Two separate flights at speeds of 32 km h^{-1} (20 mi h^{-1}) and 64 km h^{-1} (40 mi h^{-1}) were conducted using both quad-copter and fixed-wing flight platforms, respectively.

From the May 1 sensing mission, both fixed-rate N and VRN applications were made on May 8, 2021, utilizing quad-copter data (Table 4.12).

Table 4.12 Slope, root mean square error and sensitivity equivalents of indices of corn plot at V8 stage in 2021.

2021 Corn 32 km h^{-1}			2021 Corn 64 km h^{-1}		
SLOPE	SPAD	Leaf N%	*SLOPE*	SPAD	Leaf N%
NDVI	-0.00598	0.03481	NDVI	-0.00560	0.04302
GNDVI	-0.00082	0.03026	GNDVI	-0.00053	0.03593
NDRE	0.00180	0.03861	NDRE	0.00200	0.04578
SCCCI	0.00888	0.03756	SCCCI	0.00874	0.04794
FENDVI	0.03967	0.19055	FENDVI	0.05140	0.30738
BENDVI	-0.00369	0.02667	BENDVI	-0.00344	0.02989
RMSE			*RMSE*		
NDVI	0.05486	0.05462	NDVI	0.05828	0.05723
GNDVI	0.03117	0.02933	GNDVI	0.03595	0.03365
NDRE	0.02975	0.02667	NDRE	0.03278	0.02877
SCCCI	0.02365	0.02566	SCCCI	0.02971	0.02937
FENDVI	0.11304	0.11723	FENDVI	0.19119	0.18439
BENDVI	0.03407	0.03346	BENDVI	0.03312	0.03205
SEq			*SEq*		
NDVI	-0.10900	0.63731	NDVI	-0.09609	0.75170
GNDVI	-0.02646	1.03171	GNDVI	-0.01478	1.06776
NDRE	0.06050	1.44769	NDRE	0.06101	1.59124
SCCCI	**0.37548**	1.46376	SCCCI	**0.29418**	1.63228
FENDVI	0.35094	**1.62544**	FENDVI	0.26884	**1.66701**
BENDVI	-0.10831	0.79707	BENDVI	-0.10386	0.93261

Speeds are 32 km h^{-1} (20 mi h^{-1}) and 64 km h^{-1} (40 mi h^{-1})

The 2021 corn plot revealed that SCCCI, when modeled with SPAD, produced the greatest sensitivity equivalents value at a speed of 32 km h^{-1} (20 mi h^{-1}). FENDVI, a modified green band divided by the SCCCI, performed best when modeled with Leaf N at the 32 km h^{-1} (20 mi h^{-1}) speed. A decrease of 0.0813 was noted in SCCCI modeled with SPAD sensitivity equivalents among an increase of speed from 32 km h^{-1} (20 mi h^{-1}) to 64 km h^{-1} (40 mi h^{-1}). FENDVI modeled with leaf N experienced a slight increase in sensitivity equivalents of 0.04157 when speed increased from 32 km h^{-1} (20 mi h^{-1}) to 64 km h^{-1} (40 mi h^{-1}) (Table 4.12).

Among both quad-copter (32 km h^{-1} (20 mi h^{-1})) and fixed-wing platforms (64 km h^{-1} (40 mi h^{-1})), SCCCI modeled with SPAD experienced a decrease. The 0.0813 decrease in SCCCI modeled with SPAD sensitivity equivalence is likely due to the unreliability of SPAD. SPAD requires an elevated level of precision and consistency when collecting samples that is not typically present when conducting on-farm sampling. Xiong et al. (2015) found that SPAD readings are highly variable depending upon leaf and environmental characteristics.

When performing on-farm research, SPAD is not a preferred biophysical parameter by which to assay canopy leaf N status. The physically demanding and time-consuming effort required to sample using SPAD are, in themselves, tremendously limiting factors. Added effects of end-user subjectivity and inconsistent sampling method necessitates the development of objective on-the-fly field measurements techniques that can, in almost real time, determine crop canopy status. Moreover, a SPAD lacking green band assessment may also reduce its overall efficacy for use on-farm. A reduction in green band reflectance is highly and indirectly relatable to increasing canopy N status.

FENDVI modeled with leaf N produced an increase of 0.04157 in sensitivity equivalents with an increase in speed from quad-copter (32 km h^{-1} (20 mi h^{-1})) to fixed-wing platforms (64 km h^{-1} (40 mi h^{-1})). The 0.04157 increase expresses that fixed-wing flight may produce higher sensitivity equivalents than quad-copter flight.

Cotton 2021

On June 18, 2021, the first sensing mission was completed for the 2021 cotton crop during pinhead square development stage. Due to a fixed-wing platform malfunction, only a quad-copter flight was executed at a speed of 32 km h^{-1} (20 mi h^{-1}) on June 18. From the June 18 quad-copter only sensing mission, both fixed-rate N and VRN applications were made on June

20, 2021, utilizing quad-copter data (Table 4.13). A second sensing mission was accomplished on July 28, 2021, at mid-bloom development stage, employing both quad-copter (32 km h^{-1} (20 mi h^{-1})) and fixed-wing (64 km h^{-1} (40 mi h^{-1})) flight systems. The July 28 mission was necessary for comparison of quad-copter and fixed-wing flight data in similar environmental conditions (Table 4.14).

Table 4.13 details the slope, root mean square error and sensitivity equivalents of indices of cotton plot at pinhead square stage in 2021.

Table 4.13 Slope, root mean square error and sensitivity equivalents of indices of cotton plot at pinhead square stage in 2021.

2021 Cotton 32 km h^{-1}		
SLOPE	SPAD	Leaf N%
NDVI	0.00183	0.04386
GNDVI	0.00079	0.00691
NDRE	0.00069	0.01359
SCCCI	0.00003	0.02270
FENDVI	0.00070	0.07362
BENDVI	0.00086	0.00616
RMSE		
NDVI	0.03060	0.02835
GNDVI	0.01373	0.01380
NDRE	0.00964	0.00904
SCCCI	0.01264	0.01054
FENDVI	0.09051	0.08792
BENDVI	0.01804	0.01815
SEq		
NDVI	0.05980	1.54709
GNDVI	0.05748	0.50072
NDRE	**0.07171**	1.50332
SCCCI	0.00225	**2.15370**
FENDVI	0.00772	0.83735
BENDVI	0.04746	0.33939

Speed is at 32 km h^{-1} (20 mi h^{-1})

The VRN quad-copter flight for the 2021 cotton crop resulted in the NDRE modeled with SPAD sensitivity equivalents value rising above compared VIs. NDRE may be ideal when modeled with SPAD at a speed of 32 km h^{-1} (20 mi h^{-1}). When modeled with leaf N, SCCCI resulted in a greater sensitivity equivalents value than other VIs. At a speed of 32 km h^{-1} (20 mi h^{-1}), SCCCI modeled with SPAD may be preferred in terms of sensitivity equivalents (Table 4.13).

Table 4.14 details the slope, root mean square error and sensitivity equivalents of indices of cotton plot at mid-bloom stage in 2021.

Table 4.14 Slope, root mean square error and sensitivity equivalents of indices of cotton plot at mid-bloom stage in 2021.

2021 Cotton 32 km h^{-1}			2021 Cotton 64 km h^{-1}		
SLOPE	SPAD	Leaf N%	*SLOPE*	SPAD	Leaf N%
NDVI	-0.00087	0.04752	NDVI	0.00111	0.05667
GNDVI	-0.00031	0.03245	GNDVI	0.00122	0.04027
NDRE	0.00018	0.03830	NDRE	0.00179	0.04649
SCCCI	0.00073	0.01512	SCCCI	0.00122	0.01533
FENDVI	0.00234	0.05260	FENDVI	0.00391	0.04925
BENDVI	-0.00074	0.03273	BENDVI	0.00096	0.04262
RMSE			*RMSE*		
NDVI	0.04341	0.04119	NDVI	0.03496	0.03054
GNDVI	0.02815	0.02651	GNDVI	0.02159	0.01812
NDRE	0.03058	0.02845	NDRE	0.02144	0.01698
SCCCI	0.01083	0.01014	SCCCI	0.00873	0.00830
FENDVI	0.03976	0.03737	FENDVI	0.02809	0.02670
BENDVI	0.03163	0.03022	BENDVI	0.02665	0.02342
SEq			*SEq*		
NDVI	-0.02009	1.15368	NDVI	0.03175	1.85560
GNDVI	-0.01096	1.22407	GNDVI	0.05651	2.22241
NDRE	0.00589	1.34622	NDRE	0.08349	**2.73793**
SCCCI	**0.06716**	**1.49112**	SCCCI	**0.13975**	1.84699
FENDVI	0.05885	1.40755	FENDVI	0.13920	1.84457
BENDVI	-0.02343	1.08306	BENDVI	0.03603	1.81981

Speeds are 32 km h^{-1} (20 mi h^{-1}) and 64 km h^{-1} (40 mi h^{-1})

When modeled with SPAD, SCCCI possessed a greater sensitivity equivalents value than other VIs at a speed of 32 km h^{-1} (20 mi h^{-1}). Consistent with SCCCI modeled with SPAD at 32 km h^{-1} (20 mi h^{-1}), SCCCI modeled with leaf N attained a greater sensitivity equivalents value than compared VIs at 32 km h^{-1} (20 mi h^{-1}). An increase of 0.07259 was noted in SCCCI modeled with SPAD when speed was increased from 32 km h^{-1} (20 mi h^{-1}) to 64 km h^{-1} (40 mi h^{-1}). Inconsistent with leaf N sensitivity equivalents results at 32 km h^{-1} (20 mi h^{-1}), NDRE achieved the highest sensitivity equivalents value when modeled with SPAD for the 64 km h^{-1} (40 mi h^{-1}) speed (Table 4.14).

The mid-bloom sensing mission resulted in SCCCI having the greatest sensitivity equivalents when modeled with SPAD. The increase in speed from quad-copter (32 km h^{-1} (20 mi h^{-1})) to fixed-wing (64 km h^{-1} (40 mi h^{-1})) led to an increase in SCCCI modeled with SPAD sensitivity equivalents of 0.07259. The increase of 0.07259 may infer that fixed-wing is ideal to quad-copter for sensitivity equivalents in VIs modeled with SPAD. When speed increased from 32 km h^{-1} (20 mi h^{-1}) to 64 km h^{-1} (40 mi h^{-1}), VIs modeled with leaf N's sensitivity equivalents values resulted in the higher values for SCCCI and NDRE, respectively.

Concluding Remarks on Crop Canopy Sensing

Sensing missions for this study resulted in numerous novel findings. The first being that NDRE-based indices performed well in comparison to other VIs in all individual studies. Multiple studies support similar findings revealing NDRE-based VIs produced the strongest relationship with leaf N content (Varco et al., 2013; Raper and Varco, 2014; Fox, 2015; Sumner et al., 2021). Among all VIs, NDRE-based VIs may yield the greatest relationship to crop canopy N levels. This study does not suggest there is verifiable causation between canopy N status and VI efficiency without further study into the complex relationship of lateral, right red-edge shift,

and accompanying reduction in green reflectance with increasing canopy N status. However, noted to date herein, no SPAD canopy analysis tools have successfully incorporated the green band, which may further elucidate canopy N status in-field.

The prevalent and predominate VIs were found to be SCCCI and FENDVI for detecting early N status in corn and cotton during the V4-V8 and pinhead square-mid bloom stages, respectively. Means separation by way of Tukey's studentized range test was performed across all SCCCI and FENDVI values. Results revealed no statistically significant difference between SCCCI and FENDVI among all crops and flight speeds.

A loss in VI efficiency was not evident among an increase in speed from quad-copter (32 km h^{-1} (20 mi h^{-1})) to fixed-wing (64 km h^{-1} (40 mi h^{-1})). In select cases, faster but moderate sensing speeds may result in a greater level of accuracy. Fixed-wing sensing platforms provided more efficacy than quad-copter platforms in these studies, but further studies are needed. Overall, fixed-wing platforms may provide a faster alternative to quad-copter platforms without a loss of data accuracy. However, the results from this study suggest the sensor attitude onboard the aircraft may affect sensing results, but relevant research is needed to decouple speed and attitude effects.

Variable Rate N Demonstration using sUAS

The following results sections detail experiments and outcomes of a variable rate fertilizer N experiment in corn and cotton conducted between 2020 and 2021 in the Mississippi River Alluvium production areas of MS and LA.

VRN Flights and Nitrogen Applications

Autonomous, unmanned flights were conducted at critical sampling stages for corn and cotton, which allowed for adequate post-flight data processing and return of the VRN maps to the fertilizer N applicator in WGS84 gridded format [22.9 m^2 (75 ft^2)]. All missions were flown with a MicaSense RedEdge® (Seattle, WA) (MSRE) sensor onboard (no gimble). Table 4.15 details the flight dates, crop, and critical stages in relationship to a preferred speed and flight altitude.

Table 4.15 sUAS flight dates and specifications for corn and cotton VRN application calibration in 2020 and 2021

Date	Crop	Stage	Flight Platform	Altitude	Speed
June 6, 2020	Corn	V6	Quad-copter	121.92 m	32 km h^{-1}
July 11, 2020	Cotton	Mid-Bloom	Quad-copter	121.92 m	32 km h^{-1}
May 1, 2021	Corn	V8	Quad-copter	121.92 m	32 km h^{-1}
June 18, 2021	Cotton	Pinhead Square	Quad-copter	121.92 m	32 km h^{-1}

Speeds is at 32 km h^{-1} (20 mi h^{-1}). Altitude is at 121.92 m (400 ft).

Post-flight data analysis of the MSRE imagery included mosaicking of all bands and calculation of the SCCCI VI. The VRN rates were calculated in ArcGIS Desktop Spatial Analyst in WGS84 UTM15N. Post-processed maps were converted to WGS84 format. Prior to fertilizer N application, the VRN maps were uploaded to the John Deere® (Moline, IL) GreenStar™ monitor and deployed within one week after sampling. Table 4.16 details the VRN application dates and ranges of rates for both VRN and fixed N applications.

Table 4.16 VRN and fixed-rate applications and specifications for corn and cotton in 2020 and 2021

Date	Crop	VRN Rate Low	VRN Rate High	Fixed-Rate
June 8, 2020	Corn	114.33 kg ha^{-1}	170.37 kg ha^{-1}	170.37 kg ha^{-1}
July 15, 2020	Cotton	0 kg ha^{-1}	33.63 kg ha^{-1}	33.63 kg ha^{-1}
May 8, 2021	Corn	78.46 kg ha^{-1}	134.50 kg ha^{-1}	134.50 kg ha^{-1}
June 20, 2021	Cotton	56.04 kg ha^{-1}	89.67 kg ha^{-1}	89.67 kg ha^{-1}

Fertilizer N source: UAN 32% (32-0-0)
Refer to Materials and Methods for unit conversions

2020 Corn Crop

The 2020 corn crop flight was performed on June 6, 2020 (Table 4.13). A flight was conducted at a speed of 32 km h^{-1} (20 mi h^{-1}) and altitude of 121.92 m (400 ft) using a 650-class commercial quadcopter with a 10,000 mAh 4S battery capable of 15 minutes sustained flight [custom designed by Dennis Lott (UASSolutions, Clinton, MS)]. A MicaSense RedEdge® was employed aboard the quadcopter for multispectral sensing. The fixed- and variable-rate N applications were made on June 8, 2020, utilizing sensor data from the 32 km h^{-1} (20 mi h^{-1}) flight. During August of the 2020 growing season, the corn experienced yield loss from Hurricane Laura. The salvaged plot was harvested on September 9, 2020. Figure 4.13 depicts the variable- and fixed-rate N applications noted in Table 4.16.

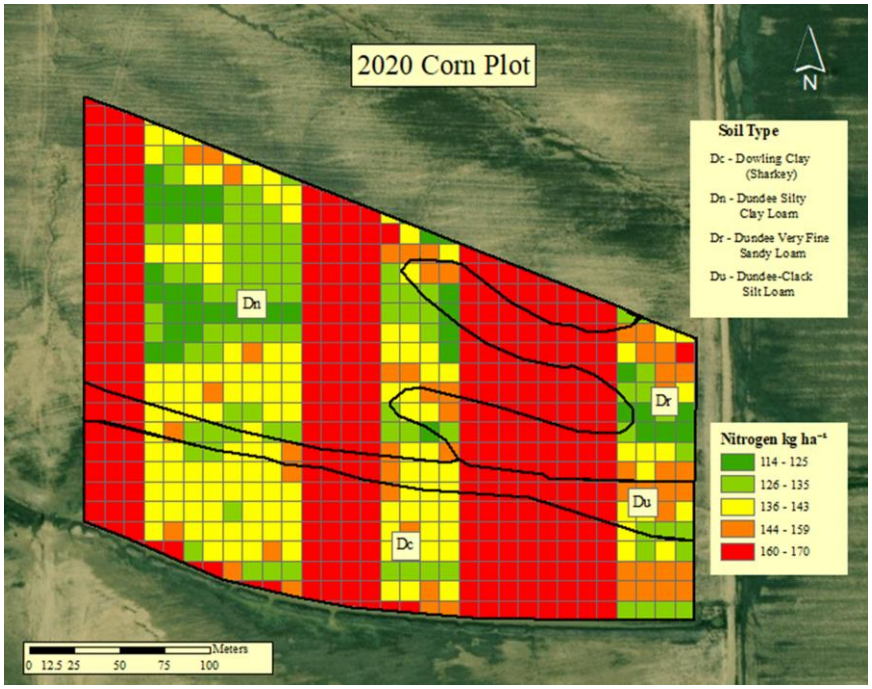

Figure 4.13 2020 corn N application including both fixed-rate and VRN applications

Soil series were described as 30% (2.43 ha) Dowling clay (Very-fine, smectitic, nonacid, thermic, Vertic Endoaquepts), 46% (3.72 ha) Dundee silty clay loam (Fine-silty, mixed, active, thermic Typic Endoaqualfs), 14% (1.13 ha) Dundee very fine sandy loam, and 10% (0.81) Dundee-clack silt loam.

An N rate of 137.87 kg ha^{-1} (123 lb ac^{-1}) was the mean, median, and mode for the VRN application dataset. The total season variable-rate N section of the plot ranged from 257.80 N kg ha^{-1} (230 N lb ac^{-1}) to 313.84 N kg ha^{-1} (280 N lb ac^{-1}) (Figure 4.13). The yield map for the 2020 corn crop is depicted in Figure 4.14.

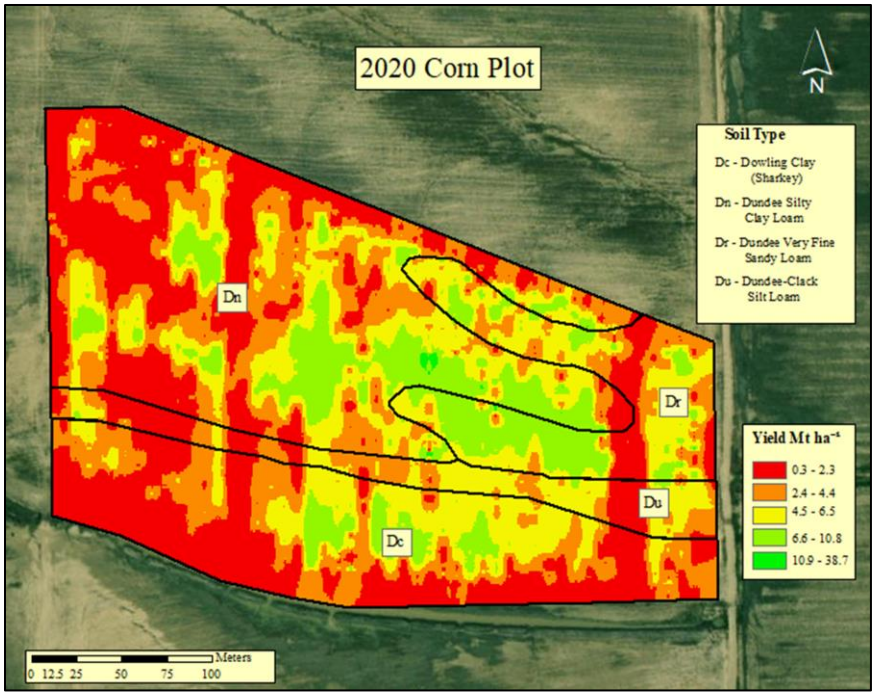

Figure 4.14 2020 corn yield map

Soil series were described as 30% (2.43 ha) Dowling clay (Very-fine, smectitic, nonacid, thermic, Vertic Endoaquepts), 46% (3.72 ha) Dundee silty clay loam (Fine-silty, mixed, active, thermic Typic Endoaqualfs), 14% (1.13 ha) Dundee very fine sandy loam, and 10% (0.81) Dundee-clack silt loam.

The 2020 corn crop resulted in unusually low yields due to damage from Hurricane Laura (Figure 4.14). Yield average for the total plot, fixed- and variable-rate combined, was 3.76 Mt ha^{-1} (56 bu ac^{-1}). The VRN section of the plot yielded an average of 3.42 Mt ha^{-1} (51 bu ac^{-1}). Fixed-rate N applicated crops produced a mean yield of 4.13 Mt ha^{-1} (61 bu ac^{-1}). Unfortunately, yield analysis cannot be accurately conducted due to total loss of the 2020 corn crop (Figure 4.15).

Figure 4.15 2020 corn crop damage as a result of Hurricane Laura

Corn is seen laid over directly in front of the harvester. The plants to the right in the photo sustained less damage, but still produced substantial yield loss

Nitrogen Use Efficiency (NUE) was an integral piece to this study. VRN applications were classified using equal interval four classes. The VRN NUE was calculated based on the yield divided by the VRN application. Total available NUE was achieved by yield divided by the available N that was available to the plant throughout the season (Residual Soil N + Total Season

N Application). The 2020 corn NUE is classed by N rate across four VRN rates and one fixed rate (Table 4.17).

Table 4.17 2020 corn plot NUE by N rate class

N Rate Class	N Rate by Class (kg ha^{-1})	Yield by N Rate (Mt ha^{-1})	N Rate NUE	Total Available NUE	Percentage of Field	Hectares per Class (ha)
VRN Low	114-129	3.01	0.02	0.01	11%	0.91
VRN Mod Low	130-142	3.45	0.03	0.01	29%	2.30
VRN Mod High	143-157	3.76	0.03	0.01	10%	0.83
VRN High	158-170	1.88	0.01	0.01	1%	0.06
Fixed Rate	170	4.13	0.02	0.01	49%	3.87

Refer to Materials and Methods for unit conversions

As depicted in Table 4.17, yield increased as VRN rate increased from 114 kg ha^{-1} (102 lb ac^{-1}) to 157 kg ha^{-1} (140 lb ac^{-1}). The VRN moderately high rate class shows evidence that 143 kg ha^{-1} (128 lb ac^{-1}) to 157 kg ha^{-1} (140 lb ac^{-1}) is the ideal N rate range before loss is experienced. A significant decrease in yield by 50% was noted when VRN rates increased from the 143 kg ha^{-1} (128 lb ac^{-1}) to 157 kg ha^{-1} (140 lb ac^{-1}) range to the 158 kg ha^{-1} (141 lb ac^{-1}) to 170 kg ha^{-1} (152 lb ac^{-1}) range. Table 4.18 details the comparison of LSMeans for the 2020 corn crop.

Table 4.18 2020 corn plot Tukey Studentized range of yield means by treatment class

	Yield LSMEAN	Treatment Class
A	4.14	2
B	3.41	1

LSMeans with same letter are not significantly different
Yield units are Mt ha^{-1}
Treatment Classes: VRN Treatment = 1 (Total N application average = 280 kg ha^{-1}).
Fixed-rate Treatment = 2 (Total N applied = 314 kg ha^{-1})

According to Tukey's studentized range test shown in Table 4.16, treatment classes one and two yield are not significantly different (Table 4.18). The fixed-rate treatment, treatment class two yield was 0.73 Mt ha^{-1} higher than treatment class one. Figure 4.16 depicts the yield for the 2020 corn plot modeled against the VRN application rates.

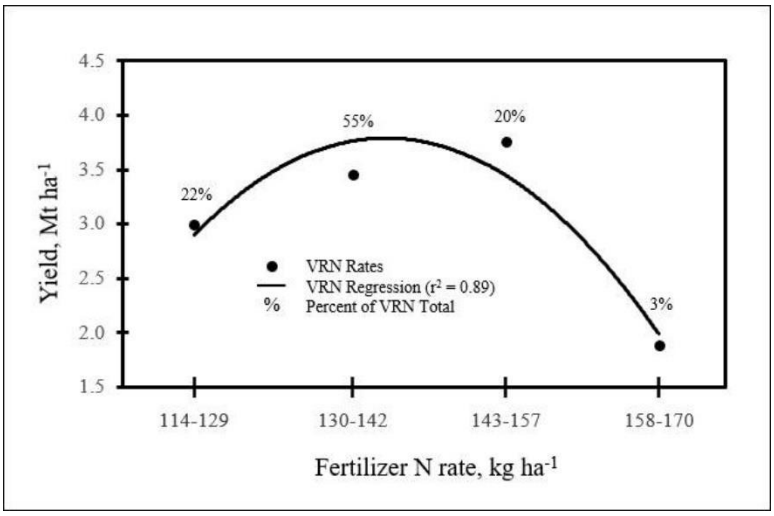

Figure 4.16 2020 corn yield modeled against VRN rates

Percentages indicate the portion of the VRN area that the rate covered

As reported by Figure 4.16, the VRN average highest fertilizer N rate produced 1/3rd the average yield of the fixed-rate N plots. Figure 4.13 displays the locations of the high rate VRN

areas of the plot. All high rate VRN locations exist on the edge of the plot. The edge of the plot was subject to higher winds due to lack of protection from surrounding plants. Figure 4.15 shows the drastic damage that the edge of the plot received.

2020 Cotton Plot North

The 2020 cotton crop sensing flight was performed on July 11, 2020 (Table 4.13). A quad-copter was employed at a speed of 32 km h^{-1} (20 mi hr^{-1}) and altitude of 121.92 m (400 ft) for the flight. Multispectral sensing was conducted by a MSRE aboard the quad-copter. Both fixed- and variable-rate N applications were made on July 15, 2020, using data from the 32 km h^{-1} (20 mi hr^{-1}) flight on July 11. The 2020 cotton plot north N application including both fixed-rate and VRN applications are shown in Figure 4.17.

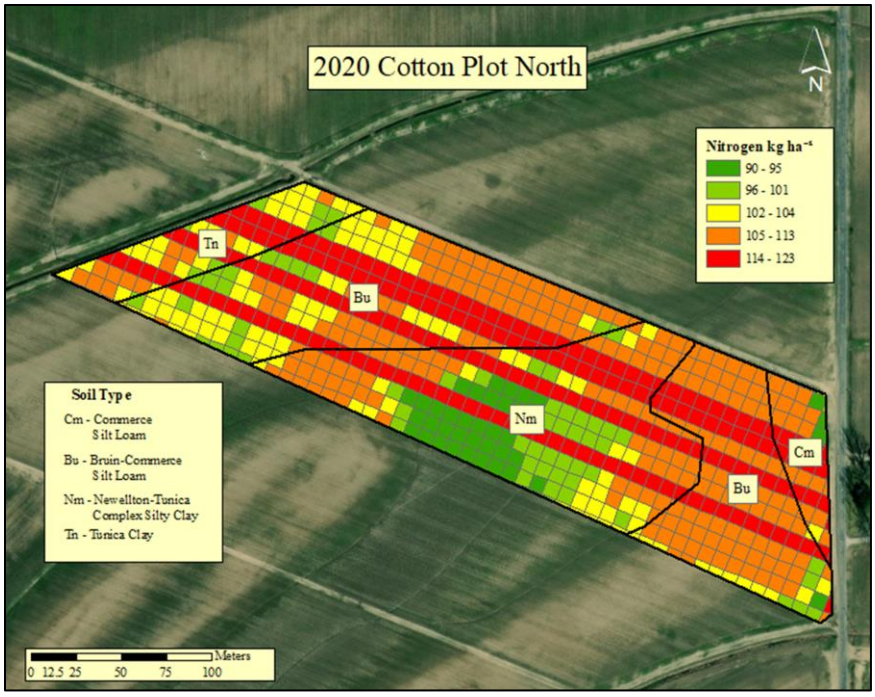

Figure 4.17 2020 cotton plot North N application including both fixed-rate and VRN applications

The soil in this plot was identified as 50% (4.05 ha) Bruin silt (loam coarse-silty, mixed, superactive, thermic, Oxyaquic Eutrudepts), 35% (2.83 ha) Newellton complex (Clayey over loamy, smectitic over mixed, superactive, nonacid, thermic, Fluvaquentic Epiaquepts), 10% (0.81 ha) Tunica clay (Clayey over loamy, smectitic over mixed, superactive, nonacid, thermic, Vertic Epiaquepts), and 5% (0.40 ha) Commerce silt (Fine-silty, mixed, superactive, nonacid, thermic Fluvaquentic Endoaquepts).

The mean N rate was 13.45 kg ha^{-1} (12 lb ac^{-1}) for the VRN application dataset (Figure 4.17). The mode for the VRN dataset was 15.69 kg ha^{-1} (14 lb ac^{-1}). A rate of 14.57 kg ha^{-1} (13 lb ac^{-1}) was found to be the median of the VRN dataset. The total season variable-rate N section of the plot ranged from 89.67 kg ha^{-1} (80 lb ac^{-1}) to 123.29 kg ha^{-1} (110 lb ac^{-1}). Figure 4.18 displays the yield map for the 2020 cotton plot north.

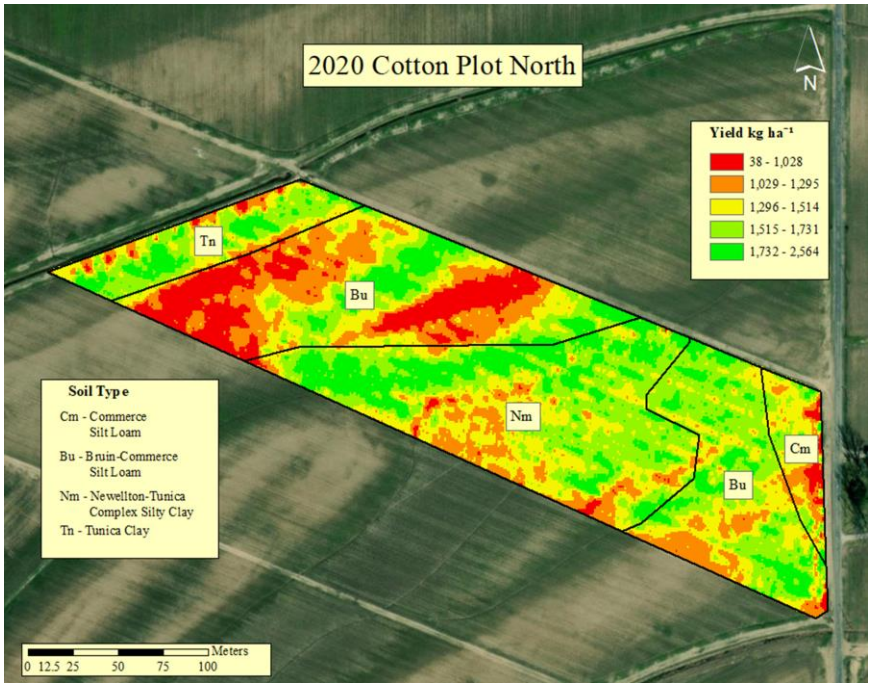

Figure 4.18 2020 cotton plot North yield map

The soil in this plot was identified as 50% (4.05 ha) Bruin silt (loam coarse-silty, mixed, superactive, thermic, Oxyaquic Eutrudepts), 35% (2.83 ha) Newellton complex (Clayey over loamy, smectitic over mixed, superactive, nonacid, thermic, Fluvaquentic Epiaquepts), 10% (0.81 ha) Tunica clay (Clayey over loamy, smectitic over mixed, superactive, nonacid, thermic, Vertic Epiaquepts), and 5% (0.40 ha) Commerce silt (Fine-silty, mixed, superactive, nonacid, thermic Fluvaquentic Endoaquepts).

The overall mean yield for the 2020 cotton plot north was 1,445.89 kg ha^{-1} (1,290 lb ac^{-1}) (Figure 4.18). An average yield of 1,448.14 kg ha^{-1} (1,292 lb ac^{-1}) was observed for the VRN application area of the plot. The fixed-rate application portion of the plot resulted in an average yield of 1,440.29 kg ha^{-1} (1,285 lb ac^{-1}). Table 4.19 depicts the fertilizer N treatment effects on yield and NUE for the 2020 cotton plot north.

Table 4.19 2020 cotton plot North NUE by N rate class

N Rate Class	N Rate by Class (kg ha^{-1})	Yield by N Rate (kg ha^{-1})	N Rate NUE	Total Available NUE	Percentage of Field	Hectares per Class (ha)
VRN Low	0-9	1,419.70	3.03	6.51	12%	1.00
VRN Mod Low	10-17	1,444.73	4.64	6.57	54%	4.39
VRN Mod High	18-26	1,422.63	4.68	7.03	3%	0.21
VRN High	27-34	1,377.65	4.76	6.35	0.1%	0.01
Fixed Rate	34	1,439.36	4.28	6.74	31%	2.48

Refer to Materials and Methods for unit conversions

An increase in yield was evident among an increase in VRN application from 0 kg ha^{-1} (0 lb ac^{-1}) to 17 kg ha^{-1} (15 lb ac^{-1}) (Table 4.19). Once yield peaked at the 10 kg ha^{-1} (9 lb ac^{-1}) to 17 kg ha^{-1} (15 lb ac^{-1}) stage, yield experienced a decrease as VRN application increased from 18 kg ha^{-1} (16 lb ac^{-1}) to 34 kg ha^{-1} (30 lb ac^{-1}). The high yield at the 10 kg ha^{-1} to 17 kg ha^{-1} class may suggest that 10 kg ha^{-1} to 17 kg ha^{-1} class is the optimal rate for cotton N application. Both VRN and total available NUE experienced an increase when VRN application increased from 0 kg ha^{-1} (0 lb ac^{-1}) to 26 kg ha^{-1} (23 lb ac^{-1}). VRN NUE continued to rise as VRN application rates increased to 34 kg ha^{-1} (30 lb ac^{-1}) while total available NUE decreased by 0.68. LSMeans comparison for the 2020 cotton plot south are detailed in Table 4.20.

Table 4.20 2020 cotton plot North Tukey Studentized range of yield means by treatment class

	Yield LSMEAN	Treatment Class
A	1,443.4	1
A		
A	1,439.4	2

LSMeans with same letter are not significantly different
Yield units are kg ha^{-1}
Treatment Classes: VRN Treatment = 1 (Total N application average = 102 kg ha^{-1}).
Fixed-rate Treatment = 2 (Total N applied = 123 kg ha^{-1})

Tukey's studentized range test revealed that the yield for treatment classes one and two were not significantly different (Table 4.20). According to Tukey's studentized range test, VRN treatment class one may be preferred to fixed-rate treatment class two due to lower input of N without a significant loss in yield. Yield for the 2020 cotton plot north modeled against VRN rate is depicted in Figure 4.19.

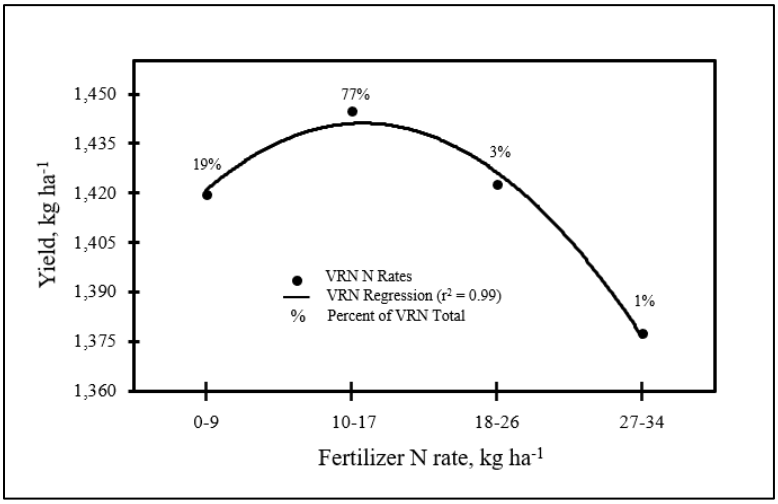

Figure 4.19 2020 cotton plot North yield modeled against VRN rates

Percentages indicate the portion of the VRN area that the rate covered

The final, high rate, VRN class resulted in a 61.71 kg ha^{-1} (55 lb ac^{-1}) lower yield than the fixed-rate N application (Figure 4.19). Edge-effect is a probable cause for the decrease in yield

since all locations for the high rate VRN applications were located on the outer edge of the plot. Future on-farm research should integrate the edge-effect and spatial dynamics related to outer rows and consider possible removal of marginal edge production from results.

The 2020 cotton plot south employed the same platform and payload as the 2020 cotton plot north did (Table 4.15). Fertilizer date and rates for the 2020 cotton plot south are consistent with 2020 cotton plot north. Figure 4.20 depicts the variable- and fixed-rate fertilizer N applications as outlined in Figure 4.16.

Figure 4.20 2020 cotton plot South N application including both fixed-rate and VRN applications

The soil series were identified as 60% (4.86 ha) Bruin silt loam (Coarse-silty, mixed, superactive, thermic, Oxyaquic Eutrudepts) and 40% (3.24 ha) Newellton-Tunica complex (Clayey over loamy, smectitic over mixed, superactive, nonacid, thermic, Fluvaquentic Epiaquepts).

A season total of 123.29 kg ha-1 (110 lb ac-1) was applied for the fixed-rate N amount (Figure 4.20). A rate of 21.29 kg ha^{-1} (19 lb ac^{-1}) was the mean for the VRN application dataset. The mode for the VRN dataset was calculated to be 26.90 kg ha^{-1} (24 lb ac^{-1}). A rate of 23.54 kg ha^{-1} (21 lb ac^{-1}) was found to be the median of the VRN dataset. The variable-rate N section of the plot received a total season amount ranging from 89.67 kg ha^{-1} (80 lb ac^{-1}) to 123.29 kg ha^{-1} (110 lb ac^{-1}). The 2020 cotton plot south yield map is depicted in Figure 4.21.

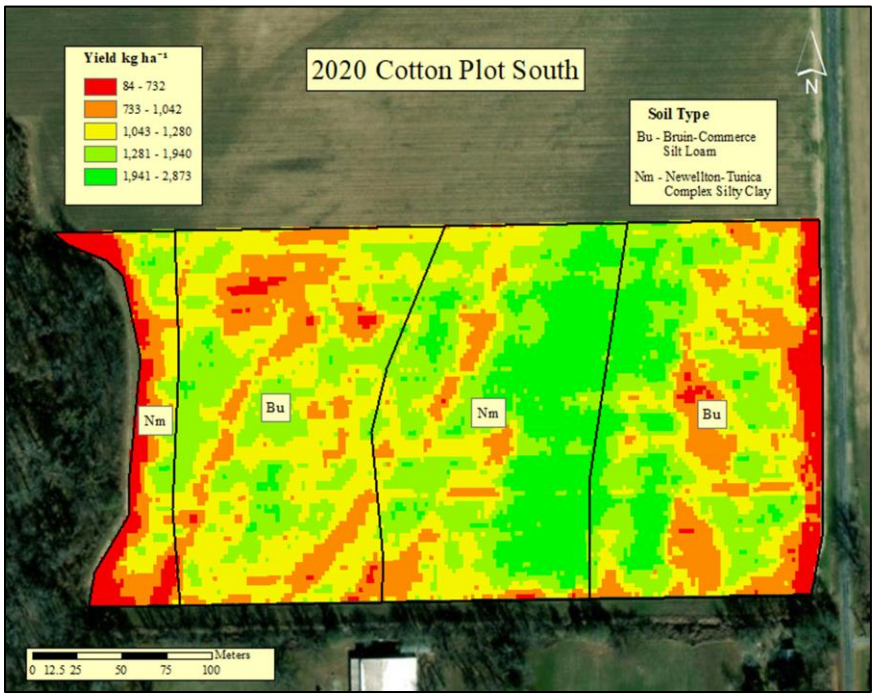

Figure 4.21 2020 cotton plot South yield map

The soil series were identified as 60% (4.86 ha) Bruin silt loam (Coarse-silty, mixed, superactive, thermic, Oxyaquic Eutrudepts) and 40% (3.24 ha) Newellton-Tunica complex (Clayey over loamy, smectitic over mixed, superactive, nonacid, thermic, Fluvaquentic Epiaquepts).

The 2020 cotton plot south attained an overall average yield of 1,173.53 kg ha^{-1} (1,047 lb ac^{-1}) (Figure 4.21). A mean yield of 1,185.86 kg ha^{-1} (1,058 lb ac^{-1}) was noted for the fixed-rate

portion of the plot. The VRN applicated portion of the plot achieved an average yield of 1,163.92 kg ha^{-1} (1,038 lb ac^{-1}). Table 4.21 denotes the fertilizer N treatment effects on yield and NUE in the 2020 cotton plot south.

Table 4.21 2020 cotton plot South NUE by N rate class

N Rate Class	N Rate by Class (kg ha^{-1})	Yield by N Rate (kg ha^{-1})	N Rate NUE	Total Available NUE	Percentage of Field	Hectares per Class (ha)
VRN Low	0-9	1,350.86	2.15	5.97	1%	0.06
VRN Mod Low	9-16	1,343.71	4.90	6.67	4%	0.34
VRN Mod High	17-24	1,203.72	5.68	6.01	24%	1.96
VRN High	25-34	1,149.32	4.46	5.64	28%	2.35
Fixed Rate	34	1,185.86	3.53	5.59	44%	3.63

Refer to Materials and Methods for unit conversions

As VRN application increased from 0 kg ha^{-1} (0 lb ac^{-1}) to 34 kg ha^{-1} (30 lb ac^{-1}), yield decreased from 1350.86 kg ha^{-1} (1205 lb ac^{-1}) to 1149.32 kg ha^{-1} (1025 lb ac^{-1}) (Table 4.21). The reason for the decrease in yield was due to heavy rain from Hurricane Laura. The heavier bolls loaded with N were shed from the plant during the heavy wind and rain (Figure 4.18). The NUE for both VRN and total available sections increased as VRN application increased from 0 kg ha^{-1} (0 lb ac^{-1}) to 16 kg ha^{-1} (14 lb ac^{-1}). The VRN NUE increase corresponded with a decrease in N rate applied as VRN application progressed from 17 kg ha^{-1} (15 lb ac^{-1}) to 34 kg ha^{-1} (30 lb ac^{-1}). Table 4.22 displays the LSMeans comparison for the 2020 cotton plot south.

Table 4.22 2020 cotton plot South Tukey Studentized range of yield means by treatment class

	Yield LSMEAN	Treatment Class
A	1,220.2	1
A		
A	1,215.8	2

LSMeans with same letter are not significantly different
Yield units are kg ha^{-1}
Treatment Classes: VRN Treatment = 1 (Total N application average = 112 kg ha^{-1}).
Fixed-rate Treatment = 2 (Total N applied = 123 kg ha^{-1})

Yield means for treatment classes one and two were not significantly different based on Tukey's studentized range test. Variable rate N treatment class one may be preferred due to the decrease in N input without significantly decreasing yield. Damage to the cotton plot sustained by Hurricane Laura is shown in (Figure 4.22).

Figure 4.22 2020 cotton plot South damage sustained during Hurricane Laura

Photograph depicting bolls laying on ground due to wind and heavy rain

Figure 4.23 depicts the 2020 cotton plot north yield modeled against VRN rates.

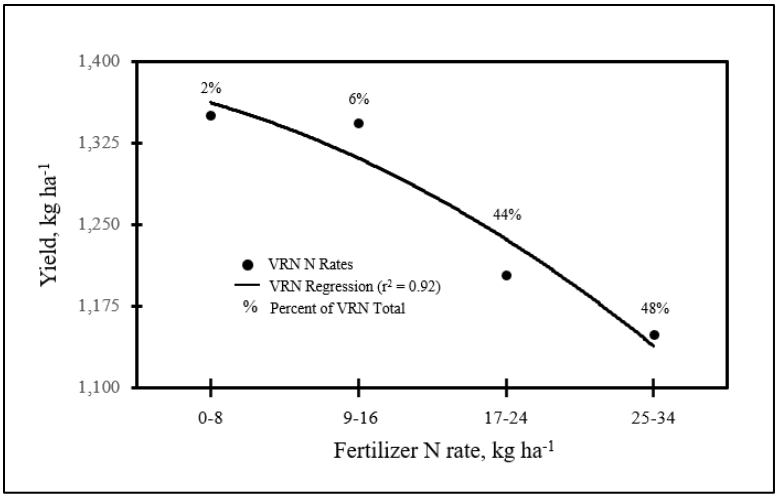

Figure 4.23 2020 cotton plot South yield modeled against VRN rates

Percentages indicate the portion of the VRN area that the rate covered

As fertilizer N rates progressed, yield encountered a drastic decrease for both the VRN applications and the fixed-rate application (Figure 4.23). Hurricane Laura produced a unique scenario where the fixed-rate N application performed poor. The heavy bolls possessed by the plants that received the high N application rate were too cumbersome to remain attached to the plant amidst high winds and heavy rain.

2021 Corn

The 2021 corn crop sensing mission was conducted on May 1, 2021 (Table 4.15). A quad-copter platform was equipped with a MicaSense RedEdge multispectral camera and flown at 32 km h^{-1} (20 mi h^{-1}). Table 4.15 outlines the variable- and fixed-rate applications that are displayed in Figure 4.24.

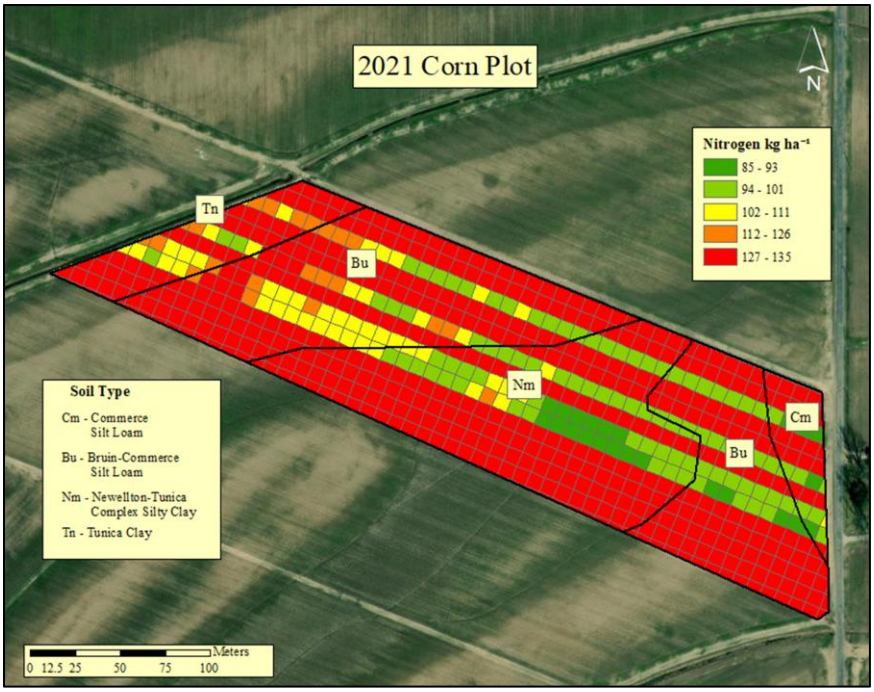

Figure 4.24 2021 corn N application including both fixed-rate and VRN applications

The soil in this plot was identified as 50% (4.05 ha) Bruin silt (loam coarse-silty, mixed, superactive, thermic, Oxyaquic Eutrudepts), 35% (2.83 ha) Newellton complex (Clayey over loamy, smectitic over mixed, superactive, nonacid, thermic, Fluvaquentic Epiaquepts), 10% (0.81 ha) Tunica clay (Clayey over loamy, smectitic over mixed, superactive, nonacid, thermic, Vertic Epiaquepts), and 5% (0.40 ha) Commerce silt (Fine-silty, mixed, superactive, nonacid, thermic Fluvaquentic Endoaquepts).

The season total fixed-rate fertilizer N amount was 302.63 kg ha^{-1} (270 lb ac^{-1}) (Figure 4.24). The mean rate for the VRN application dataset was 102.25 kg ha^{-1} (91 lb ac^{-1}). 96.41 kg ac^{-1} (86 lb ac^{-1}) served as the mode for VRN application dataset. A rate of 99.77 kg ha^{-1} (89 lb ac^{-1}) was discovered to be the median of the VRN application dataset. A season total range of 246 kg ha^{-1} (220 lb ac^{-1}) to 302.63 kg ha^{-1} (270 lb ac^{-1}) was applied to the VRN portion of the plot. Figure 4.25 shows the yield map for the 2021 corn plot.

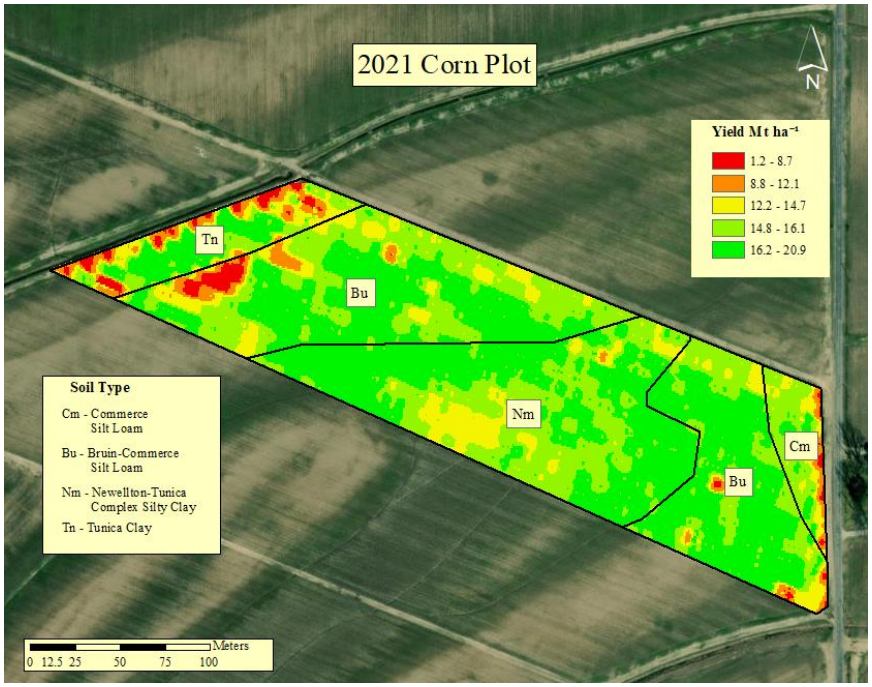

Figure 4.25 2021 corn plot yield map

The soil in this plot was identified as 50% (4.05 ha) Bruin silt (loam coarse-silty, mixed, superactive, thermic, Oxyaquic Eutrudepts), 35% (2.83 ha) Newellton complex (Clayey over loamy, smectitic over mixed, superactive, nonacid, thermic, Fluvaquentic Epiaquepts), 10% (0.81 ha) Tunica clay (Clayey over loamy, smectitic over mixed, superactive, nonacid, thermic, Vertic Epiaquepts), and 5% (0.40 ha) Commerce silt (Fine-silty, mixed, superactive, nonacid, thermic Fluvaquentic Endoaquepts).

An overall average and fixed-rate average yield of 14.66 Mt ha^{-1} (217 bu ac^{-1}) was observed for the 2021 corn plot (Figure 4.25). The VRN application portion of the plot exceeded the overall average with a yield of 14.69 Mt ha^{-1} (218 bu ac^{-1}). Fertilizer N treatment effects on yield and NUE for the 2021 corn plot are denoted in Table 4.23.

Table 4.23 2021 corn plot NUE by N rate class

N Rate Class	N Rate by Class (kg ha^{-1})	Yield by N Rate (Mt ha^{-1})	N Rate NUE	Total Available NUE	Percentage of Field	Hectares per Class (ha)
VRN Low	85-98	14.90	0.15	0.04	13%	1.09
VRN Mod Low	99-110	14.98	0.14	0.04	12%	0.94
VRN Mod High	111-122	15.23	0.13	0.04	4%	0.30
VRN High	123-134	15.16	0.12	0.04	2%	0.13
Fixed Rate	134	15.11	0.12	0.04	70%	5.66

Refer to Materials and Methods for unit conversions

Corn yield increased from 14.90 Mt ha^{-1} (221 bu ac^{-1}) to 15.23 Mt ha^{-1} (226 bu ac^{-1}) as VRN application increased from 85 kg ha^{-1} (75 lb ac^{-1}) to 122 kg ha^{-1} (108 lb ac^{-1}) (Table 4.23). The peak in yield at 15.23 Mt ha^{-1} (226 bu ac^{-1}) may suggest that the VRN application range of 111 kg ha^{-1} (99 lb ac^{-1}) to 122 kg ha^{-1} (108 lb ac^{-1}) is the optimal rate. Furthermore, corn yield decreased as VRN application reached the 123 kg ha^{-1} (110 lb ac^{-1}) to 134 kg ha^{-1} (120 lb ac^{-1}) range. The VRN NUE exhibited a decrease as VRN application increased. Table 4.24 details the 2021 corn plot LSMeans yield comparison.

Table 4.24 2021 Corn plot Tukey Studentized range of yield means by treatment class

	Yield LSMEAN	Treatment Class
A	14.99	1
A		
A	14.66	2

LSMeans with same letter are not significantly different
Yield units are Mt ha^{-1}
Treatment Classes: VRN Treatment = 1 (Total N application average = 270 kg ha^{-1}).
Fixed-rate Treatment = 2 (Total N applied = 303 kg ha^{-1})

Tukey's studentized range test discovered that the yield of treatments one and two were not significantly different (Table 4.24). A difference of 0.33 Mt ha^{-1} separated treatment one from treatment three. Treatment one may be favored to treatment two due to reduced N input

without significant decrease in yield. The 2021 corn plot yield modeled against VRN rates is shown in Figure 4.26.

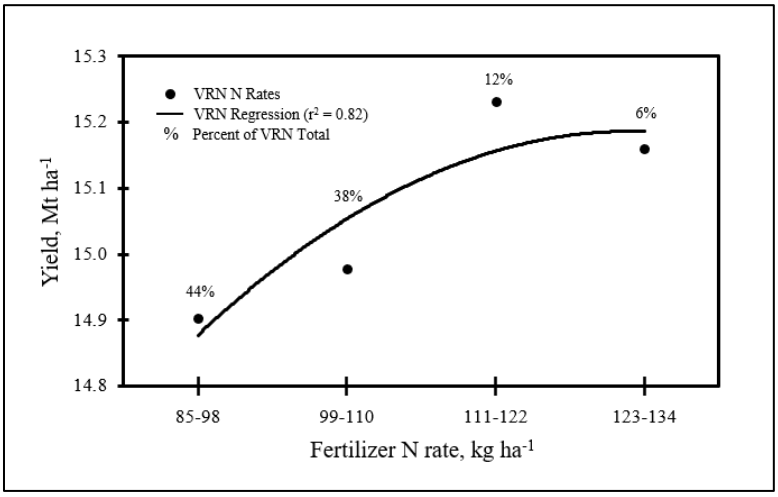

Figure 4.26 2021 corn yield modeled against VRN rates.
Percentages indicate the portion of the VRN area that the rate covered

Yield peaked at 15.23 Mt ha^{-1} (226 bu ac^{-1}) followed by a decline to 15.16 Mt ha^{-1} (225 bu ac^{-1}) (Figure 4.26). The fixed-rate portion of the plot performed lower than the highest VRN application rate at a yield of 15.11 (224 bu ac^{-1}). Edge-effect may be a likely culprit to the decline of yield among the highest VRN application and the fixed-rate application.

2021 Cotton

The crop sensing mission for the 2021 cotton crop was conducted on June 18, 2021 (Table 4.15). A quad-copter platform was equipped with a MicaSense RedEdge multispectral camera and flown at 32 km h^{-1} (20 mi h^{-1}). Table 4.16 notes the variable- and fixed-rate N applications that are mapped in Figure 4.27.

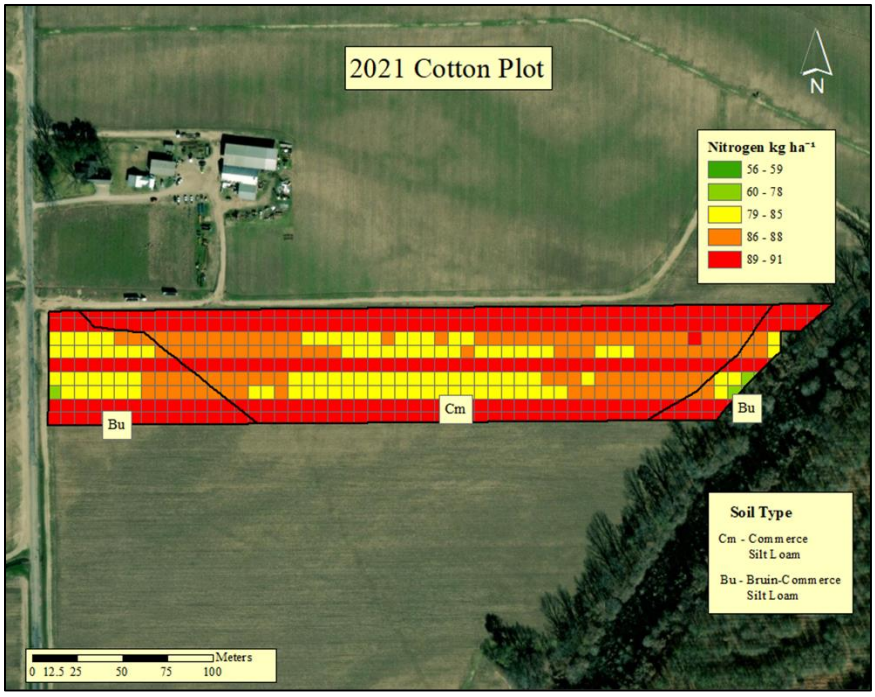

Figure 4.27 2021 cotton N application including both fixed-rate and VRN applications

The soil series consisted of 26% (2.10 ha) Bruin silt loam (Coarse-silty, mixed, superactive, thermic, Oxyaquic Eutrudepts), 71% (5.75 ha) Commerce silt loam (Fine-silty, mixed, superactive, nonacid, thermic Fluvaquentic Endoaquepts), and 3% (0.24 ha) Newellton-Tunica complex (Clayey over loamy, smectitic over mixed, superactive, nonacid, thermic, Fluvaquentic Epiaquepts).

The fixed-rate total season N application that the crop received was 89.67 kg ha^{-1} (80 lb ac^{-1}) (Figure 4.27). A rate of 84.87 kg ha^{-1} (75 lb ac^{-1}) served as the mean for the VRN application dataset. The mode and median for the VRN application dataset were 85.34 kg ha^{-1} (76 lb ac^{-1}). Total season range of the VRN applicated portion of the plot was 56 kg ha^{-1} (50 lb ac^{-1}) to 89.67 kg ha^{-1} (80 lb ac^{-1}).

For the 2020 season, a heavier, early season N treatment of 89.67 kg ha^{-1} (80 lb ac^{-1}) was applied as the starter N rate. The 2021 cotton crop only received a starter N rate of 33.63 kg ha^{-1} (30 lb ac^{-1}). The decrease in VRN application variability for the 2021 season may be linked to a

reduced need for N at pinhead square as a result of the heavier starter N rate. Figure 4.28 depicts the 2021 cotton plot yield map.

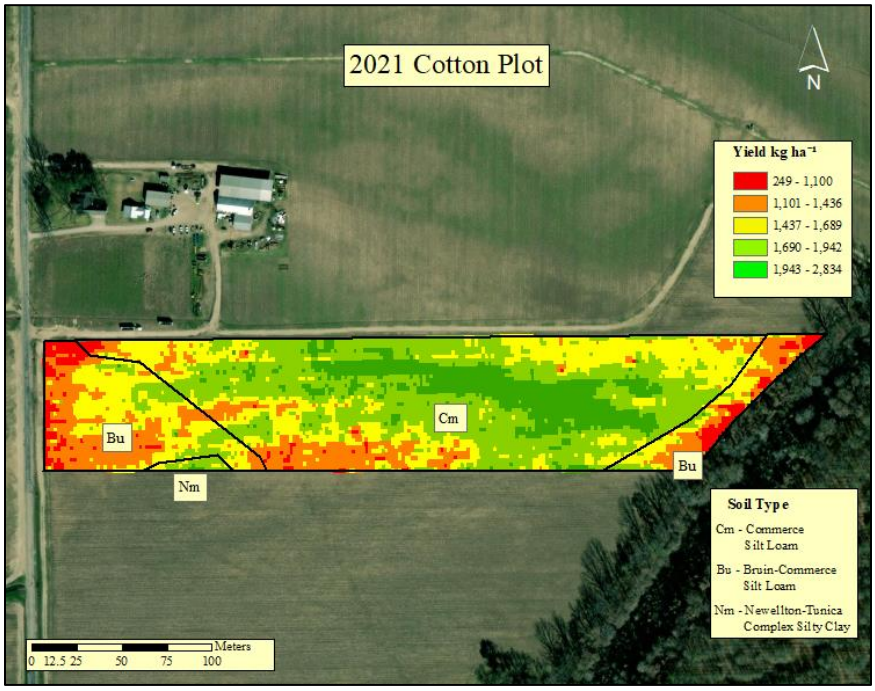

Figure 4.28 2021 cotton plot yield map

The soil series consisted of 26% (2.10 ha) Bruin silt loam (Coarse-silty, mixed, superactive, thermic, Oxyaquic Eutrudepts), 71% (5.75 ha) Commerce silt loam (Fine-silty, mixed, superactive, nonacid, thermic Fluvaquentic Endoaquepts), and 3% (0.24 ha) Newellton-Tunica complex (Clayey over loamy, smectitic over mixed, superactive, nonacid, thermic, Fluvaquentic Epiaquepts).

An overall average yield of 91.93 kg ha^{-1} (1,366 lb ac^{-1}) was noted for the 2021 cotton plot (Figure 4.28). The fixed-rate only portion of the plot achieved a mean yield of 92.66 kg ha^{-1} (1,377 lb ac^{-1}). Plants that received the VRN application achieved an average yield of 91.01 kg ha^{-1} (1,352 lb ac^{-1}). Low topographic field areas are noted to have a significantly reduced yield. Fertilizer N treatment effect on yield and NUE for the 2021 cotton plot is noted in Table 4.25.

Table 4.25 2021 cotton plot NUE by N rate classes

N Rate Class	N Rate by Class (kg ha^{-1})	Yield by N Rate (kg ha^{-1})	N Rate NUE	Total Available NUE	Percentage of Field	Hectares per Class (ha)
VRN Low	73-76	1,586.50	21.41	8.31	0.3%	0.02
VRN Mod Low	77-81	1,645.63	20.61	8.62	0.7%	0.04
VRN Mod High	82-84	1,663.44	19.98	8.08	3%	0.17
VRN High	85-89	1,559.24	18.09	8.31	33%	1.73
Fixed Rate	89	1,542.29	17.21	7.28	63%	3.30

Yield increased from 1586.50 kg ha^{-1} (1415 lb ac^{-1}) to 1663.44 kg ha^{-1} (1483 lb ac^{-1}) as VRN application rate increased from 73 kg ha^{-1} (65 lb ac^{-1}) to 84 kg ha^{-1} (75 lb ac^{-1}) (Table 4.25). A decrease in yield was found as VRN application rate increased from 85 kg ha^{-1} (76 lb ac^{-1}) to 89 kg ha^{-1} (79 lb ac^{-1}). Total available NUE increased from 8.31 to 8.62 with transition from the first VRN application class to the second. After peaking at 8.62, total available NUE decreased as VRN application increased. Variable rate N NUE consistently decreased as VRN application increased from 73 kg ha^{-1} (65 lb ac^{-1}) to 89 kg ha^{-1} (79 lb ac^{-1}). The 2021 LSMeans comparison is displayed in Table 4.26.

Table 4.26 2021 cotton plot Tukey Studentized range of yield means by treatment class.

	Yield LSMEAN	Treatment Class
A	1,543.5	2
A		
A	1,519.6	1

LSMeans with same letter are not significantly different
Yield units are kg ha^{-1}
Treatment Classes: VRN Treatment = 1 (Total N application average = 119 kg ha^{-1}).
Fixed-rate Treatment = 2 (Total N applied = 123 kg ha^{-1})

According to Tukey's studentized range test, treatment classes one and two are not significantly different (Table 4.26). Although class one and two were not significantly different,

fixed-rate treatment class two yielded 23.9 kg ha^{-1} greater than VRN treatment class one. Variable rate N treatment class one may be the preferred rate due to decreased input N without a significant yield loss. 2021 cotton yield modeled against variable- and fixed-rate application rate and is noted in Figure 4.29.

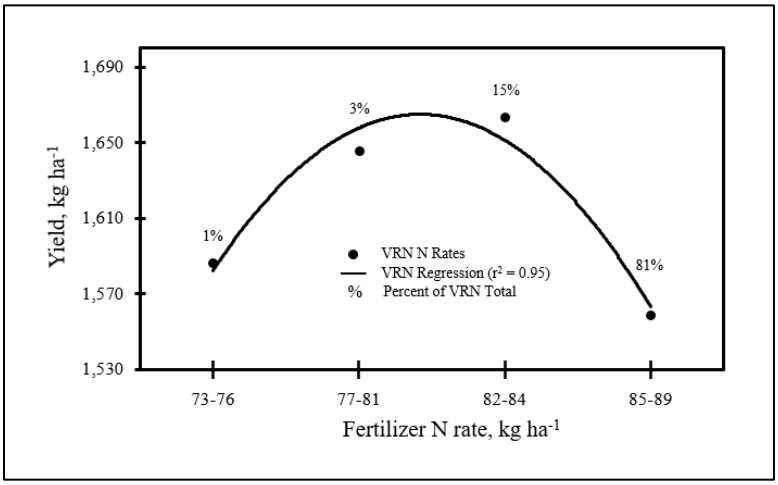

Figure 4.29 2021 cotton yield modeled against VRN rates

Percentages indicate the portion of the VRN area that the rate covered

Yield increased as fertilizer rate increased from 73 kg ha^{-1} (65 lb ac^{-1}) to 84 kg ha^{-1} (75 lb ac^{-1}) (Figure 4.29). A decrease in yield occurred as fertilizer rate increased from 85 kg ha^{-1} (76 lb ac^{-1}) to 89 kg ha^{-1} (79 lb ac^{-1}). The highest VRN application (89 kg ha^{-1} (79 lb ac^{-1})) resulted in an 83 kg ha^{-1} (74 lb ac^{-1}) lower yield than the fixed-rate applied area. The low yield of the final VRN application point may be due to limited sample locations that fell within the highest VRN applied area.

Discussion on Variable Rate N Demonstration Using sUAS

The variable rate N demonstration using sUAS provided insightful results. Variable rate N demonstration data from 2020 and 2021 found that farmers may reduce N input without a significant reduction in yield. Reduced N input would improve sustainability for the future of our crop land and the wildlife that surrounds the land. This study confirmed that sUAS can successfully be used to implement variable rate N practices in an on-farm situation.

Results Conclusions

Through the results of this study, the following is inferred:

1. sUAS sensing mission data provided sufficient evidence suggesting that fixed-wing flight platforms may be successfully deployed to estimate crop canopy N status most effectively, and the results of fixed-wing missions were not significantly different than that of the slower, quad-copter missions.

2. The SCCCI and FENDVI VIs most often were highly related by *SEq* to early corn and cotton canopy N status. In general, compound red-edge VIs outperformed simple slope-based VIs in most cases.

3. The VariRite™ technology was successfully implemented in a producer's field using VI calibrated imagery captured on an sUAS. Deployment of a VRN prescription across corn and cotton provided evidence for reduction of fertilizer N inputs towards the mutual goals of N redistribution and sustained yield.

This concludes the Chapter 4 Results section of this paper.

CHAPTER V

CONCLUSIONS AND RECOMMENDATIONS

The research detailed in the previous sections cultivated many ideas that should be considered for future research. Objective outcomes, issues, and shortcomings in this research, as stated below, must be noted and mitigated in research to come. In a 1675 letter to Robert Hooke, Sir Isaac Newton stated, "If I have seen further, it is by standing on the shoulders of Giants." Researchers are charged to use the past as a steppingstone for the future. Future research must continuously build upon past findings and failures to ensure the advancement of our people. Finding such as the ones listed below should be accounted for and closely considered when performing future research.

Review of Research Results

In this study, the following results were noted:

1. sUAS sensing mission data provided sufficient evidence suggesting that fixed-wing flight platforms may be successfully deployed to estimate crop canopy N status most effectively, and the results of fixed-winged missions were not significantly different than that of the slower, quad-copter missions.

2. The SCCCI and FENDVI VIs most often were highly related by *SEq* to early corn and cotton canopy N status. In general, compound red-edge VIs outperformed simple slope-based VIs in most cases.

3. The VariRite™ technology was successfully implemented in a producer's field using VI calibrated imagery captured on an sUAS. Deployment of a VRN prescription across corn and cotton provided evidence for reduction of fertilizer N inputs towards the mutual goals of N redistribution and sustained yield.

The study results ally with the stated objectives and hypothesis in the deployment of red-edge VIs to assess canopy N status in early corn and cotton will successfully demonstrate the practical utility of reducing fertilizer N applications through remote sensing calibrated re-distribution techniques.

Limitations of On-Farm sUAS Research and Future Recommendations

This study was conducted in a highly variable, on-farm theater in lieu of a highly-constrained and limited-variability research plot array. A primary and limiting issue exposed during the 2020 research was the limited number of soil and *in situ* sample locations. Ample soil and biophysical data sample count should be taken into consideration for future research. Too few of soil sample locations will increase the likelihood of outlying statistical samples being integrated into the soil N dataset. SPAD data collection is problematic and, therefore, necessitates increased sampling to improve relationships with objective leaf N% sample datasets. Noted in this research are outliers occurring in the highly variable on-farm research and must be excluded to ensure accuracy. Increasing sample number may also lead to a better understanding of phenomenon actually occurring in the soil beneath the surface.

Quad-copter "tilt" was also noted as a prominent issue in this research. Tilting of the quad-copter, thus skewing the camera angle, resulted in variable sensitivity equivalents values as speed increased. The implementation of a gimble on a quad-copter platform is proposed for use in future research scenarios. A gimble would allow the sensor to maintain a constant perspective of the ground regardless of quad-copter attitude. Gimble implementation is necessary in future research to resolve data variability due to inconsistent camera angles.

Vegetation indices testing also encountered hurtles that should be addressed in future research. Needed is a SPAD sensor that incorporates the green (550 nm) reflectance band.

Currently, SPAD measures the absorbance in red and NIR wavelengths. Vegetation indices in this study, such as FENDVI stated previously, require a green band incorporated testing tool to determine efficacy of VIs that incorporate the green band. Green band reflectance is indirectly related with canopy N status during photosynthesis, thus, coextended in detectable by SPAD meters (Mutanga and Skidmore, 2004). SPAD, in addition, does not account for red-colored soil albedo detected with sensors above canopy level. SPAD developed with a green band may increase understanding of individual band reflectance's and improve canopy N detection through proximal and sUAS sensing methods.

The red-edge shift relation to canopy leaf N% is an important connection that must be discussed in future research. A 'rubberbanding' effect occurs as reflective bands stretch within the red to NIR region. The stretch among the reflective bands may be linked to increase and decrease of canopy reflectance that correlate canopy N levels. A biochemical phenomenon has not been linked to the lateral red-edge shift that may occur with increased N status and/or availability. Gitelson et al. (1999) proposed the ratio of F737/F700 nm detectable florescence is directly correlated to canopy chlorophyll, and thus, highly relatable to canopy N status. Laboratory research is necessary to decouple red-edge shift from red-to-NIR reflectance decrease and increase. Moreover, research is needed to discover why red-edge is superior in detecting canopy N status. Little, if any, research has been done to dissect the true cause of success among red-edge based indices in canopy N related research.

Final recommendations for this research are to expand the study beyond small plot canopy N status assessment to larger, broader field landscapes using fixed-wing sUAS parallel with continued deployment of the VariRite VRN algorithm. The stated purpose of this research was to reduce N fertilization by redistributing resources to field areas of greater need and

maintaining sustainable yields, although likely not highest attainable yields. Future research is needed to expand the results of the study herein and advance the technologies to ensure the safety of our environment parallel to profitable, sustainable farm production.

This concludes the research results and recommendations for this study.

REFERENCES

Ashburn, P. 1979. The vegetative index number and crop indentification. Proc. Tech. Sess. vols 1 2 lacie Symp. Houston, Oct. 1978,: 843–855. https://www.researchgate.net/publication/24296447_The_vegetative_index_number_and_crop_identification (accessed 24 February 2020).

Associated Press, T. 2021. NOAA: Average-sized "dead zone" likely off Louisiana | AP News. https://apnews.com/article/louisiana-science-environment-and-nature-d1ed9eee3c81e10012cf293295639924 (accessed 20 December 2021).

Ballester, C., J. Hornbuckle, J. Brinkhoff, J. Smith, and W. Quayle. 2017. Assessment of In-Season Cotton Nitrogen Status and Lint Yield Prediction from Unmanned Aerial System Imagery. Remote Sens. 9(11): 1149. doi: 10.3390/rs9111149.

Baret, F., and G. Guyot. 1991. Potentials and limits of vegetation indices for LAI and APAR assessment. Remote Sens. Environ. 35(2–3): 161–173. doi: 10.1016/0034-4257(91)90009-U.

Baret, F., V. Houlès, and M. Guérif. 2007. Quantification of plant stress using remote sensing observations and crop models: the case of nitrogen management. J. Exp. Bot. 58(4): 869–80. doi: 10.1093/jxb/erl231.

Barnes, E., T. Clarke, S. Richards, P. Colaizzi, J. Haberland, et al. 2000. Coincident detection of crop water stress, nitrogen status and canopy density using ground-based multispectral data.

Birth, G.S., and G.R. McVey. 1968. Measuring the Color of Growing Turf with a Reflectance Spectrophotometer 1. Agron. J. 60(6): 640–643. doi: 10.2134/agronj1968.00021962006000060016x.

Boon, M.A., A.P. Drijfhout, and S. Tesfamichael. 2017. Comparison of a fixed-wing and multi-rotor UAV for environmental mapping applications: A case study. International Archives of the Photogrammetry, Remote Sensing and Spatial Information Sciences - ISPRS Archives. International Society for Photogrammetry and Remote Sensing. p. 47–54

Broge, N.H., and E. Leblanc. 2001. Comparing prediction power and stability of broadband and hyperspectral vegetation indices for estimation of green leaf area index and canopy chlorophyll density. Remote Sens. Environ. 76(2): 156–172. doi: 10.1016/S0034-4257(00)00197-8.

Bruckner, M. 2019. NOAA forecasts very large ‘dead zone’ for Gulf of Mexico | National Oceanic and Atmospheric Administration. https://www.noaa.gov/media-release/noaa-forecasts-very-large-dead-zone-for-gulf-of-mexico (accessed 5 March 2020).

Bulanon, D.M., J. Lonai, H. Skovgard, and E. Fallahi. 2016. Evaluation of different irrigation methods for an apple orchard using an aerial imaging system. ISPRS Int. J. Geo-Information 5(6). doi: 10.3390/ijgi5060079.

Byrum, J. 2017. How Remote Sensing Powers Precision Agriculture. AgFunder News. https://agfundernews.com/remote-sensing-powers-precision-agriculture.html (accessed 15 February 2020).

Cammarano, D., G. Fitzgerald, B. Basso, G. O’Leary, D. Chen, et al. 2011. Use of the Canopy Chlorophyl Content Index (CCCI) for remote estimation of wheat nitrogen content in rainfed environments. Agron. J. 103(6): 1597–1603. doi: 10.2134/agronj2011.0124.

Cellania, M. 2010. 10 Ways We Use Corn | Mental Floss. https://www.mentalfloss.com/article/26030/10-ways-we-use-corn (accessed 24 February 2020).

Chaturvedi, A. 2019. Do you know how many satellites are currently orbiting around the Earth? https://www.geospatialworld.net/blogs/do-you-know-how-many-satellites-earth/ (accessed 16 February 2020).

Chen, P. 2019. Cotton Leaf Area Index Estimation Using Unmanned Aerial Vehicle Multi-Spectral Images. International Geoscience and Remote Sensing Symposium (IGARSS). Institute of Electrical and Electronics Engineers Inc. p. 6251–6254

Chen, H., A. Kasterine, M. Lewkowitz, A. MacDonald, and P. Ton. 2005. 5.1-Market Segments-Types of cotton. http://www.cottonguide.org/cotton-guide/market-segments-types-of-cotton/ (accessed 24 February 2020).

Christiano, D. 2017. Blue Baby Syndrome: Causes, Symptoms, and More. https://www.healthline.com/health/blue-baby-syndrome#causes (accessed 5 March 2020).

Ciampitti, I.A., and T.J. Vyn. 2014. Nutrient Sufficiency Concepts for Modern Corn Hybrids: Impacts of Management Practices and Yield Levels. Crop Manag. 13(1): CM-2013-0022-RS. doi: 10.2134/CM-2013-0022-RS.

Clevers, J. 1988. The derivation of a simplified reflectance model for the estimation of LAI. | Request PDF. https://www.researchgate.net/publication/40216025_The_derivation_of_a_simplified_reflectance_model_for_the_estimation_of_LAI (accessed 24 February 2020).

Collins, G. 2017. Tips for Successful Cotton Planting (Collins, Edmisten, York, Reisig, & Crozier) | NC State Extension. https://cotton.ces.ncsu.edu/2017/04/tips-for-successful-cotton-planting-collins-edmisten-york-reisig-crozier/ (accessed 20 December 2021).

Colomina, I., and P. Molina. 2014. Unmanned aerial systems for photogrammetry and remote sensing: A review. ISPRS J. Photogramm. Remote Sens. 92: 79–97. doi: 10.1016/j.isprsjprs.2014.02.013.

Cook, R. 2020. Ranking Of States That Produce The Most Corn - Beef2Live | Eat Beef * Live Better. http://beef2live.com/story-states-produce-corn-0-107129 (accessed 24 February 2020).

Corti, M., D. Cavalli, G. Cabassi, A. Vigoni, L. Degano, et al. 2019. Application of a low-cost camera on a UAV to estimate maize nitrogen-related variables. Precis. Agric. 20(4): 675–696. doi: 10.1007/s11119-018-9609-y.

Diaz, B. 2018. Dead Zones | Virginia Institute of Marine Science. https://www.vims.edu/research/topics/dead_zones/index.php (accessed 5 March 2020).

Dodds, D.., C.. Main, C.. Banks, L.. Barber, R.. Boman, et al. 2010. Utility of Plant Growth Regulation in Cotton Production. Cotton: 8–11. https://www.cottoninc.com/wp-content/uploads/2015/12/Utility-Plant-Growth-Regulation.pdf (accessed 30 October 2020).

Dukowitz, Z. 2019. What Types of Drones Are There? 3 Ways of Looking at Drone Types. https://uavcoach.com/types-of-drones/ (accessed 20 February 2020).

Erisman, J.W., J.N. Galloway, S. Seitzinger, A. Bleeker, N.B. Dise, et al. 2013. Consequences of human modification of the global nitrogen cycle. Philos. Trans. R. Soc. B Biol. Sci. 368(1621). doi: 10.1098/rstb.2013.0116.

Foley, J. 2013. It’s Time to Rethink America’s Corn System - Scientific American. https://www.scientificamerican.com/article/time-to-rethink-corn/ (accessed 3 March 2020).

Fox, A.A. 2015. An integrated approach for predicting nitrogen status in early cotton and corn.

Gitelson, A.A. 2004. Wide Dynamic Range Vegetation Index for Remote Quantification of Biophysical Characteristics of Vegetation. J. Plant Physiol. 161(2): 165–173. doi: 10.1078/0176-1617-01176.

Gitelson, A.A., C. Buschmann, and H.K. Lichtenthaler. 1999. The Chlorophyll Fluorescence Ratio F 735 /F 700 as an Accurate Measure of the Chlorophyll Content in Plants.

Gitelson, A.A., Y.J. Kaufman, and M.N. Merzlyak. 1996. Use of a green channel in remote sensing of global vegetation from EOS- MODIS. Remote Sens. Environ. 58(3): 289–298. doi: 10.1016/S0034-4257(96)00072-7.

Glenn, E.P., C.M.U. Neale, D.J. Hunsaker, and P.L. Nagler. 2011. Vegetation index-based crop coefficients to estimate evapotranspiration by remote sensing in agricultural and natural ecosystems. Hydrol. Process. 25(26): 4050–4062. doi: 10.1002/hyp.8392.

Green, D. 2019. The Future Of Agriculture: Producing More From Less | U.S. Soy. https://ussoy.org/the-future-of-agriculture-producing-more-from-less/ (accessed 5 March 2020).

Haboudane, D., J.R. Miller, E. Pattey, P.J. Zarco-Tejada, and I.B. Strachan. 2004. Hyperspectral vegetation indices and novel algorithms for predicting green LAI of crop canopies: Modeling and validation in the context of precision agriculture. Remote Sens. Environ. 90(3): 337–352. doi: 10.1016/j.rse.2003.12.013.

Herrick, S. 2017. The 3 main categories of drones and their advantages and disadvantages. Botlink: 1. https://botlink.com/blog/the-3-main-categories-of-drones-and-their-advantages-and-disadvantages (accessed 20 February 2020).

Huete, A., C. Justice, and H. Liu. 1994. Development of vegetation and soil indices for MODIS-EOS. Remote Sens. Environ. 49(3): 224–234. doi: 10.1016/0034-4257(94)90018-3.

Igor, I. 2017. How Satellites Are Making Agriculture More Efficient. https://medium.com/remote-sensing-in-agriculture/how-satellites-are-making-agriculture-more-efficient-4b8dc6d443bf (accessed 16 February 2020).

Jarman, M.;Dimmock, J. 2018. Satellites for agriculture 1. : 1–20. https://projectblue.blob.core.windows.net/media/Default/Imported Publication Docs/SatellitesForAgriculture1825_181217_WEB.pdf (accessed 16 February 2020).

Katz, B. 2018. Rethinking the Corny History of Maize | Smart News | Smithsonian Magazine. https://www.smithsonianmag.com/smart-news/rethinking-corny-history-maize-180971038/ (accessed 24 February 2020).

Khot, L.R. 2016. Unmanned aerial systems in agriculture : part 3 (mid-sized uas) unmanned aerial systems in agriculture : part 3 (mid-. 3. http://knowbeforeyoufly.org/. (accessed 20 February 2020).

Khot, L.R., and A. Engineering. 2017. Unmanned aerial systems in agriculture : part 2 (sensors) Unmanned Aerial Systems in Agriculture : Part 2 (Sensors). 2: 1–8. http://pubs.cahnrs.wsu.edu/publications/pubs/fs285e/ (accessed 20 February 2020).

Knobeloch, L., B. Salna, A. Hogan, J. Postle, and H. Anderson. 2000. Blue babies and nitrate-contaminated well water. Environ. Health Perspect. 108(7): 675–678. doi: 10.1289/ehp.00108675.

Lardy, G. 2018. Feeding Corn to Beef Cattle — Publications. https://www.ag.ndsu.edu/publications/livestock/feeding-corn-to-beef-cattle (accessed 4 March 2020).

Larson, E.J., and L. Oldham. 2021. Corn Fertilization. Mississippi State Univ. http://extension.msstate.edu/publications/corn-fertilization (accessed 26 January 2022).

Leslie, R. 2018. Spatial Resolution - an overview (pdf) | ScienceDirect Topics. https://www.sciencedirect.com/topics/earth-and-planetary-sciences/spatial-resolution/pdf (accessed 17 February 2020).

Lewandrowski, J., and B. Hohenstein. 2017. Alternative Fuels Data Center: Ethanol Fuel Basics. https://afdc.energy.gov/fuels/ethanol_fuel_basics.html (accessed 4 March 2020).

Licht, M. 2021. Corn Growth Stages | Integrated Crop Management. : 1–6. https://crops.extension.iastate.edu/encyclopedia/corn-growth-stages (accessed 21 December 2021).

Mai, T. 2015. What are passive and active sensors? https://www.nasa.gov/directorates/heo/scan/communications/outreach/funfacts/txt_passive_active.html (accessed 17 February 2020).

Main, C.L. 2012. Cotton Growth and Development. https://extension.tennessee.edu/publications/Documents/W287.pdf (accessed 20 December 2021).

McConnell, A. 2018. Corn Growing 101 | Successful Farming. https://www.agriculture.com/crops/corn/corn-growing-101 (accessed 24 February 2020).

Meyer, L. 2019. Cotton Sector at a Glance. USDA. https://www.ers.usda.gov/topics/crops/cotton-wool/cotton-sector-at-a-glance/ (accessed 24 February 2020).

MicaSense. 2019. RedEdge Camera Radiometric Calibration Model – MicaSense Knowledge Base. https://support.micasense.com/hc/en-us/articles/115000351194-RedEdge-Camera-Radiometric-Calibration-Model (accessed 17 February 2020).

Moore, B.H. 1981. LACIE and AgRISTARS. Proc. 2nd East. Reg. Remote Sens. Appl. Conf. Danvers, MA, March 1981: 47–50.

Moran, S., G. Fitzgerald, A. Rango, C. Walthall, E. Barnes, et al. 2003. Sensor development and radiometric correction for agricultural applications. Photogramm. Eng. Remote Sensing 69(6): 705–718. doi: 10.14358/PERS.69.6.705.

Mosheim, R. 2019. USDA ERS - Fertilizer Use and Price. https://www.ers.usda.gov/data-products/fertilizer-use-and-price.aspx (accessed 5 March 2020).

Mukherjee, C., H. White, and M. Wuyts. 1998. Econometrics and Data Analysis for Developing Countries - Chandan Mukherjee, Howard White, Marc Wuyts - Google Books. https://books.google.com/books?id=Ib3bAAAAQBAJ&pg=PA145&lpg=PA145&dq=dfbeta+rules&source=bl&ots=pZIbHVSIkF&sig=ACfU3U3R7d9hvk30T7Qag8DD_v_j6AT5tg&hl=en&sa=X&ved=2ahUKEwiIp77utZv1AhXGlmoFHTOgAPQQ6AF6BAgfEAM#v=onepage&q&f=false (accessed 5 January 2022).

Mutanga, O., and A. Skidmore. 2004. Narrow band vegetation indices overcome the saturation problem in biomass estimation. Taylor Fr. doi: 10.1080/01431160310001654923.

Nag, O. 2017. World Leaders In Corn (Maize) Production, By Country - WorldAtlas.com. https://www.worldatlas.com/articles/world-leaders-in-corn-maize-production-by-country.html (accessed 24 February 2020).

Ose, K. 2016. Radiometric Resolution - an overview (pdf) | ScienceDirect Topics. https://www.sciencedirect.com/topics/earth-and-planetary-sciences/radiometric-resolution/pdf (accessed 17 February 2020).

Paiao, G. 2018. Canopy sensing for nitrogen management in corn | Precision Agriculture Center. http://precisionag.umn.edu/canopy-sensing-nitrogen-management-corn (accessed 24 February 2020).

Qi, J., A. Chehbouni, A.R. Huete, Y.H. Kerr, and S. Sorooshian. 1994. A modified soil adjusted vegetation index. Remote Sens. Environ. 48(2): 119–126. doi: 10.1016/0034-4257(94)90134-1.

Raper, T.B., and J.J. Varco. 2014. Canopy-scale wavelength and vegetative index sensitivities to cotton growth parameters and nitrogen status. Precis. Agric. 16(1): 62–76. doi: 10.1007/s11119-014-9383-4.

Raper, T.B., J.J. Varco, and K.J. Hubbard. 2013. Canopy-based normalized difference vegetation index sensors for monitoring cotton nitrogen status. Agron. J. 105(5): 1345–1354. doi: 10.2134/AGRONJ2013.0080.

Richardson, A.J., and C.L. Wiegand. 1977. Distinguishing vegetation from soil background information. [by gray mapping of Landsat MSS data].

Rodriguez, D., G.J. Fitzgerald, R. Belford, and L.K. Christensen. 2006. Detection of nitrogen deficiency in wheat from spectral reflectance indices and basic crop eco-physiological concepts. Aust. J. Agric. Res. 57(7): 781–789. doi: 10.1071/AR05361.

Rondeaux, G., M. Steven, and F. Baret. 1996. Optimization of soil-adjusted vegetation indices. Remote Sens. Environ. 55(2): 95–107. doi: 10.1016/0034-4257(95)00186-7.

Roozeboom, K., and A. Sindelar. 2017. Corn Growth & Development | Corn | Crop Production | Agronomy | Kansas State University. https://www.agronomy.k-state.edu/extension/crop-production/corn/corn-growth-and-development.html (accessed 20 December 2021).

Rouse, J. 1974. Monitoring the vernal advancement and retrogradation (green wave effect) of...: Discovery Service for Mississippi State University. https://eds.b.ebscohost.com/eds/detail/detail?vid=6&sid=c6e4a716-4e83-40b0-9b9b-143eaec33943%40pdc-v-sessmgr05&bdata=JmxvZ2luLmFzcCUzZmN1c3RpZCUzZG1hZ24xMzA3JnNpdGU9ZWRzLWxpdmUmc2NvcGU9c2l0ZQ%3D%3D#AN=edsnas.19740022555&db=edsnas (accessed 24 February 2020).

Samborski, S.M., N. Tremblay, and E. Fallon. 2009. Strategies to make use of plant sensors-based diagnostic information for nitrogen recommendations. Agron. J. 101(4): 800–816. doi: 10.2134/AGRONJ2008.0162RX.

Schmidt, J.P., A.E. Dellinger, and D.B. Beegle. 2009. Nitrogen recommendations for corn: An on-the-go sensor compared with current recommendation methods. Agron. J. 101(4): 916–924. doi: 10.2134/agronj2008.0231x.

Shahbandeh, M. 2018. Cotton - Statistics & Facts | Statista. https://www.statista.com/topics/1542/cotton/ (accessed 23 February 2020).

Sharpe, K. 2019. What Kind of Climate Does the Cotton Plant Require? | Hunker. https://www.hunker.com/12459242/what-kind-of-climate-does-the-cotton-plant-require (accessed 23 February 2020).

Shaver, T.M., R. Khosla, and D.G. Westfall. 2011. Evaluation of two crop canopy sensors for nitrogen variability determination in irrigated maize. Precis. Agric. 12(6): 892–904. doi: 10.1007/s11119-011-9229-2.

Solari, F., J. Shanahan, R.B. Ferguson, J.S. Schepers, A.A. Gitelson, et al. 2008. Active Sensor Reflectance Measurements of Corn Nitrogen Status Active Sensor Reflectance Measurements of Corn Nitrogen Status and Yield Potential and Yield Potential. doi: 10.2134/agronj2007.0244.

Stevens, G. 2019. Cotton Fertility Management | MU Extension. https://extension.missouri.edu/publications/g4256 (accessed 21 December 2021).

Stevens, G. 2020. Plant Growth Regulators for Cotton | MU Extension. https://extension.missouri.edu/g4258/ (accessed 29 October 2020).

Stewart, J., D. Oosterhuis, J. Heitholt, and J. Mauney. 2010. Physiology of Cotton. Physiol. Cott. doi: 10.1007/978-90-481-3195-2.

Sumner, Z., J. Varco, J. Dhillon, A. Fox, J. Czarnecki, et al. 2021. Ground versus aerial canopy reflectance of corn: Red-edge and non-red edge vegetation indices. https://mail.google.com/mail/u/0/#inbox (accessed 16 January 2022).

Taipale, E. 2019. NDVI vs. NDRE: What's the Difference? | Sentera. https://sentera.com/ndvi-vs-ndre-whats-difference/ (accessed 2 March 2020).

Tsouros, D.C., S. Bibi, and P.G. Sarigiannidis. 2019. A review on UAV-based applications for precision agriculture. Inf. 10(11). doi: 10.3390/info10110349.

Tu. 2002. NDVI and ENDVI. Situ. https://maxmax.com/maincamerapage/remote-sensing/enhanced-normalized-difference-vegetation-index/ndvi-and-endvi (accessed 1 March 2020).

UCS. 2021. Satellite Database | Union of Concerned Scientists. https://www.ucsusa.org/resources/satellite-database (accessed 21 December 2021).

USDA Quick Stats. 2019. Mississippi Agriculture Overview | Mississippi Department of Agriculture and Commerce. https://www.mdac.ms.gov/agency-info/mississippi-agriculture-snapshot/ (accessed 24 February 2020).

Varco, J.J., A.A. Fox, T.B. Raper, and K.J. Hubbard. 2013. Development of sensor based detection of crop nitrogen status for utilization in variable rate nitrogen fertilization. : 145–150. doi: 10.3920/978-90-8686-778-3_16.

Viña, A., and A.A. Gitelson. 2005. New developments in the remote estimation of the fraction of absorbed photosynthetically active radiation in crops. Geophys. Res. Lett. 32(17): 1–4. doi: 10.1029/2005GL023647.

Watson, J. 2019. Agriculture Drones Market To Reach USD 6.52 Billion By 2026 | Reports And Data. https://www.globenewswire.com/news-release/2019/07/10/1881014/0/en/Agriculture-Drones-Market-To-Reach-USD-6-52-Billion-By-2026-Reports-And-Data.html (accessed 18 February 2020).

Weigmann, H. 2020. cotton | Description, History, Production, Uses, & Facts | Britannica. https://www.britannica.com/topic/cotton-fibre-and-plant (accessed 24 February 2020).

Wendel, J.F., C.L. Brubaker, and T. Seelanan. 2010. The Origin and Evolution of Gossypium. Physiology of Cotton. Springer Netherlands. p. 1–18

Wickison, M. 2019. The Many Ways We Use Cottonseeds | Owlcation. https://owlcation.com/agriculture/cottonseed-oil (accessed 24 February 2020).

Worcester, M. 2017. Why Cotton Is Used in Clothing. https://oureverydaylife.com/why-cotton-is-used-in-clothing-12197443.html (accessed 24 February 2020).

Workman, D. 2019. Corn Exports by Country. http://www.worldstopexports.com/corn-exports-country/ (accessed 24 February 2020).

Xiong, D., J. Chen, T. Yu, W. Gao, X. Ling, et al. 2015. SPAD-based leaf nitrogen estimation is impacted by environmental factors and crop leaf characteristics. Sci. Reports 2015 51 5(1): 1–12. doi: 10.1038/srep13389.

Xu, M., R. Liu, J.M. Chen, Y. Liu, R. Shang, et al. 2019. Retrieving leaf chlorophyll content using a matrix-based vegetation index combination approach. Remote Sens. Environ. 224: 60–73. doi: 10.1016/j.rse.2019.01.039.

YANG, F., J. HUANG, Y. TANG, and X. WANG. 2007. New Vegetation Index and Its Application in Estimating Leaf Area Index of Rice. Rice Sci. 14(3): 195–203. doi: 10.1016/s1672-6308(07)60027-4.

Yinka-Banjo, C., and O. Ajayi. 2019. Sky-Farmers: Applications of Unmanned Aerial Vehicles (UAV) in Agriculture. Unmanned Aerial Vehicles [Working Title]. IntechOpen

APPENDIX A

RESEARCH PHOTOGRAPHS

Figure A.1 2020 corn crop at V4 stage

Figure A.2 2020 corn crop at V4 stage in field

Figure A.3 2020 cotton plot north at pinhead square stage

Figure A.4 2020 cotton plot north receiving VRN application

Figure A.5 2020 cotton plot south at mid bloom stage

Figure A.6 2020 cotton plot south post-Hurricane Laura

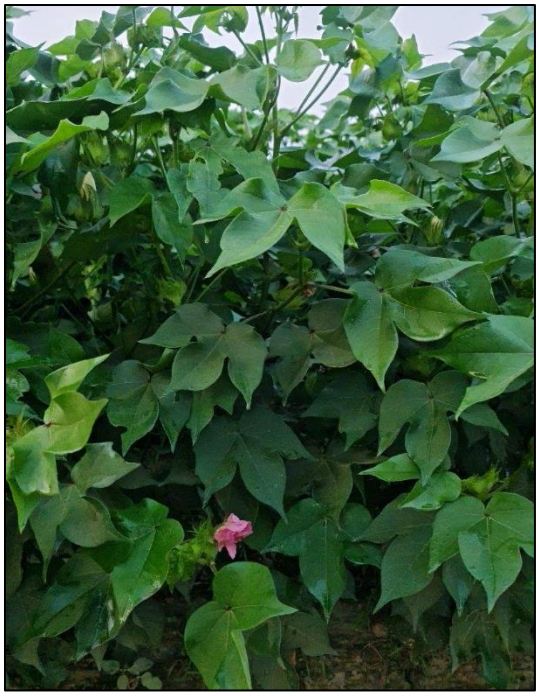

Figure A.7 2021 cotton plot at boll development stage

Figure A.8 2021 cotton plot ready to be harvested

Figure A.9 Quad-copter platform used in this study

Measures .65 m (2.13 ft) across

Figure A.10 Fixed-wing platform used in this study

Wingspan is 2.06 m (6.76 ft)

APPENDIX B

SAS CODE FOR ANALYSIS

```
OPTION PS=55 LS=85 NODATE;
DATA VIs;
INFILE '****';
INPUT Num SOM SNO3 SNH4 LN LNO3 SPAD NDVI GNDVI NDRE SCCCI FENDVI BENDVI
SCCCI2;
RUN;
PROC REG;
MODEL NDVI = LN;
RUN;
QUIT;
PROC REG;
MODEL GNDVI = LN;
RUN;
QUIT;
PROC REG;
MODEL NDRE = LN;
RUN;
QUIT;
PROC REG;
MODEL SCCCI = LN;
RUN;
QUIT;
PROC REG;
MODEL FENDVI = LN;
RUN;
QUIT;
PROC REG;
MODEL BENDVI = LN;
RUN;
QUIT;
```

Figure B.1 SAS code used for all datasets VI comparison to LN for *SEq* calculations

```
OPTION PS=55 LS=85 NODATE;
DATA VIs;
INFILE '****';
INPUT Num SOM SNO3 SNH4 LN LNO3 SPAD NDVI GNDVI NDRE SCCCI FENDVI BENDVI
SCCCI2;
RUN;
PROC REG;
MODEL NDVI = SPAD;
RUN;
QUIT;
PROC REG;
MODEL GNDVI = SPAD;
RUN;
QUIT;
PROC REG;
MODEL NDRE = SPAD;
RUN;
QUIT;
PROC REG;
MODEL SCCCI = SPAD;
RUN;
QUIT;
PROC REG;
MODEL FENDVI = SPAD;
RUN;
QUIT;
PROC REG;
MODEL BENDVI = SPAD;
RUN;
QUIT;
```

Figure B.2 SAS code used for all datasets VI comparison to SPAD for SEq calculations

Table B.2 DFBetas test on 2020 corn quad data conducted in SAS for Leaf N

Output Statistics							
Obs	Residual	RStudent	Hat Diag H	Cov Ratio	DFFITS	DFBETAS	
						Intercept	LN
1	-0.0152	-1.8384	0.1283	0.5881	-0.7052	0.0647	-0.1125
2	0.0064	0.6219	0.1283	1.4232	0.2385	-0.0219	0.0380
3	-0.0043	-0.6385	0.6152	3.1996	-0.8074	0.6942	-0.7207
4	-0.0110	-1.3240	0.2848	1.1039	-0.8356	-0.6622	0.6259
5	0.0093	0.9667	0.1558	1.2108	0.4153	-0.1589	0.1847
6	-0.0001	-0.0124	0.1266	1.6487	-0.0047	0.0002	-0.0005
7	0.0027	0.3252	0.4298	2.4220	0.2824	0.2476	-0.2378
8	0.0122	1.3274	0.1311	0.9062	0.5157	0.1455	-0.1115

```
OPTION PS=55 LS=85 NODATE;
DATA VIs;
INPUT LN SCCCI;
 X1 = 'LN';
      Y = 'SCCCI';
      Cards;
3.71 0.563844825
3.84 0.564979426
3.21 0.560055286
3.38 0.526104882
3.6 0.582152638
3.47 0.58226504
3.39 0.560443916
3.37 0.573725916
;
RUN;
ODS HTML STYLE = STATISTICAL;
ODS GRAPHICS ON;
PROC REG DATA = VIs;
MODEL SCCCI = LN / INFLUENCE;
OUTPUT OUT = TEMP1 COOKD = COOKSD P = YHAT R = RESID;
RUN;
QUIT;
PROC PRINT DATA = TEMP1;
RUN;
AXIS1 ORDER = (0.35 to 0.45 by 0.01);
AXIS2 ORDER = (-0.05 to 0.05 by 0.01) label = (angle=90 h=1 color = black
'Studentized Resid');
PROC GPLOT DATA = TEMP1;
BUBBLE RESID*YHAT = COOKSD / HAXIS = AXIS1 VAXIS = AXIS2 bsize = 10 hminor =
0 VREF = 0;
LABEL RESID = 'Studentized Residuals';
LABEL YHAT = 'YHAT';
RUN;
QUIT;
PROC REG DATA = VIs PLOTS = (dfbetas dffits);
      model LN = SCCCI;
RUN;
QUIT;

ODS GRAPHICS OFF;

ODS HTML CLOSE;
```

Figure B.3 SAS code used for all LN DFBetas tests

Table B.3 DFBetas test on 2020 corn quad data conducted in SAS for SPAD

Output Statistics							
Obs	Residual	RStudent	Hat Diag H	Cov Ratio	DFFITS	DFBETAS	
						Intercept	SPAD
1	-0.0088	-1.6647	0.1575	0.7076	-0.7199	-0.3689	0.3271
2	0.0057	0.9211	0.1291	1.2086	0.3547	-0.0401	0.0634
3	-0.0047	-0.9088	0.3919	1.7443	-0.7296	0.5735	-0.6021
4	-0.0004	-0.0970	0.5570	3.2384	-0.1088	-0.0990	0.0958
5	0.0041	0.6745	0.2203	1.5517	0.3585	-0.2175	0.2358
6	-0.0056	-0.9383	0.1748	1.2616	-0.4318	0.2058	-0.2305
7	0.0011	0.1819	0.2401	1.8703	0.1023	0.0755	-0.0708
8	0.0087	1.5908	0.1291	0.7289	0.6125	-0.0693	0.1094

```
OPTION PS=55 LS=85 NODATE;
DATA VIs;
INPUT SPAD SCCCI;
 X1 = 'SPAD';
      Y = 'SCCCI';
      Cards;
43.8 0.563844825
47.5 0.564979426
45.3 0.560055286
39.8 0.526104882
45.5 0.582152638
45.2 0.58226504
43 0.560443916
44.6 0.573725916
;
RUN;
ODS HTML STYLE = STATISTICAL;
ODS GRAPHICS ON;
PROC REG DATA = VIs;
MODEL SCCCI = SPAD / INFLUENCE;
OUTPUT OUT = TEMP1 COOKD = COOKSD P = YHAT R = RESID;
RUN;
QUIT;
PROC PRINT DATA = TEMP1;
RUN;
AXIS1 ORDER = (0.35 to 0.45 by 0.01);
AXIS2 ORDER = (-0.05 to 0.05 by 0.01) label = (angle=90 h=1 color = black
'Studentized Resid');
PROC GPLOT DATA = TEMP1;
BUBBLE RESID*YHAT = COOKSD / HAXIS = AXIS1 VAXIS = AXIS2 bsize = 10 hminor =
0 VREF = 0;
LABEL RESID = 'Studentized Residuals';
LABEL YHAT = 'YHAT';
RUN;
QUIT;
PROC REG DATA = VIs PLOTS = (dfbetas dffits);
      model SPAD = SCCCI;
RUN;
QUIT;

ODS GRAPHICS OFF;
ODS HTML CLOSE;
```

Figure B.4 SAS code used for all SPAD DFBetas tests

Table B.4 DFBetas test on 2020 cotton north quad data conducted in SAS for Leaf N

Output Statistics							
Obs	Residual	RStudent	Hat Diag H	Cov Ratio	DFFITS	DFBETAS	
						Intercept	LN
1	0.0079	0.1997	0.1267	1.6230	0.0761	-0.0028	0.0089
2	0.0274	0.7416	0.1791	1.4238	0.3465	-0.1667	0.1905
3	0.0071	0.1799	0.1277	1.6296	0.0688	-0.0044	0.0099
4	0.0249	0.6585	0.1620	1.4551	0.2896	-0.1176	0.1384
5	-0.0369	-1.1519	0.2962	1.2779	-0.7473	0.5274	-0.5682
6	-0.0000	-0.0025	0.8544	9.8871	-0.0062	-0.0059	0.0057
7	-0.0697	-2.7555	0.1285	0.2605	-1.0581	-0.2576	0.1745
8	0.0392	1.0831	0.1254	1.0801	0.4100	0.0546	-0.0218

Table B.5 DFBetas test on 2020 cotton north quad data conducted in SAS for SPAD

Output Statistics							
Obs	Residual	RStudent	Hat Diag H	Cov Ratio	DFFITS	DFBETAS	
						Intercept	SPAD
1	0.0059	0.1522	0.1407	1.6603	0.0616	0.0223	-0.0206
2	0.0202	0.6017	0.3283	1.8640	0.4206	0.3385	-0.3310
3	0.0084	0.2155	0.1306	1.6261	0.0835	-0.0150	0.0174
4	0.0246	0.6460	0.1256	1.4029	0.2449	0.0245	-0.0173
5	-0.0416	-1.2757	0.2153	1.0445	-0.6683	-0.4476	0.4329
6	-0.0051	-0.1370	0.2009	1.7886	-0.0687	-0.0438	0.0422
7	-0.0611	-3.3756	0.4017	0.2238	-2.7657	2.2491	-2.2954
8	0.0486	2.1729	0.4569	0.7013	1.9929	-1.6672	1.6985

Table B.6 DFBetas test on 2020 cotton south quad data conducted in SAS for Leaf N

Output Statistics							
Obs	Residual	RStudent	Hat Diag H	Cov Ratio	DFFITS	DFBETAS	
						Intercept	LN
1	-0.0049	-0.2869	0.2783	1.9313	-0.1781	0.1254	-0.1322
2	-0.0065	-0.4770	0.5215	2.7534	-0.4980	0.4202	-0.4343
3	0.0019	0.1265	0.4000	2.3846	0.1033	0.0887	-0.0857
4	-0.0356	-3.6991	0.1704	0.1243	-1.6762	-0.9427	0.8649
5	0.0157	0.9076	0.1611	1.2653	0.3978	-0.1687	0.1883
6	0.0186	1.0856	0.1273	1.0807	0.4146	0.0784	-0.0559
7	-0.0014	-0.0789	0.1629	1.7159	-0.0348	-0.0184	0.0168
8	0.0122	0.6920	0.1785	1.4598	0.3226	0.1912	-0.1766

Table B.7 DFBetas test on 2020 cotton south quad data conducted in SAS for SPAD

Output Statistics							
Obs	Residual	RStudent	Hat Diag H	Cov Ratio	DFFITS	DFBETAS	
						Intercept	SPAD
1	0.0028	0.2293	0.1331	1.6267	0.0899	0.0263	-0.0221
2	-0.0183	-2.7803	0.4047	0.3731	-2.2924	1.8429	-1.9058
3	-0.0099	-0.8489	0.1509	1.2955	-0.3579	0.1326	-0.1483
4	-0.0107	-1.8939	0.7008	1.6316	-2.8984	-2.6825	2.6272
5	0.0110	0.9577	0.1628	1.2281	0.4223	-0.1856	0.2035
6	0.0129	1.1525	0.1458	1.0524	0.4762	-0.1587	0.1799
7	0.0043	0.3532	0.1750	1.6616	0.1627	0.0934	-0.0870
8	0.0079	0.6517	0.1269	1.4012	0.2485	-0.0188	0.0306

Table B.8 DFBetas test on 2021 corn quad data conducted in SAS for Leaf N

Output Statistics							
Obs	Residual	RStudent	Hat Diag H	Cov Ratio	DFFITS	DFBETAS	
						Intercept	LN
1	0.0150	0.3973	0.0550	1.1442	0.0959	-0.0385	0.0473
2	0.0465	1.2936	0.0787	1.0219	0.3780	-0.2297	0.2592
3	0.0001	0.0048	0.0528	1.1587	0.0011	-0.0004	0.0005
4	0.0747	2.1732	0.0440	0.7651	0.4660	0.1525	-0.1065
5	0.0289	0.7705	0.0441	1.0859	0.1655	-0.0221	0.0388
6	-0.0576	-1.6576	0.0961	0.9495	-0.5404	0.3680	-0.4067
7	0.0077	0.2036	0.0417	1.1408	0.0425	0.0058	-0.0015
8	-0.0525	-1.6943	0.2794	1.1788	-1.0551	-1.0099	0.9732
9	-0.0510	-1.5645	0.2147	1.1211	-0.8182	-0.7676	0.7345
10	-0.0196	-0.5192	0.0417	1.1165	-0.1083	-0.0067	-0.0044
11	-0.0629	-1.9000	0.1508	0.9411	-0.8008	-0.6345	**0.6812**
12	-0.0544	-1.5087	0.0465	0.9369	-0.3332	0.0747	-0.1076
13	-0.0150	-0.4028	0.0712	1.1636	-0.1115	0.0627	-0.0719
14	-0.0024	-0.0639	0.0627	1.1705	-0.0165	-0.0109	0.0096
15	0.0115	0.3132	0.1107	1.2226	0.1105	0.0937	-0.0872
16	0.0223	0.5901	0.0431	1.1098	0.1252	0.0352	-0.0227
17	0.0241	0.6937	0.1824	1.2829	0.3276	0.3023	-0.2878
18	0.0195	0.5181	0.0536	1.1306	0.1233	0.0690	-0.0582
19	0.0239	0.6384	0.0517	1.1137	0.1491	-0.0517	0.0658
20	0.0277	0.7379	0.0428	1.0894	0.1561	-0.0096	0.0255
21	0.0300	0.8043	0.0550	1.0931	0.1941	-0.0779	0.0957
22	0.0198	0.5232	0.0428	1.1173	0.1107	-0.0068	0.0181
23	0.0122	0.3235	0.0616	1.1580	0.0829	-0.0399	0.0472
24	-0.0483	-1.3461	0.0767	1.0074	-0.3880	0.2316	-0.2623

Table B.9 DFBetas test on 2021 corn quad data conducted in SAS for SPAD

Output Statistics							
Obs	Residual	RStudent	Hat Diag H	Cov Ratio	DFFITS	DFBETAS	
						Intercept	SPAD
1	0.0043	0.1665	0.0524	1.1551	0.0391	-0.0161	0.0177
2	0.0260	1.0343	0.0791	1.0791	0.3032	-0.1983	0.2086
3	-0.0014	-0.0562	0.0428	1.1462	-0.0119	0.0014	-0.0019
4	0.0361	1.5121	0.1221	1.0168	0.5640	-0.4421	0.4578
5	0.0099	0.3856	0.0652	1.1576	0.1019	-0.0574	0.0612
6	-0.0389	-1.5711	0.0510	0.9260	-0.3643	-0.1711	0.1561
7	-0.0020	-0.0799	0.0471	1.1510	-0.0178	0.0052	-0.0060
8	-0.0300	-1.2269	0.1130	1.0773	-0.4378	-0.3597	0.3478
9	-0.0491	-2.0561	0.0510	0.8014	-0.4768	-0.2239	0.2043
10	-0.0212	-0.8187	0.0418	1.0757	-0.1711	0.0033	-0.0112
11	-0.0324	-1.3007	0.0695	1.0102	-0.3555	-0.2375	0.2250
12	-0.0188	-0.7520	0.1077	1.1663	-0.2613	-0.2119	0.2046
13	-0.0031	-0.1193	0.0449	1.1475	-0.0259	-0.0081	0.0069
14	0.0158	0.6150	0.0695	1.1381	0.1681	0.1123	-0.1064
15	0.0556	2.6626	0.1915	0.7588	1.2960	1.1731	-1.1465
16	0.0130	0.4966	0.0457	1.1235	0.1087	-0.0274	0.0322
17	-0.0216	-0.8704	0.1166	1.1573	-0.3162	0.2444	-0.2534
18	-0.0088	-0.3428	0.0791	1.1786	-0.1005	0.0657	-0.0691
19	0.0222	0.8579	0.0428	1.0702	0.1814	-0.0210	0.0293
20	0.0110	0.4258	0.0595	1.1470	0.1071	-0.0544	0.0586
21	-0.0202	-0.8568	0.2047	1.2884	-0.4348	0.3786	-0.3880
22	0.0123	0.4721	0.0457	1.1260	0.1033	-0.0261	0.0306
23	0.0325	1.2955	0.0578	0.9987	0.3207	0.1816	-0.1693
24	0.0088	0.3680	0.1994	1.3533	0.1836	0.1670	-0.1633

Table B.10 DFBetas test on 2021 cotton quad data conducted in SAS for Leaf N

Output Statistics							
Obs	Residual	RStudent	Hat Diag H	Cov Ratio	DFFITS	DFBETAS	
						Intercept	LN
1	0.0110	0.9475	0.0945	1.1148	0.3062	0.2427	-0.2290
2	0.0013	0.1114	0.0501	1.1541	0.0256	0.0121	-0.0105
3	-0.0142	-1.2114	0.0510	1.0104	-0.2809	0.1023	-0.1204
4	-0.0050	-0.4317	0.1003	1.1984	-0.1441	0.1034	-0.1102
5	-0.0025	-0.2204	0.1075	1.2240	-0.0765	0.0564	-0.0599
6	0.0048	0.4053	0.0902	1.1876	0.1276	-0.0873	0.0936
7	0.0042	0.3559	0.1003	1.2052	0.1188	-0.0852	0.0908
8	0.0026	0.2334	0.1649	1.3074	0.1037	-0.0858	0.0896
9	-0.0041	-0.3384	0.0453	1.1372	-0.0737	0.0159	-0.0210
10	-0.0037	-0.3085	0.0417	1.1349	-0.0643	-0.0060	0.0015
11	-0.0135	-1.1419	0.0477	1.0216	-0.2555	-0.1072	0.0906
12	-0.0296	-2.8960	0.0621	0.5975	-0.7450	-0.4688	0.4271
13	6.6809	0.0005	0.0428	1.1466	0.0001	0.0000	-0.0000
14	-0.0041	-0.3449	0.0530	1.1459	-0.0816	-0.0427	0.0378
15	-0.0036	-0.2972	0.0466	1.1415	-0.0657	-0.0257	0.0214
16	-0.0232	-2.0957	0.0488	0.7892	-0.4749	-0.2124	0.1820
17	0.0048	0.4042	0.0621	1.1521	0.1040	0.0654	-0.0596
18	0.0132	1.1173	0.0510	1.0304	0.2591	-0.0944	0.1111
19	0.0081	0.6851	0.0704	1.1295	0.1885	-0.1099	0.1204
20	0.0062	0.5232	0.0614	1.1394	0.1338	-0.0679	0.0758
21	0.0185	1.6234	0.0594	0.9211	0.4079	-0.1983	0.2229
22	0.0012	0.1002	0.0664	1.1745	0.0267	0.0178	-0.0163
23	0.0043	0.4307	0.3357	1.6232	0.3061	0.2934	-0.2865
24	0.0232	2.2441	0.1469	0.8369	0.9311	0.8209	-0.7881

Table B.11 DFBetas test on 2021 cotton quad data conducted in SAS for Leaf N

Output Statistics							
Obs	Residual	RStudent	Hat Diag H	Cov Ratio	DFFITS	DFBETAS	
						Intercept	SPAD
1	0.0144	1.3126	0.2179	1.1985	0.6928	-0.6007	0.6231
2	0.0029	0.2378	0.1083	1.2242	0.0829	0.0684	-0.0650
3	-0.0157	-1.3178	0.0861	1.0245	-0.4044	-0.3092	0.2905
4	-0.0090	-0.7766	0.1704	1.2501	-0.3520	0.2932	-0.3059
5	-0.0065	-0.5279	0.0729	1.1530	-0.1481	-0.1044	0.0970
6	0.0012	0.1031	0.0801	1.1919	0.0304	-0.0195	0.0211
7	0.0004	0.0339	0.0429	1.1465	0.0072	0.0017	-0.0012
8	-0.0028	-0.2295	0.0564	1.1573	-0.0561	0.0253	-0.0287
9	-0.0048	-0.4332	0.2364	1.4119	-0.2410	-0.2252	0.2187
10	-0.0036	-0.2909	0.0421	1.1366	-0.0610	-0.0104	0.0062
11	-0.0124	-1.0192	0.0775	1.0802	-0.2954	0.1855	-0.2009
12	-0.0274	-2.4515	0.0424	0.6928	-0.5157	0.0311	-0.0665
13	0.0005	0.0404	0.0453	1.1494	0.0088	-0.0019	0.0025
14	-0.0024	-0.1960	0.0567	1.1592	-0.0480	-0.0275	0.0247
15	-0.0024	-0.1963	0.0584	1.1613	-0.0489	-0.0290	0.0262
16	-0.0219	-1.8656	0.0421	0.8431	-0.3909	0.0108	-0.0377
17	0.0071	0.5735	0.0567	1.1279	0.1406	0.0805	-0.0724
18	0.0116	0.9450	0.0564	1.0702	0.2311	-0.1042	0.1182
19	0.0054	0.4355	0.0533	1.1386	0.1034	-0.0419	0.0483
20	0.0039	0.3311	0.1429	1.2671	0.1352	-0.1085	0.1138
21	0.0164	1.3532	0.0433	0.9705	0.2878	-0.0359	0.0555
22	0.0036	0.2925	0.0447	1.1395	0.0632	0.0206	-0.0164
23	0.0129	1.0679	0.0779	1.0708	0.3104	0.2269	-0.2117
24	0.0284	2.6583	0.0890	0.6744	0.8308	0.6436	-0.6058

```
title RDMean;
ODS GRAPHICS OFF;
data RDMean;
input SCCCI1FENDVI2 Value;
datalines;
1 2.9743
2 2.7274
1 4.5474
2 3.2577
1 3.3234
2 2.2511
1 4.7828
2 4.3338
1 -0.0070
2 0.03317
1 -0.5029
2 0.5599
1 -0.02925
2 0.0598
1 -0.7062
2 0.7540
1 0.1650
2 0.1615
1 -0.3313
2 -0.32465
1 1.1507
2 1.1751
1 1.8246
2 1.8259
1 1.4637
2 1.6254
1 1.6322
2 1.6670
1 2.1537
2 0.8373
1 1.4911
2 1.4075
1 1.8469
2 1.8445
;
proc glm data=RDMean;
class SCCCI1FENDVI2 Value;
model Value = SCCCI1FENDVI2;
means SCCCI1FENDVI2 /lsd  Tukey lines;
means SCCCI1FENDVI2/DUNNETT;
LSMEANS SCCCI1FENDVI2/PDIFF;
run;
quit;
```

Figure B.5 SAS code used for SCCCI vs FENDVI means separation

Table B.12 Tukey's Studentized Range test to determine if SCCCI and FENDVI modeled with Leaf N were significantly different

The GLM Procedure

Tukey's Studentized Range (HSD) Test for Value

Alpha	0.05
Error Degrees of Freedom	32
Error Mean Square	2.177344
Critical Value of Studentized Range	2.88062
Minimum Significant Difference	1.0309

Means with the same letter are not significantly different.

Tukey Grouping	Mean	N	SCCCI1FENDVI2
A	1.5164	17	1
A			
A	1.4233	17	2

```
title RDMean;
ODS GRAPHICS OFF;
data RDMean;
input SASclass Mean_Yield;
datalines;
2      1156.401131
2      1319.33859
2      1325.033221
2      1416.731076
1      1654.539895
2      1627.142721
3      1943.287163
2      1851.241869
2      1637.70259
2      1718.930206
2      1866.431337
2      1645.448602
2      1668.115326
2      1846.533587
5      1626.481369
2      1537.126366
1      1259.208134
5      1329.517221
2      1402.146855
5      1325.268587
2      1324.439058
5      1281.572029
2      1330.369192
2      1480.717706
2      1291.19016
5      1408.009663
5      1063.313315
2      1430.149413
5      1283.668294
;
proc glm data=RDMean;
class SASClass Mean_Yield;
model Mean_Yield = SASclass;
means SASclass /lsd  Tukey lines;
means SASclass/DUNNETT;
LSMEANS SASclass/PDIFF;
run;
quit;
```

Figure B.6 SAS code used for separation of means for yield across all datasets

Data cards are concatenated for space constrictions